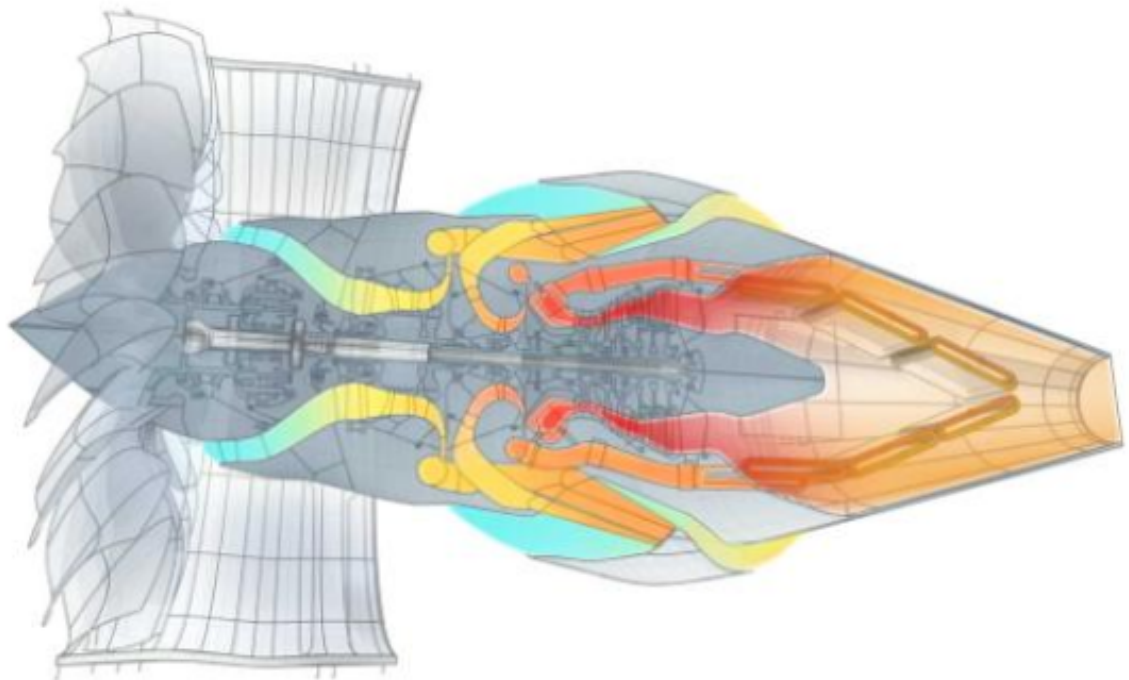


Preliminary design optimization of the Combined Cycle Engine

Patrick Jahn

Technische Universiteit Delft



PRELIMINARY DESIGN OPTIMIZATION OF THE COMBINED CYCLE ENGINE

by

Patrick Jahn

in partial fulfillment of the requirements for the degree of

Master of Science
in Aerospace Engineering

at the Delft University of Technology,
to be defended publicly on Thursday December 14, 2017 at 09:30 AM.

1. Supervisor:	Dr. A. Gangoli Rao	TU Delft
2. Supervisor:	L.Azzini	TU Delft
Thesis committee:	Prof. dr. ir. P. Colonna,	TU Delft
	Dr. A. Gangoli Rao,	TU Delft
	Dr. R. Pecnik,	TU Delft
	M.Sc. L. Azzini,	TU Delft

An electronic version of this thesis is available at <http://repository.tudelft.nl/>.

Thesis registration number: 171#17#MT#FPP

PREFACE

During the writing of this thesis I learned many things. No just about the combined cycle engine and the thermodynamics but also about motivation and the working of the human mind. I could not have done this alone. I want to thank my supervisor Dr. Arvind Gagoli Rao for his inspiration and guidance. Moreover, I want to thank Lucia Azzini for the patience, support and her valuable feedback.

Lastly I want to thank my family and friends.

Patrick Jahn
Delft, November 2017

ABSTRACT

Aviation has to reduce its emission. In the past the improvements of aero engine technology have been achieved by higher turbine inlet temperatures, higher overall pressure ratios, higher bypass ratios and more efficient components. However, these methods hold only limited potential for further improvements. Therefore, research into alternative cycle concepts started. No best solution for future aircraft engines has been identified yet and thus this research continues.

As part of this research, the combined cycle engine has been proposed as a new solution. It has been realised that the thermal energy of the exhaust gases is the biggest energy loss in a turbofan engine. The combined cycle engine uses a combination of a conventional turbofan engine and an additional supercritical Brayton cycle to use this exhaust gas heat to produce additional thrust power. A heat exchanger uses the exhaust gases of the main engine as the heat source for the supercritical cycle. Initial investigations showed many difficulties in the application of this cycle and limited potential for fuel burn reduction. This study aims at investigating the behaviour of different combined cycle engine designs to find an optimal design and to be able to estimate the potential of the concept based on this optimal design.

To predict the behaviour of the combined cycle engine, a simulation framework has been created and the results have been compared to similar investigations in literature. In addition to this, a gradient based optimization routine has been implemented to be able to optimize the system for the maximum range. With this methodology, the effect of the supercritical cycle operating conditions, the configuration of the main engine, the supercritical working fluid, the supercritical cycle configuration and the heat exchanger design have been investigated.

It was found that the behaviour of the system is very non linear. The optimum performance becomes a trade off between the specific fuel consumption and the weight. The operating parameters of the supercritical cycle and the heat exchanger design have the biggest impact on the system performance. The heat exchanger technology plays an important role in enabling good heat exchanger designs in that it limits the minimum size and wall thickness of the heat exchanger tubes. The addition of an inter turbine burner to the main engine was found to be beneficial to the performance of the supercritical cycle and the combined cycle engine as a whole. While a turboshaft configuration of the main engine brings thermodynamic benefits for the combined cycle engine, it causes a higher weight of the heater. Therefore, a turbofan engine is the superior main engine for the combined cycle engine.

The combination of a turbofan engine with an inter turbine burner and a simple recuperated supercritical carbon dioxide cycle has been identified as the best configuration of the combined cycle engine. In this configuration, the cooler is placed downstream of the fan of the main engine. The application of this cycle on a Boeing 777ER could increase the range of the aircraft by 0.46 %. With more advanced production techniques for the heat exchangers, a range increase of 2.15 % becomes possible. However, more in depth research has to be performed, to confirm these results.

CONTENTS

Abstract	v
List of Figures	ix
List of Tables	xi
Nomenclature	xiii
1 Introduction	1
1.1 The combined cycle engine	1
1.1.1 The supercritical power cycle	1
1.1.2 Research on the supercritical power cycle	4
1.2 Motivation and Scope	4
1.2.1 Thesis outline	5
2 Modelling methodology	7
2.1 Simulation framework	7
2.2 Turbomachinery	7
2.3 Combustion chamber	8
2.3.1 Turbine Cooling	8
2.4 Nozzles	8
2.5 Heat exchangers	9
2.5.1 Weight estimation	11
2.5.2 Regenerator	11
2.6 System modelling	13
2.6.1 Design mode	13
2.7 Verification	13
2.7.1 Main engine	13
2.7.2 Influence of the heat exchanger discretisation	14
2.7.3 Reference case 1	14
2.7.4 Reference case 2	15
2.8 Limitations of the methodology	16
2.9 Conclusions	17
3 Initial combined cycle engine design	19
3.1 Reference case	19
3.2 Results	19
3.2.1 Comparison to a turbofan engine	22
3.2.2 Design sensitivities	22
3.2.3 Heat exchanger behaviour	25
3.3 Conclusions	26
4 Analysis of the combined cycle engine	29
4.1 Optimization	29
4.1.1 Optimization set-up	29
4.1.2 Results	30
4.2 Top level analysis	31
4.2.1 Weight breakdown	32
4.2.2 Thermodynamic analysis	32
4.2.3 Pressure losses	35
4.2.4 System level	35
4.2.5 Derivation non choked nozzle	36
4.2.6 Placement of the cooler	39

4.3	Application to an Inter turbine burner turboshaft	40
4.3.1	Reference engines	40
4.4	Influence of the supercritical working fluid	42
4.4.1	Fluid requirements.	42
4.4.2	Critical temperature	43
4.4.3	Critical pressure	43
4.4.4	Candidate fluids	43
4.4.5	Performance comparison	43
4.4.6	Mixtures of working fluids	45
4.5	Technological barriers	45
4.6	Influence of the heat exchanger design	46
4.6.1	Effect of the wall thickness	46
4.6.2	Effect of the heat exchanger tube diameter.	47
4.6.3	Effect of the thermal conductivity of the material	47
4.6.4	Effect of the spacing between heat exchanger tubes	47
4.6.5	Effect of the tube aspect ratio in the heat exchanger	47
4.7	Influence of the supercritical cycle configuration	48
4.7.1	Effect of the supercritical cycle components	48
4.8	Conclusions.	49
5	System optimization	51
5.1	Modified methodology	51
5.1.1	Numerical implementation	51
5.1.2	Verification	54
5.2	Main engines	56
5.3	Results	58
5.3.1	Carbon dioxide cycles	60
5.3.2	Xenon cycles	60
5.3.3	Perfluorobutane cycles.	61
5.4	Conclusions.	61
6	Results	63
6.1	Optimization of the system	63
6.1.1	Investigated cases	64
6.2	Results	64
6.2.1	The optimal design	65
6.3	Effect of technological barriers	65
6.4	Conclusions.	66
7	Conclusions	67
7.1	Recommendations	68
	Bibliography	69

LIST OF FIGURES

1.1	Sankey diagram of the energy within a typical aircraft engine	2
1.2	T-s diagram of a simple ideal Brayton cycle from [1]	2
1.3	Work required to compress 1 kg of CO ₂ from the critical pressure to a variable outlet pressure	3
1.4	Schematic of the heat exchanger placement in [2]	5
2.1	Explanation of the governing equations of the turbomachinery	8
2.2	Graphical impression of the heat exchanger	9
2.3	Discretisation of the heat exchangers in cross flow configuration	10
2.4	Illustration of the regenerator layout from [2]	12
2.5	Illustration of the influence of the number of cells used for the discretisation of the heat exchangers	15
2.6	Comparison of the fluid properties discretisations	15
3.1	Dymola model of the reference case	20
3.2	Dymola model of the supercritical cycle of the reference case	20
3.3	Sensitivities of the cycle parameters	24
3.4	C_p value of CO ₂ for different temperatures and pressures	25
3.5	Temperature profile in the heat exchangers	26
3.6	Temperature distribution in the high pressure side of a regenerator	27
4.1	Changes between initial and optimized CCE design	30
4.2	GSP model to represent the combined cycle engine	31
4.3	Efficiency variation of a recuperated sCO ₂ cycle with maximum temperature	35
4.4	Effect of added heat in front of a converging nozzle	36
4.5	h-s diagram of the optimum cycle for the application of waste heat recovery	37
4.6	h-s diagram of an inter turbine burner cycle	37
4.7	Effect of pressure losses and temperature increase on an exemplary unchoked nozzle	39
4.8	Thermodynamic properties of a CO ₂ - C ₄ F ₁₀ mixture dependent on the mixture fraction	45
4.9	Layout of a recompression cycle from [3]	49
5.1	Information flow in the new simulation framework	52
5.2	Main calculation steps in the system simulation	53
5.3	Initial and final temperature distribution of a cooler with CO ₂	53
5.4	Convergence history of a typical cooler with CO ₂	54
5.5	Main calculation steps in the system simulation	55
5.6	Heat exchanger weight for a given heat duty	57
5.7	GSP models of the main engines	58
5.8	Weight distribution of different CCE configurations	60

LIST OF TABLES

2.1	Verification of the main engine model	14
2.2	Comparison of the CCE model and the results from [2]	14
2.3	Comparison of the CCE model using the results of [4]	16
3.1	Main cycle characteristics of the baseline 2035 CCE	19
3.2	Supercritical cycle characteristics of the baseline 2035 CCE	21
3.3	Performance of the baseline 2035 CCE	21
3.4	Required change in SFC to compensate for 1000 kg of additional engine weight for different aircraft	22
3.5	Required change power density for the supercritical cycle for different aircraft	22
3.6	Comparison between baseline 2035 CCE and the corresponding turbofan engine	22
4.1	Overview of different engine performances	30
4.2	Top level sensitivities	31
4.3	Applied top level sensitivities	32
4.4	Breakdown of the three heat exchangers	32
4.5	Weight estimation of the cooler	40
4.6	Flue gas properties	41
4.7	Top level sensitivities of the heater for different architectures, values give the change in SFC in %	41
4.8	Weight estimation of the heater	42
4.9	Properties of the candidate working fluids	43
4.10	Operating conditions of the heat exchangers	44
4.11	Performance of the working fluids for different heat exchangers	44
5.1	Comparison of results from Dymola and the modified methodology	56
5.2	Performance of the engines without waste heat recovery unit	57
5.3	Performance of the investigated turbofan engines	59
5.4	Performance of the investigated turboshaft engines	59
6.1	Properties of the investigated cases	64
6.2	Results of the second optimization step	64
6.3	Characteristics of the optimized engine 1 design	65

NOMENCLATURE

Symbols

ITB_{frac}	ITB energy fraction	Pr	Prandtl number
A	Cross sectional area	Q	Heat duty
Ar	Aspect ratio	Q	Heat transfer rate
C_p	Specific heat for constant pressure	R	Individual Gas constant
CO ₂	Carbon dioxide	R	Range
csi	Skin friction coefficient	R	Tube radius
cst	Skin friction coefficient	Ra	Ratio of internal to external diameter
D	Drag	Re	Reynolds number
D	Tube diameter	S	Sensitivity
E	Energy	s	Specific entropy
F	Thrust force	T	Temperature
g	Gravitational acceleration	t	Thickness
h	Channel height	u	Velocity
h	Convective heat transfer coefficient	V	Velocity
h	Specific enthalpy	W	Work
J	Performance parameter	w	Channel width
k	Conductive heat transfer coefficient	Abbreviations	
k	Constant	API	Application Programming Interface
k	constant factor	CC	Combustion Chamber
L	Lift	CCE	Combined Cycle Engine
l	Length	CSP	Concentrated Solar Power
m	Mass flow rate	GSP	Gas turbine Simulation Program
N ₂ O	Nitrous oxide	HEX	Heat EXchanger
NO _x	Nitrogen oxide	HP	High Pressure
Nu	Nusselt number	HPC	High Pressure Compressor
P	Power	HPT	High Pressure Turbine
P	Pressure	IRE	Intercooled Recuperated Engine
		ITB	Inter Turbine Burner
		LHV	Lower Heating Value

LP	Low Pressure	δ	Geometric parameter
LPC	Low Pressure Compressor	η	Isentropic efficiency
LPT	Low Pressure Turbine	γ	Geometric parameter
OPR	Overall Pressure Ratio	κ	Heat capacity ratio
PR	Pressure Ratio	λ	Thermal conductivity
SFC	Specific Fuel Consumption	μ	Dynamic viscosity
TIT	Turbine Inlet Temperature	ρ	Density
Greek symbols			
α	Geometric parameter	σ	Material yield strength

1

INTRODUCTION

The emissions of aviation have become an important part of the global emissions. These emissions are projected to further increase [5]. As a result, solutions to reduce the emissions of aviation are in high demand. Because the engine technology based on the Brayton cycle is well understood and mature, only small future efficiency increases are expected from this technology [6]. Therefore, research in new types of engine cycles started. Several studies have investigated the benefits of the intercooled cycle [7], the intercooled recuperated cycle [8], the composite cycle [9] or other alternative cycles [10]. However, no best concept has been identified yet. In the scope of these research efforts, the combined cycle engine has recently been proposed as a new working concept for aircraft propulsion.

1.1. THE COMBINED CYCLE ENGINE

In aero engines a large fraction of the chemical energy that enters the engine in the form of the fuel ends up in the high temperature of the exhaust gas stream. The Sankey diagram in figure 1.1 shows how the chemical energy is transformed in a typical turbofan engine. The diagram has been created from a simplified thermodynamic analysis of an typical modern aero engine during cruise. As can be seen, around 45 % of the total energy is lost in the exhaust heat while only around 38 % is transformed into the desired thrust.

The idea behind the combined cycle engine(CCE) is to use the high temperature of the exhaust to create additional useful power. In this way, less energy is wasted in the exhaust heat. The energy transformation takes place in an additional supercritical power cycle, the waste heat recovery unit(WHR). The combined cycle engine is thus a combination of a supercritical power cycle and a turbofan engine. In this configuration the hot gas leaving the turbine of the turbofan engine is used as the heat source of the supercritical cycle. In this way the efficiency of the system can be increased. The heat is added to the supercritical cycle by means of heat exchangers. Therefore, the supercritical cycle is operated as a closed cycle.

1.1.1. THE SUPERCRITICAL POWER CYCLE

The basic principle of the supercritical cycle resembles the Brayton cycle. It consists of an isentropic compression, an isobaric heat addition, an isentropic expansion and an isobaric heat removal. Figure 1.2 shows a T-s diagram of a typical Brayton cycle.

The advantage of the supercritical cycle is the compression of a fluid close to its critical point. Close to the critical point, the compression of a fluid requires less energy compared to the same fluid in its gas phase. Through heat addition, the fluid behaves more like an ideal gas and the work extracted during the expansion in a turbine is big. In this way high efficiencies can be achieved. In addition to this, the high density of the supercritical working fluid enables the use of compact turbomachinery and heat exchangers. Therefore, the supercritical cycle can achieve a high power density. The effect on the compression work is demonstrated in figure 1.3. This figure shows the work that is required to compress CO₂ isentropically. The three graphs correspond to three different inlet temperatures. The red line represents the inlet temperature of 305 K. This temperature is very close to the critical temperature of CO₂ and in the supercritical state. The blue line repre-

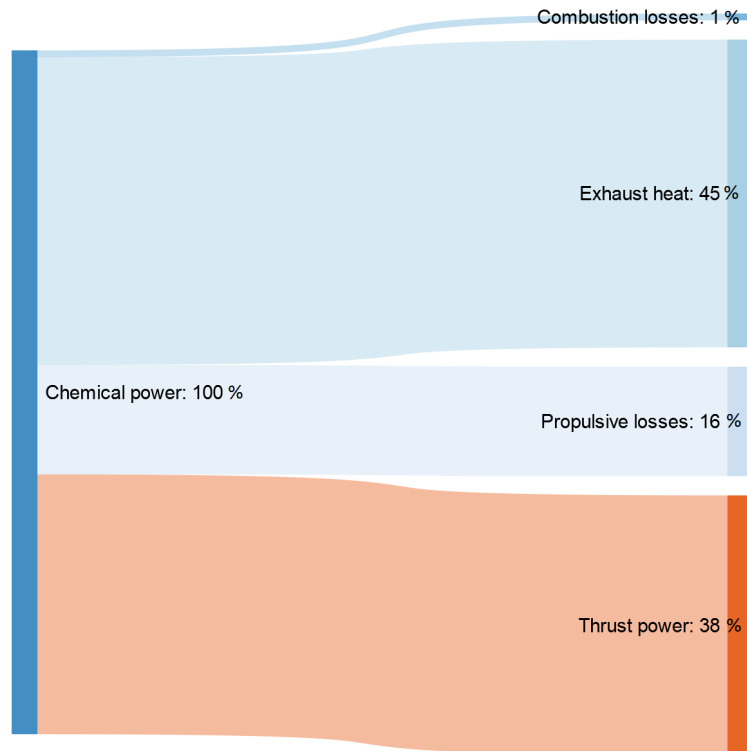


Figure 1.1: Sankey diagram of the energy within a typical aircraft engine

sents a subcritical state and the yellow line represents a temperature above the critical temperature. All three lines start at the critical pressure of CO_2 at 7,375 MPa.

It can be seen that the work that is required to reach a certain pressure ratio is lower for the starting temperature 305 K than it is for the starting temperature 324 K. The required work for a starting temperature of 284 K is even lower. However, the starting temperature below the critical temperature results in the fluid reaching the liquid phase. If this is the case, cavitations can occur. These cavitations can damage the compressor and reduce its efficiency. Therefore, the option of a phase change is not investigated in this thesis.

After the heat addition, the influence of the starting temperature is much lower. Almost the same amount of energy can be extracted from the fluids. Therefore, the efficiency of the cycle with the fluid being compressed from the critical point is higher. If the starting temperature of the fluid is even lower than the critical temperature, the efficiency can be further increased. As the critical pressure of suitable fluids is in the order of 50 bar, only low pressure ratios are achievable due to the high maximum pressures resulting from this.

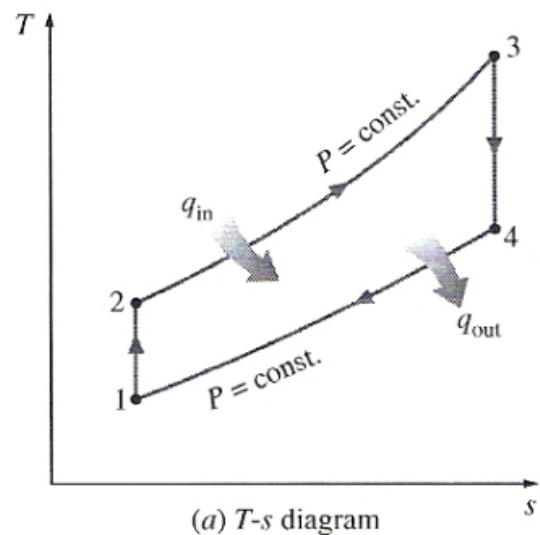


Figure 1.2: T-s diagram of a simple ideal Brayton cycle from [1]

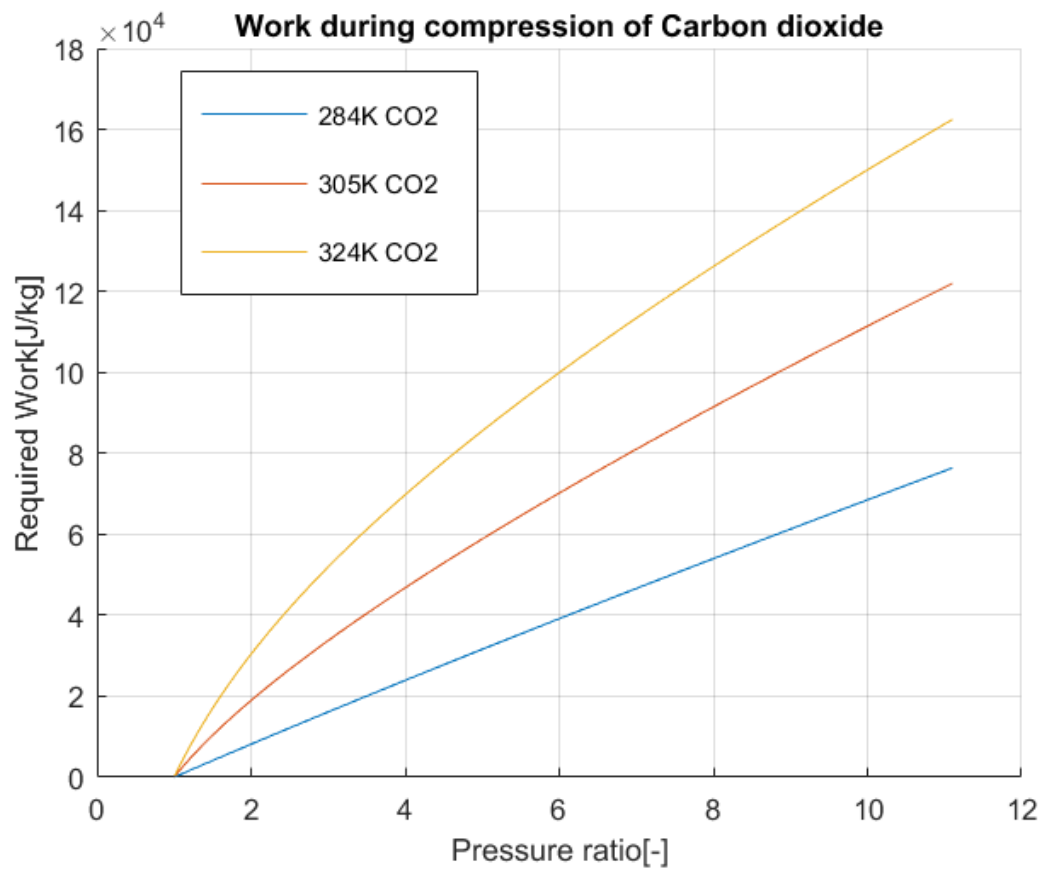


Figure 1.3: Work required to compress 1 kg of CO₂ from the critical pressure to a variable outlet pressure

1.1.2. RESEARCH ON THE SUPERCRITICAL POWER CYCLE

The foundation for the supercritical cycle was laid in 1967 by Feher and Angelino [11] [12]. Although a potential was discovered, the research did not continue due to the absence of suitable turbomachinery and heat exchangers at that time [13]. Occasionally some research had been conducted on the supercritical cycle but it stayed largely unnoticed [14]. In 2004 Dostal *et al.* [13] proposed the supercritical CO₂ cycle for the use in nuclear power plants. This analysis extensively investigated the performance of different configuration with the possibilities of that time. The recompression cycle showed to be the best candidate. This study was the starting point of extensive research at different places and many studies were published. Most investigations are related to the turbomachinery involved in the cycle and thermodynamic analyses of the overall layout of the cycle. The research was still eyeing the application in nuclear power plants. In these efforts also several test cycles have been build. Recently research on the application of the supercritical CO₂ cycle for other forms of energy have started [15]. One study also investigated the use of an supercritical CO₂ power cycle in a nuclear reactor for maritime applications [16].

There are at least four test set-ups that are currently researching the operations of the supercritical CO₂ cycle. These test set-ups are located at the Institute of applied science in Tokyo, the Sandia National Laboratory, Bettis atomic power laboratory, both located in the USA, and the Korean Atomic Energy Research Institute in South Korea [17]. These studies showed the feasibility of the supercritical CO₂ cycle as energy could be produced with the demonstrators. The research at these demonstrators is mostly related to the practical matters that are required for the operation of a supercritical power cycle. These topics include the design and operation of the required turbomachinery, especially the compressor [18] [19] [20], the control of the system [21] and the behaviour of the system in off design conditions [22] [23]. In the demonstrators, many issues related to the small size of the demonstrators were found. For this reason a bigger demonstrator with a power output of 10 MW is planned to be operational in 2019 [24] [25] [26].

Next to the research on the demonstrators, also research on possible improvements to the cycle was conducted. These studies manly focussed on the use of different working fluids or mixtures of working fluids [27] [28] [29] [29] [30] [31], different applications of the cycle or the use of different cycle configurations [3] [13] [32] [33].

1.2. MOTIVATION AND SCOPE

In a preliminary study the combined cycle engine has been identified as a promising solution for future aircraft propulsion. A possible SFC reduction of 7 % was found compared to a conventional turbofan engine [2]. Furthermore it was found that the combined cycle engine gives big advantages for high overall pressure ratios (OPR) of the core engine. A comparison of the achieved heat transfer rates in the heat exchangers showed that the heat duty is lower for the combined cycle engine compared to the IRE. This can lead to more compact heat exchangers for the combined cycle engine. However during an sizing exercise, fitting a supercritical CO₂ cycle on a GE90 engine, the systems did not yield any benefits. This was because the size constraint of the engine enclosure limited the heat exchanger size. Therefore the SFC reduction was only 2.8 %. At the same time the weight per engine increased by 3 tons. This weight increase compensated for the reduction in SFC and no fuel burn reduction could be achieved. In the investigation, the heater of the supercritical cycle was placed in the bypass duct of the fan. The heater was placed between the LPT and the nozzle of the turbofan engine. The power generated by the supercritical cycle was used to produce thrust outside the core engine. The configuration is shown in figure 1.4.

In another investigation the combined cycle engine could be designed to achieve a fuel burn reduction of 1.9 % [4]. In this study an advanced geared turbofan engine of the year 2050 was equipped with a supercritical CO₂ cycle to generate power from the waste heat. The power of the supercritical cycle was calculated to be around 0.8 MW and was introduced into the low speed spool. The additional weight of the heat exchangers was calculated to be around 600 kg per engine. However, the weight estimation did not take the effect of the high pressure working fluid into account and assumed the ability to produce very thin-walled and small tubes in the heat exchangers. The configuration was the same as in the study of de Servi *et al.* The power of the supercritical cycle was transferred into the low pressure spool of the main engine.

Based on the literature, the true potential of the combined cycle engine can not be assessed sufficiently.

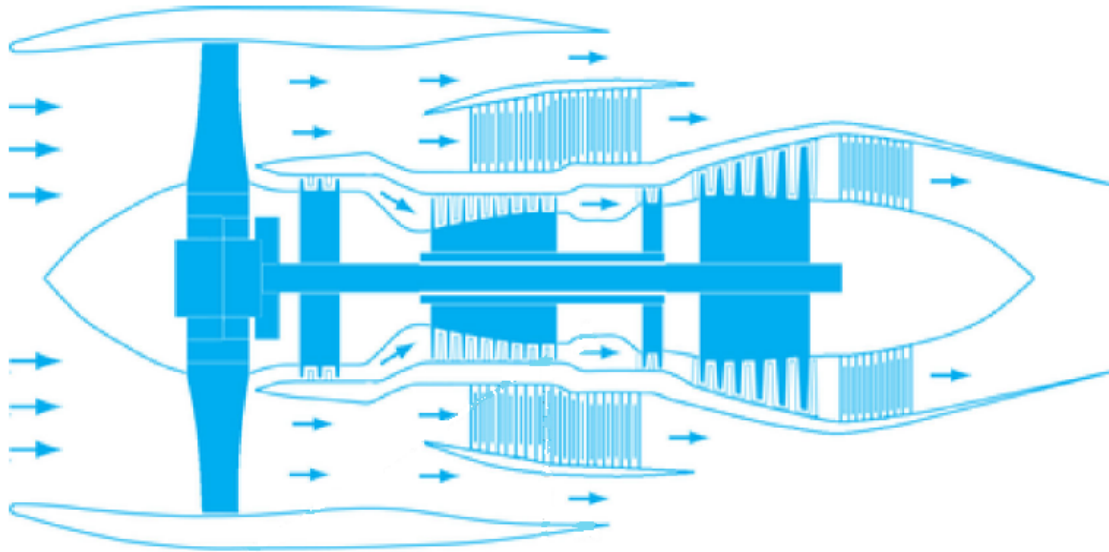


Figure 1.4: Schematic of the heat exchanger placement in [2]

Therefore more knowledge about the behaviour of the combined cycle engine and the potential for improvements is required. To gain this knowledge, the behaviour of the CCE will be investigated and the influence of the most important parameters on the performance of the CCE will be analysed. The optimal combination of the CCE concept will be evaluated and its performance determined. This will show the potential benefits of the introduction of the CCE and can be used as a decision ground about the future research on the concept. The study will only investigate supercritical waste heat recovery cycles. The possibility of a supercritical condensation cycle will not be investigated. The study will also highlight the assumptions about the technological possibilities and show their impact on the feasibility of the CCE. This will be done by relatively low fidelity methods that capture all important effects and still enable the exploration of a large design space.

1.2.1. THESIS OUTLINE

The goal of the thesis is to find the possible benefits of the use of a combined cycle engine for the use as aircraft propulsor. For this purpose an optimal design shall be found, analysed and compared to other possible solutions. To be able to analyse the performance of the designs, a modelling methodology has to be established. This simulation framework will be reasoned and explained in chapter 2. In this chapter the core assumptions and verification of the model will be shown as well. Chapter 3 will introduce the reference design and the starting point for the optimization. In addition to this, the performance will be calculated and presented. The optimization of the combined cycle engine will be elaborated on in chapter 4. This chapter contains the main part of this thesis. It will show the impact of different parameters like the heat exchanger design or the working fluid on the system performance and also clarify how these results are found. Based on these findings, several improved designs will be proposed. These designs will be specified and evaluated in chapter 5. The best concept design will be further optimized in a more in depth approach to show the full potential of the combined cycle engine. This process and the results will be explained in chapter 6. In chapter 7 conclusions will be drawn and recommendations for further work will be proposed.

2

MODELLING METHODOLOGY

This section contains the thermodynamic modelling and the weight estimation methods that are used for the components and the entire system. Most components are represented by zero dimensional thermodynamic models. This enables a fast computation with a low number of required parameters.

2.1. SIMULATION FRAMEWORK

The model is built adopting the Modelica language, through the Dymola user interface. Modelica is a symbolic language that allow for the simulation of complex systems through their constitutive equations. Such systems are well-posed, i.e. the number of variables and degree of freedom are equal. This simplifies the implementation of the model, as iterative procedures are conducted automatically. However, the implementation becomes less intuitive, as the problem has to be described as a well posed system of equations. Furthermore the automatic solution of the equation system makes it harder to detect errors or unphysical behaviour. For this reason, the verification of the results is crucial to determine the reliability of the model.

The fluid properties of the gases like the flue gas or the air in the main engine are calculated using the standard fluid library of Dymola. This enables quick calculation of the properties and allows the use of standard component libraries in the main engine. The fluid properties of the supercritical working fluid of the waste heat recovery unit is calculated using the Modelica interface to Refprop. Although the computational time required by this external library is higher, the choice was deemed necessary to keep into account the highly non-ideal behaviour of the working fluid in the considered thermodynamic region.

2.2. TURBOMACHINERY

The turbomachinery components in the gas turbine as well as in the supercritical cycle are modelled by means of a simple 0-D model with isentropic efficiency. To define the operating conditions of these components, three main parameters have to be set: i.) the inlet conditions ii.) the isentropic efficiency iii.) either the pressure ratio or the required work output. As an example, equation 2.1, 2.2, 2.3, 2.4 and 2.5 show the governing equations to model a turbine. In these equations h is the specific enthalpy, P the pressure, s the specific entropy, W the power and m the mass flow rate. The subscripts *in* and *out* depict the property at the inlet or the outlet of the turbine. The subscript *isen* describes the properties at the outlet of an isentropic process. As an example, the procedure for a turbine is illustrated in figure 2.1. The black lines represent the isobars of the inlet and the outlet pressure of the turbine. The point *isen* represents, the process that would take place in an isentropic process. As the pressure and entropy are known, the enthalpy is uniquely defined. An equivalent procedure can be applied to model a compressor.

$$h_{out} = h_{in} + \eta * (h_{isen} - h_{in}) \quad (2.1)$$

$$P_{isen} = P_{out} \quad (2.2)$$

$$s_{isen} = s_{in} \quad (2.3)$$

$$h_{isen} = f(s_{isen}, P_{isen}) \quad (2.4)$$

$$W = m * (h_{in} - h_{out}) \quad (2.5)$$

2.3. COMBUSTION CHAMBER

The combustion chamber is also represented by a 0-D model. The temperature increases according to the amount of fuel that is injected $m_{fuel_{in}}$ and its caloric value LHV . A total pressure loss from the inlet to the outlet of the combustion chamber is imposed. Equation 2.6 shows the energy balance of the combustion chamber. $\eta_{combustion}$ is the efficiency of the combustion process and is a measure of how much of the chemical energy of the fuel is transferred into heat.

$$m_{out} * h_{out} = m_{air_{in}} * h_{air_{in}} + m_{fuel_{in}} * (h_{fuel_{in}} + \eta_{combustion} * LHV) \quad (2.6)$$

The composition of the flue gases is calculated keeping into account only some of the reactions that take place during the combustion. In particular the reaction of air and methane to water and CO_2 according to the chemical equilibrium. The formation of CO or nitrous oxides is not taken into account.

2.3.1. TURBINE COOLING

In order to ensure acceptable material temperatures in the HPT, cooling air from the outlet of the HPC is injected into the HPT. This process is modelled as additional air entering between the combustion chamber and the HPT. The temperature of the mixture is calculated using the energy balance. For both properties, the gas composition and the pressure, the values from the gas leaving the combustion chamber are assumed. The amount of cooling air is calculated based on the mass flow rate at the exit of the HPC, the ratio of the total pressure at the fan inlet and the HPC outlet and the turbine inlet temperature. This method enables a quick estimation of the required cooling air, taking into account the most important factors pressure ratio (and thus cooling air temperature) and TIT.

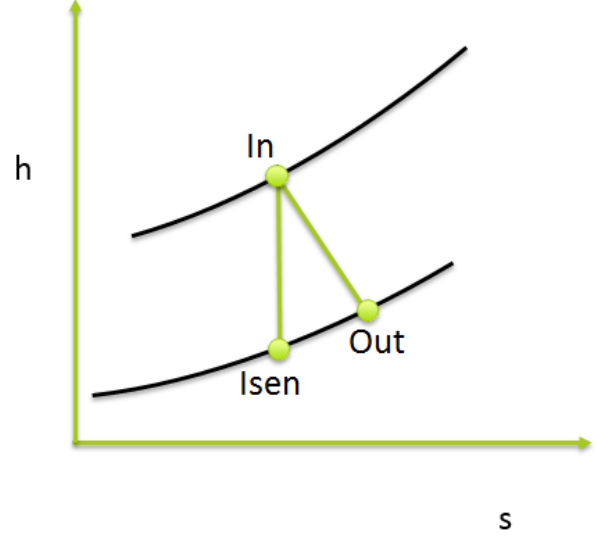


Figure 2.1: Explanation of the governing equations of the turbomachinery

2.4. NOZZLES

The thrust F of the nozzle is calculated using a momentum balance of the flight velocity V_0 , the exit velocity of the gas V and the pressure difference between the exit pressure P and the ambient pressure P_0 acting on A , the exit area of the nozzle.

$$F = m * (V - V_0) + A * (P - P_0). \quad (2.7)$$

The cross sectional area of the nozzle is calculated using a mass balance.

$$A = \frac{m}{\rho * V} \quad (2.8)$$

ρ in this equation is the density of the gas. The nozzles are assumed to be choked. I.e. the flow reaches sonic velocity at the outlet. According to the isentropic flow relations, the pressure P can thus be calculated dependent on the total inlet pressure $P_{t_{in}}$ and the specific heat ratio of the gas κ_{gas} .

$$P = \frac{P_{t_{in}}}{\frac{1}{\left(1 - \frac{1}{\eta_j} * \frac{\kappa_{gas}-1}{\kappa_{gas}+1}\right)^{\frac{\kappa_{gas}}{\kappa_{gas}-1}}}} \quad (2.9)$$

The exit velocity equals the speed of sound and is calculated as

$$V = \sqrt{\kappa_{gas} * R * T} \quad (2.10)$$

where R is the individual gas constant and the temperature T can be calculated using the isentropic relations.

$$T = T_{in} * \frac{2}{\kappa_{gas}} \quad (2.11)$$

2.5. HEAT EXCHANGERS

The heat exchanger is modelled as a stack of elliptical tubes that goes around the full diameter of the engine core. This geometry is shown in figure 2.2. As can be seen, the curvature of the tubes itself is very low. The cross sectional area is filled with the tubes. The length of the heat exchanger along the shaft of the main engine depends on the requirement for the heat duty. The tubes are small but long. This causes high temperature differences for the fluid in the first tubes and might result in parts of the fluid entering the liquid phase. With different heat exchanger configurations, this can be avoided. However, this heat exchanger design is beyond the scope of this thesis. Therefore it is noted that the phase change of parts of the working fluid, especially in the cooler has to be investigated in further research.



Figure 2.2: Graphical impression of the heat exchanger

inside the cell known, the updated value of the outlet conditions can be calculated. In this fashion, the iterations continue until convergence is reached. The interaction between the cells is realised through the media streams. I.e. A2 represents the outlet conditions of the CO_2 stream through cell 1 and at the same time the inlet conditions of this stream through cell 2 and so forth.

Different schemes are available to model the properties in the heat exchanger cells. The model uses the central discretisation scheme, i.e. the calculations are carried out using the average properties of the fluid for each cell.

The pressure losses on the outside of the heat exchanger are estimated using the correlation of Ibrahim Gooma. The correlation is based on experiments and is shown in equation 2.12 [34]. In this relation u is the velocity and csi the skin friction coefficient.

$$dp = 0.5 * l * \rho * u^2 * csi \quad (2.12)$$

The heat exchangers are modelled in 2-D to allow an accurate estimation of their weight and pressure losses. For this model, the heat exchangers are discretised to take the variation in the heat transfer coefficient and pressure loss along the component into account. The discretisation of the heat exchangers happens in 2-D and is shown for a cooler in figure 2.3. The heat exchangers operate as a cross flow configuration. In this case 2x2 cells are used for the discretisation. The cooling air follows the blue arrows and flows from the top to the bottom in the independent streams I and II. The CO_2 follows the black arrows and flows from left to right in the independent streams A and B. The functioning of the discretisation is explained on the example of the top left cell 1:

The air stream I and the CO_2 stream A cross in cell number 1. The inlet conditions of the air stream are depicted by I1 and the outlet conditions by I2. For the CO_2 stream, the inlet conditions are at A1 and the outlet conditions at A2. The conditions inside the cell, e.g. the temperature are calculated based on the inlet and outlet conditions. With the values

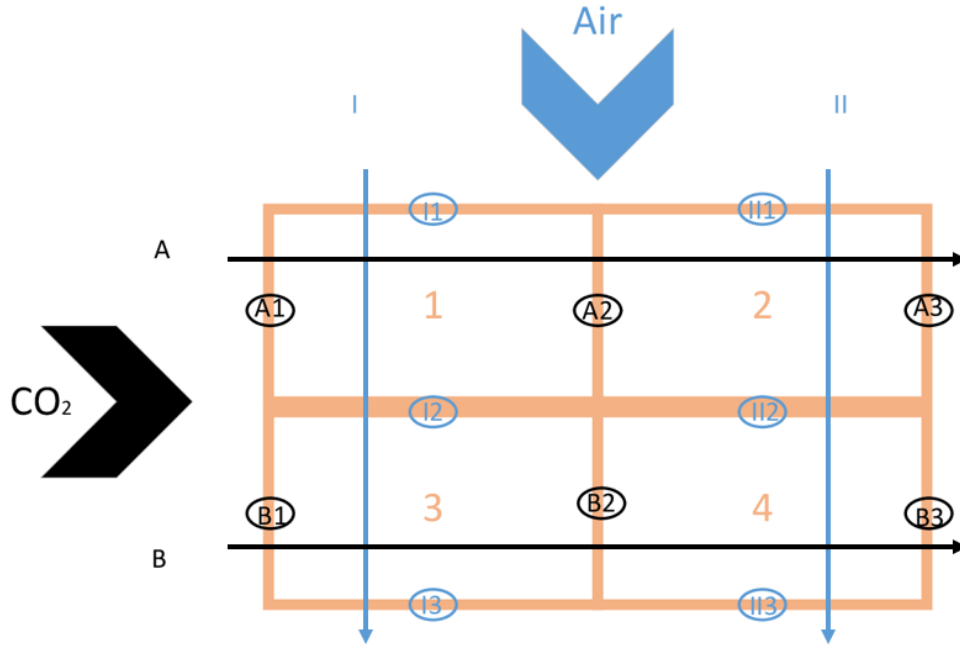


Figure 2.3: Discretisation of the heat exchangers in cross flow configuration

The skin friction coefficient csi is estimated using equation 2.13. It depends on the Reynolds number Re , the Prandtl number Pr and the aspect ratio of the tubes Ar .

$$csi = 0.195 * Re^{-0.0466} * Pr^{0.33} * Ar^{-2.29} * \sin\left(\frac{\pi}{18}\right)^{0.052} \quad (2.13)$$

The Reynolds number is calculated to be

$$Re = \frac{u * \rho * D_{hydo}}{\mu} \quad (2.14)$$

D_{hyd} is the hydraulic diameter of the tube and depends on the maximum diameter D_{min} and the maximum diameter D_{max} of the tubes. On the outside, the hydraulic diameter is defined as

$$D_{hydo} = 2 * \sqrt{D_{min} * D_{max}} \quad (2.15)$$

On the inside, the wall thickness t is also taken into account and the hydraulic diameter is defined as

$$D_{hyd} = 2 * \sqrt{(D_{min} - t) * (D_{max} - t)} \quad (2.16)$$

The Prandtl number is given by

$$Pr = \frac{C_p * \mu}{\lambda} \quad (2.17)$$

where μ is the dynamic viscosity of the fluid and λ its thermal conductivity. For the internal pressure losses, as similar correlation has been established. This correlation is shown in equation 2.18 [35]. l is the length of the tube and D_{hyd} is the hydraulic diameter of the tubes.

$$dp = 0.5 * csi * \frac{l}{D_{hyd}} * \rho * u^2 \quad (2.18)$$

In this correlation, the skin friction coefficient csi is estimated using equation 2.19.

$$csi = 0.3164 * Re^{-0.25} + 0.03 * Ar^{-0.05} \quad (2.19)$$

The heat transfer coefficient ht on the outside is calculated by the correlation of Gooma, given in equation 2.20 [34]. In this equation Nu is the Nusselt number of the flow and λ is the conductivity of the gas.

$$ht = Nu * \frac{\lambda}{D} \quad (2.20)$$

The Nusselt number Nu is estimated using equation 2.21.

$$Nu = 0.452 * Re^{0.537} * Pr^{0.33} * Ar^{-0.079} * \sin\left(\frac{\pi}{18}\right)^{0.2} \quad (2.21)$$

The heat transfer coefficient ht on the inside is calculated by the correlation of Chiesa given in equation 2.22 [35]. This equation is based on relations for the Nusselt number that have been found in experiments [36].

$$ht = \frac{csi * Re * Pr}{8 * \left(1 + 12.7 * \sqrt{\frac{csi}{8}} * Pr^{\frac{2}{3}} - 1\right)} * \frac{\lambda}{D} \quad (2.22)$$

It has to be noted that the curvature of the heat exchangers is not taken into account. The tubes are modelled to be straight rather than forming a circle. Therefore, the correction factors mentioned in [35] do not apply. As the internal medium velocity is relatively low and the curvature of the heat exchangers is low as well, this is a reasonable assumption.

The total heat transfer coefficient is calculated using equation 2.23.

$$G_{tot} = \frac{1}{\frac{1}{ht_{out}} + R_{wall} + \frac{Ra}{ht_{in}}} \quad (2.23)$$

Ra is a measure for the ratio of inside and outside diameter of the heat exchanger tubes. 2.24.

$$Ra = \frac{D_{max} * D_{min}}{(D_{max} - t) * (D_{min} - t)} \quad (2.24)$$

In this equation 2.23, the heat transfer resistance of the wall R_{wall} is derived from equation 2.25.

$$R_{wall} = \frac{t_{wall}}{\lambda_{wall}} \quad (2.25)$$

The total heat transfer dh in an element is calculated using equation 2.26.

$$dh = G_{tot} * \Delta T * A \quad (2.26)$$

2.5.1. WEIGHT ESTIMATION

An accurate estimation of the weight of the supercritical cycle is important to determine the performance of the combined cycle engine. As the weight of the heat exchangers is the majority of the total weight of the supercritical cycle, only the weight of the heat exchangers is taken into account. The weight is calculated to be the volume of the heat exchanger times the density. The required thickness t of the tubes is based on the maximum tube diameter D_{max} , aspect ratio, material yield stress $\sigma_{material}$ as well as the maximum pressure difference P_{max} between inside and outside. As a material, the titanium alloy Ti-6Al-4V is used. Equation 2.27 is used to calculate the required thickness [37].

$$t = P_{max} * D_{max} * \frac{\sqrt{3 + Ar^4 - 3 * Ar^2}}{2 * \sigma_{material}} \quad (2.27)$$

2.5.2. REGENERATOR

The regenerator is modelled as a printed circuit heat exchanger. An illustration of the regenerator is shown in figure 2.4. As the channels are rectangular, the required thickness is calculated using equation 2.28. In this equation, ΔP is the pressure difference between the two flows. h is the height of a channel and $\sigma_{material}$ is the yield strength of the material.

$$t = \frac{\Delta P * h}{2 * \sigma_{material}} \quad (2.28)$$

The estimation of the heat transfer coefficient and the pressure losses is based on the experimental work of Manglik and Bergles [38]. The heat transfer coefficient is calculated using equation 2.29.

$$ht = Nu * \frac{A}{m} * c_p * Pr^{-0.66} \quad (2.29)$$

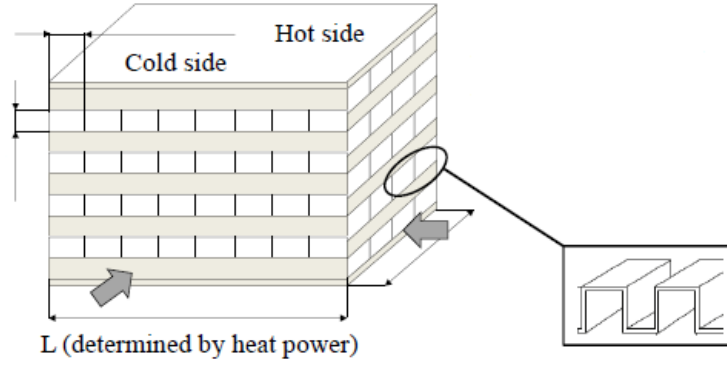


Figure 2.4: Illustration of the regenerator layout from [2]

In this relation Pr is the Prandtl number, m the mass flow rate and A is the cross sectional area of the channels. c_p is the specific heat for constant pressure of the working fluid. The Nusselt number Nu is estimated using equation 2.30 [38],

$$Nu = 0.6522 * Re^{-0.5403} * \alpha^{-0.1541} * \delta^{0.1499} * \gamma^{-0.0678} * (1 + 5.269 * 10^{-5} * Re^{1.34} * \alpha^{0.504} * \delta^{0.456} * \gamma^{-1.066})^{0.1} \quad (2.30)$$

where several geometric properties are present. The parameter α is the ratio of the channel dimensions

$$\alpha = \frac{w}{h}, \quad (2.31)$$

where h is the height of the channel and w is the width. δ is the ratio of the wall thickness to the width and γ the ratio of wall thickness to the height of a channel.

$$\delta = \frac{t}{w} \quad (2.32)$$

$$\gamma = \frac{t}{h} \quad (2.33)$$

The Reynolds number Re is calculated as

$$Re = \frac{u * \rho * D_{hyd}}{\mu}. \quad (2.34)$$

In this equation η is the dynamic viscosity of the working fluid and D_{hyd} is the hydraulic diameter and calculated in equation 2.35.

$$D_{hyd} = \frac{4 * w * h * (h - t)}{2 * (w * h + h^2 + h * t) + t * w} \quad (2.35)$$

The pressure losses are calculated using equation 2.36.

$$dp = \frac{2 * csi * l * \frac{m^2}{A} * 0.9}{\rho * D_{hyd}} \quad (2.36)$$

In this equation l is the length of the channel, ρ is the density of the fluid and D is the hydraulic diameter. The skin friction coefficient csi is calculated using equation 2.37 [38].

$$csi = 9.6243 * Re^{-0.7442} * \alpha^{-0.1856} * \delta^{0.3053} * \gamma^{-0.2659} * (1 + 7.669 * 10^{-8} * Re^{4.429} * \alpha^{0.92} * \delta^{3.767} * \gamma^{0.236})^{0.1} \quad (2.37)$$

The regenerator has the form of a cuboid. The height of the cuboid is fixed by the amount of layers and the height of a single channel. The length is the design variable that is used to size the regenerator. The width equals the length times the pressure ratio of the supercritical cycle. This is to ensure similar flow velocities in both sides of the regenerator and thus also similar pressure losses.

2.6. SYSTEM MODELLING

The model is run in design mode. The environmental conditions as well as the total thrust are kept constant at an prescribed value. This section reports some details of the gas turbine modelling.

2.6.1. DESIGN MODE

There are three main components in the model of the CCE:

- Main engine: In the design mode, the pressure ratios of the fan, the lower pressure as well as the high pressure compressor and the supercritical compressor are fixed. The low pressure and the high pressure turbine of the main engine have a fixed power output that they have to deliver.
- Heat exchangers: For the cooler, a certain mass flow of bypass air is prescribed. Furthermore, the minimum temperature differences of the heat exchangers is an input parameter. The size of the heat exchangers are varied accordingly. In this procedure, the length as well as the maximum and minimum diameter of the heat exchanger are given as well. The variation of the geometry is thus limited to the amount of columns of tubes and thus the total amount of tubes.
- Supercritical cycle: For the CO₂ cycle, the mass flow of the supercritical fluid is fixed. Furthermore, the minimum and maximum pressure in the cycle are fixed. The temperatures are dependent on the minimum temperature differences in the heat exchangers and the conditions of the fluids on the outside of the heat exchangers. The turbine of the supercritical cycle has a fixed pressure ratio. This is the case, as the turbine outlet pressure in the closed cycle is fixed and excessive power from the turbine can be used to provide additional thrust.

The analysis is limited to the design point. Off-design analysis is beyond the scope of this thesis. Therefore, the methodology will not be further elaborated on. For more information, the reader is referred to [39].

The thermodynamic performance of the engine is measured in terms of the specific fuel consumption SFC. In this context it is defined as

$$SFC = \frac{m_{fuel}}{F_{mainengine} + F_{WHR}} \quad (2.38)$$

in which m_{fuel} is the fuel flow, $F_{mainengine}$ the thrust produced by the main engine and F_{WHR} is the equivalent thrust produced by the supercritical cycle, calculated as

$$F_{WHR} = 0.9 * \frac{P_{WHR}}{V}, \quad (2.39)$$

where V is the cruise speed of the aircraft and P_{WHR} is the power produced by the supercritical cycle.

2.7. VERIFICATION

In this section, the procedure of the verification will be described and discussed. Three different tests have been performed in order to verify the model. First the model for the main engine without supercritical bottoming cycle has been compared to an equivalent model in GSP. GSP is a 0-D simulation program for gas turbines [40]. Much experience is available with the tools and its accuracy has been proven. It is used as a benchmark tool for the verification, as it enables quick and accurate results. Second and third, the CCE model has been modified in order to meet the conditions described in [2] and [4]. The results of these calculations are then compared to the published results. The simulation of the heat exchangers involves a 2-D model which is associated with a discretisation. The best discretisation scheme and the required number of cells is determined before the CCE results are compared.

2.7.1. MAIN ENGINE

To verify the validity of the used models, a turbofan model was composed and compared to a similar model in GSP. The models consisted of components with identical performance and following from this, the resulting performance and dimensions should be the same for the two models. Table 2.1 compares the results for both models. A small discrepancy between the models was observed. This is likely due to the different adopted

Table 2.1: Verification of the main engine model

	Dymola	GSP	Difference in %
Thrust [kN]	72	71.71	0.404
SFC [kg/kN*h]	52.94	52.88	0.12
m_{air} [kg/s]	687.969	687.969	0
m_{fuel} [kg/s]	1.05887	1.0534	0.519
PT3 [bar]	16.4088	16.4351	-0.16
TT3 [K]	798.792	800.61	-0.227
TT4 [K]	1500	1500	0
PT5 [bar]	0.554734	0.54708	1.399
TT5 [K]	716.022	710.88	0.723
$A_{nozzle_{core}}$ [m ²]	0.663619	0.670044	-0.959
P_{HPT} [MW]	26.430	26.637	-0.776
P_{LPT} [MW]	22.072	22.221	-0.671

Table 2.2: Comparison of the CCE model and the results from [2]

	Dymola	Model from [2]	Difference in %
Thrust [kN]	70.6	70.6	0
SFC [kg/kN*h]	52.73	55.13	-4.35
Fluegas mass flow through heater [kg/s]	54,64	54,29	0,65
Fluegas temperature heater inlet [K]	737.38	743.96	-0.88
Air temperature cooler inlet [K]	278.1	277.18	0.33
Cooler weight [kg]	1668	3175	-47.46
Heater weight [kg]	733.9	702.56	4.46
Regenerator weight [kg]	509.67	517.74	-1.56

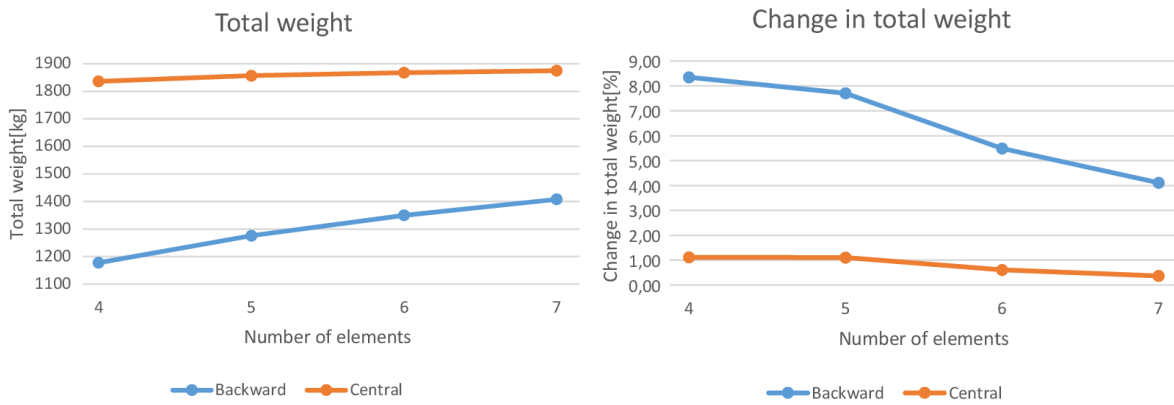
fluid models. As can be seen, the different air properties already produce small differences in the order of 0.2 %. After the combustion process, the flue gas composition is slightly different. The changes in composition are in the order of 0.5 %. This further increases the differences between the two models. However, the biggest deviation is in the total pressure at the outlet of the LPT. This error is 1.4 %. As a fuel methane has been used in both models, as otherwise the flue gas composition is different and errors in the order of magnitude of 3 % are induced downstream of the combustion chamber. When methane is used as a fuel for both models, the errors are below 1.5 % and likely due to the different thermodynamic models that are used. This is deemed acceptable for the present study.

2.7.2. INFLUENCE OF THE HEAT EXCHANGER DISCRETISATION

More elements yield a more accurate results as the non linear behaviour of the fluid properties is better approximated. At the same time, a higher amount of elements increases the computational time. Because of that, it is desirable to use the minimum amount of elements that is required to get accurate results. To find this amount of elements the changes of results for different amount of elements has been analysed. When the results do not change for different amount of cells any more, the required number of cells is reached. Figure 2.5 shows the calculated heat exchanger weight of an engine dependent on the number of cells that have been used to discretise the heat exchangers. In addition to this, the relative change in the result, if an additional cell is used for the discretisation is shown. The graphs show that indeed, the backward scheme underestimates the heat exchanger weight. Furthermore the method is much more dependent on the number of cells than the central scheme. For $n = 7$, the change in weight for the central scheme is below 0.5 %. It was decided to use 8 elements for the discretisation of the heat exchangers, as the dependency on the number of cells is very small at this amount. In addition to this, the required calculation times are still acceptable.

2.7.3. REFERENCE CASE 1

After the modelling capabilities for the main engine have been verified, the results of a combined cycle engine are compared to results from literature in order to verify the correct working of the additional computations. For this purpose, the model from [2] was used. The results of this comparison can be found in table 2.2. As



(a) Calculated weight of the heat exchangers in dependency of the number of cells used for the discretisation (b) Change between the weight for different number of cells used for the discretisation

Figure 2.5: Illustration of the influence of the number of cells used for the discretisation of the heat exchangers

can be seen, the thermodynamic results as well as the flue gas mass flow are very close with deviations below 1 %. However, significant deviations are observed in the heat exchanger weight, especially for the cooler. This difference can be explained as follows: The model employed in [2] uses an average value for the fluid properties in the entire heat exchanger. The heat exchangers are not discretised in several cells. In Dymola, the heat exchanger is split up into several parts and the fluid properties are calculated for every one of them. As the fluid properties close to the critical point vary strongly, the weight estimation of the two methods deviates the most. In this case however the Dymola results represent the reality better.

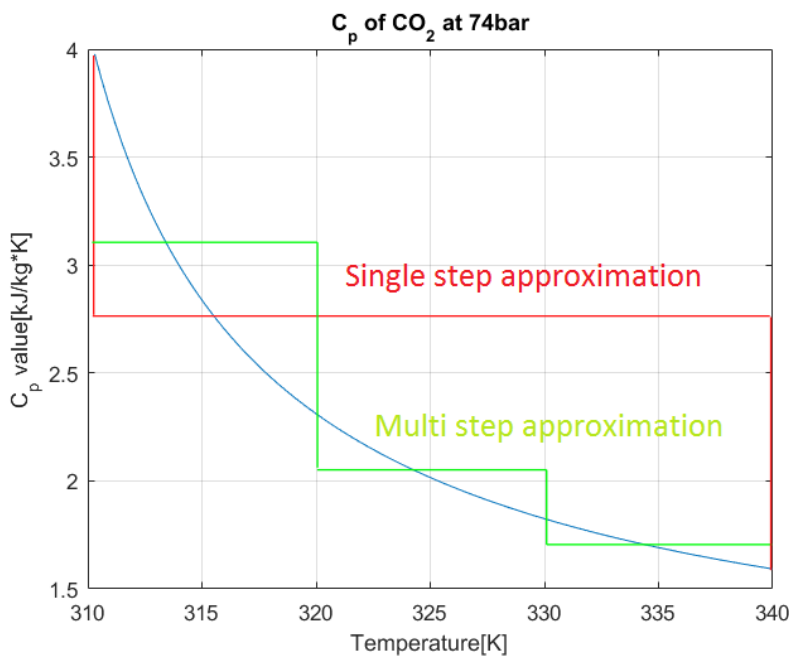


Figure 2.6: Comparison of the fluid properties discretisations

The reason for the better representation of the fluid properties in Dymola is illustrated in figure 2.6. The blue line represents the exact c_p value of CO₂. The red line uses the average of the total heat exchanger. The green line represent the case where the heat exchanger is discretised in three parts. The properties of the fluid are represented by the average inside this part. As shown, the actual fluid properties are much better represented, when multiple zones are used. The results improve further for discretisation into more parts.

2.7.4. REFERENCE CASE 2

In addition to the comparison of the results to the results found in [2], the results were also compared to the results from a similar study [4]. For this comparison, a combined cycle engine for the year 2050 has been

Table 2.3: Comparison of the CCE model using the results of [4]

	Dymola	[4]	Difference in %
Thrust [kN]	49	49	0
SFC [kg/kN*h]	12.04	12.88	-6.53
Flue gas mass flow through heater [kg/s]	30.73	32	-3.969
Flue gas temperature heater inlet [K]	611.85	615	-0.51
Cooling air temperature at cooler inlet [K]	269.8	270	-0.06
CO ₂ cycle power [MW]	0.847	0.8	5.86

modelled using Dymola.

The results are shown in table 2.3. The weight of the heat exchangers is not considered, as the model of Jacob *et. al* do not consider for the high pressures of the working fluid. Therefore unreasonably low weights are calculated. Looking at the results, again, the thermodynamic values are in good agreement with the ones given in the paper. The SFC and the power of the supercritical power cycle deviate more from each other. However, the differences stay below 7 % and can be explained with different fluid models being used and different pressure losses in the heat exchangers due to different models being used. In addition to this, not all parameters of the design from Jacob *et al.* were known due to restrictions of the publication. Therefore, the design might vary in certain aspects.

2.8. LIMITATIONS OF THE METHODOLOGY

The presented method is suitable for the performance evaluation of the combined cycle engine. However, the model can be further improved. The fluid properties are calculated using the Modelica interface to Refprop. At certain conditions, when approaching the critical point, the numerical uncertainties in the thermodynamic properties becomes significant, causing the simulation to fail. This happens most often at conditions close to the critical point of the fluid or at very high temperatures. This can lead to failure of the performance evaluation for certain configurations. Due to the big temperature fluctuations in parts of the heat exchangers and the numerical solving algorithm, it can not be accurately predicted, when this phenomena occurs and there is no solution without adjusting the Refprop program. Measures have been taken to replace especially vulnerable functions like the property evaluation based on the entropy, but the errors still occur. This limits the design space as for example very small heat exchanger tubes can not be modelled. For the initial evaluations and investigations, these problems are acceptable.

In addition to this, the validity bounds of the fluid models had to be extended, to allow the calculation at all occurring points. For this reason, the accuracy of the fluid models might be lower than expected. The points in question are at very high temperatures or at the border between the liquid and the supercritical phase. At very high temperatures, the behaviour is similar to an ideal gas and the properties do not vary strongly any more. The second region in question is very small, less than 1 K. These conditions are only reached occasionally. For these reasons, the extension of the bounds is acceptable. Due to missing reference models it is also unclear whether the accuracy of the fluid models actually decreases outside the initial validity bounds.

The heat exchangers are modelled as a bundle of tubes running around the engine core as shown in figure 2.2. The length is then assumed to be equal to the average values for all tubes. When the difference between minimum and maximum diameter increases, this becomes a bad representation of the reality as the inner tubes will be much shorter than the outer ones. The focus of the thesis is to find the potential of the system rather than the optimization of certain components. As it can be also thought of a rectangular heat exchanger layout, where this assumption does not impose errors, the assumption is judged as sufficient for the further analysis. A quick comparison to a different model with a smaller difference between assumed and actual tube length showed a roughly 15 % lower heat transfer for equal weight and identical operating conditions. At the same time, the pressure losses on both sides of the heat exchanger were much smaller.

The weight estimation takes only the weight of the heat exchangers into account. The weight of the additional tubomachinery, piping or installation effects are not taken into account. These effects will have to be investigated in further research. The weight of the main engine is not simulated. Therefore, the effect on

weight from changing main engine parameters like the bypass ratio, OPR or TIT is not taken into account. This is deemed acceptable, as the effect of the additional cycle is to be investigated. Therefore, comparisons will only be made between equivalent main engines with and without WHR. In this case, the induced error in the main engine weight is the same for both cases.

2.9. CONCLUSIONS

In this chapter, the modelling methodology was introduced and verified. The combined cycle engine will be analysed using a Dymola model representing a simple 0-D gas turbine analysis. The heat exchanger will be simulated using a 1-D model with a central discretisation scheme. The model will be used in design mode only. This means that efficiencies, thrust, pressure ratios and turbine inlet temperatures are fixed and the engine is sized to reach these values.

The validity of the results could be proven by comparison to different models and results from literature. Overall, the performance of the main engine can be calculated with high accuracy. The differences are below 1.4 %. Also the thermodynamic performance of the additional cycle could be shown to deviate from other models by less than 7 %. The results for size and weight of the heat exchangers could not be validated due to the lack of suitable results from literature. The method has some limitations. These limitations were discussed and it was concluded that the method still a good choice for the purposes of this thesis work. Therefore, the model can be used to investigate the performance of the CCE in the next chapter.

3

INITIAL COMBINED CYCLE ENGINE DESIGN

This chapter introduces the configuration that has been used as the starting point of the optimization. The engine parameters will be elaborated on and its performance will be computed and presented. A sensitivity analysis will be presented and discussed. Finally, the performance of important components will be analysed to gain more insight into the behaviour of the combined cycle engine.

3.1. REFERENCE CASE

The reference case is the same as de Servi *et al.* [2] and a similar to Jacob *et al.* [4]. The combined cycle engine uses a recuperated supercritical CO₂ cycle as waste heat recovery unit. The heater is placed between the LPT and the core nozzle and the cooler is incorporated in separate duct inside the bypass duct of the fan. The power of the supercritical CO₂ cycle is converted to thrust with an efficiency of 90 %. Figure 3.1 shows the model that has been used to determine the performance. The upper half of the figure shows the main engine whereas the waste heat recovery cycle is shown in the lower part of the image. Additional control and configuration components are shown in the top left corner. Figure 3.2 shows the configuration of the supercritical cycle more in detail. As can be seen, the supercritical unit is based on the simple regenerative cycle. The engine is designed to deliver a thrust of 72 kN at cruise conditions. Table 3.1 shows the main characteristics of the baseline CCE. The main engine characteristics are based on an expected geared turbofan engine as expected for the year 2035. The design is described in the report by Yin *et al.* [41].

Table 3.1: Main cycle characteristics of the baseline 2035 CCE

Property	Value
Thrust [kN]	72
BPR [-]	15
Fan pressure ratio [-]	1.4
OPR [-]	70
TIT [K]	1900

The heat exchangers were modelled with an imposed minimum temperature difference between hot and cold side. Therefore, the CO₂ temperature after the cooler (T_{min}) depends on the bypass air temperature. The the temperature of the CO₂ at low pressure after the regenerator depends on the CO₂ compressor outlet temperature and the maximum temperature (T_{max}) in the supercritical cycle depends on the temperature of the flue gases leaving the main engine turbine. According to the prescribed temperature differences, the heat exchangers are sized and the pressure losses as well as the weight is calculated. Table 3.2 shows the parameters that are used for the reference model.

3.2. RESULTS

The results of the calculation are summarized in table 3.3. As can be seen, the supercritical waste heat recovery cycle produces 465 kW of extra power. However, its efficiency is relatively low with only 26.04 %. This is a consequence of the high minimum temperature difference in the cooler, 45 K. The minimum temperature

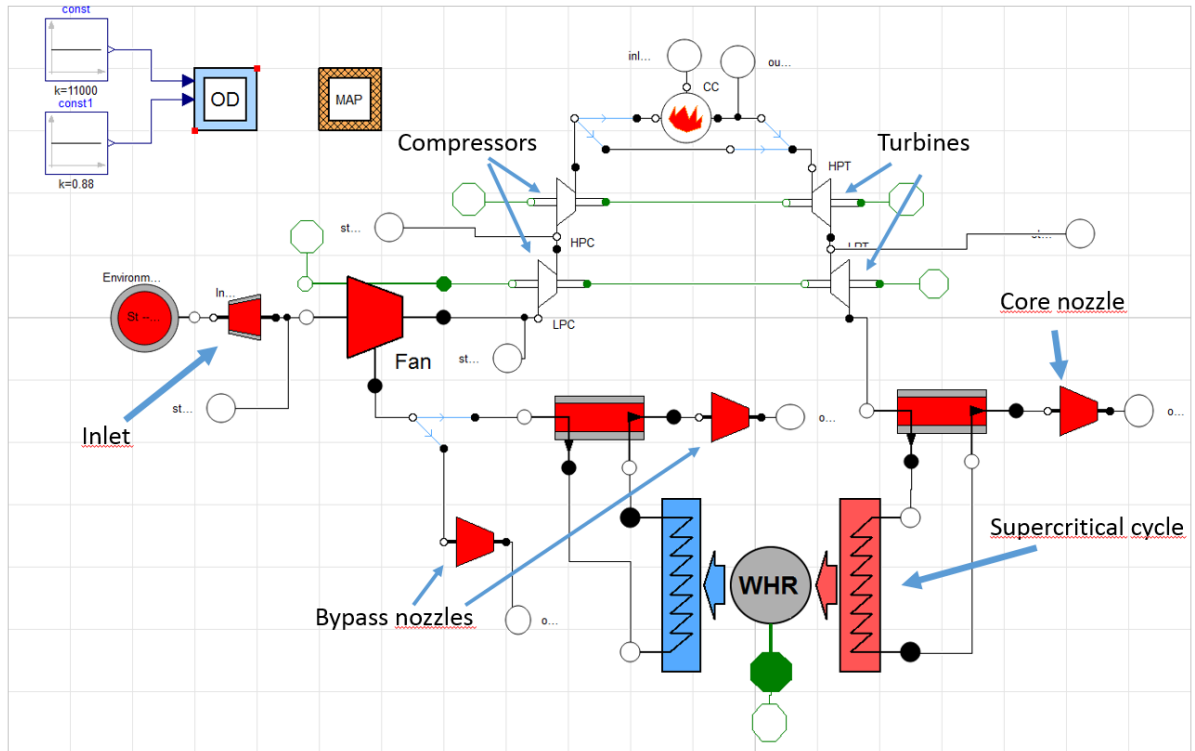


Figure 3.1: Dymola model of the reference case

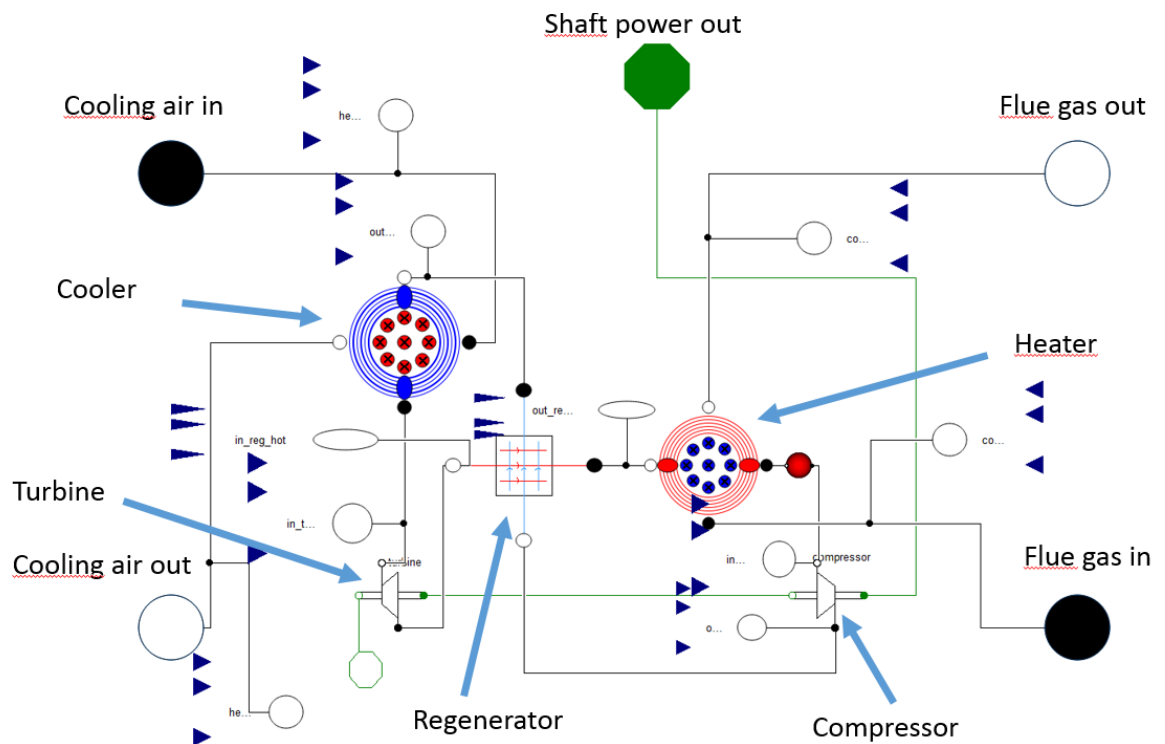


Figure 3.2: Dymola model of the supercritical cycle of the reference case

Table 3.2: Supercritical cycle characteristics of the baseline 2035 CCE

Property	Value
CO ₂ mass flow rate [kg/s]	7
Pinch temperature cooler [K]	45
Pinch temperature heater [K]	20
Pinch temperature regenerator [K]	15
Cooling air mass flow [kg/s]	30
Minimum pressure [bar]	105
Maximum pressure [bar]	400

Table 3.3: Performance of the baseline 2035 CCE

Property	Value
SFC [kg/kN*h]	47.62
CO ₂ cycle power [MW]	0.465
CO ₂ cycle efficiency [%]	26.04
HEX weight [kg]	2768.68
Cooler weight [kg]	635.44
Cooler heat duty [MW]	1.306
Heater weight [kg]	1397.95
Heater heat duty [MW]	1.786
Regenerator weight [kg]	717.29
Regenerator heat duty [MW]	0.924
Minimum CO ₂ temperature [K]	334.93

in the cycle of 335 K is 30 K above the critical temperature of CO₂. This increases the required work of the compressor. The heater is the heaviest heat exchanger and has the highest heat duty. The cooler is lighter than the regenerator even though it has a higher heat duty. This can be explained with the bigger temperature difference, that the cooler operates on. In addition to this, the heater and the regenerator operate at higher pressures. This increases the wall thickness that is necessary to withstand the stresses. At the same time, the wall material yield stress reduces due to the higher temperatures in the regenerator and heater. This also increases the required wall thickness and thus the weight of the heat exchangers.

The Breguet range equation is shown in equation 3.1. In this, equation, $W_{initials}$ is the aircraft weight at the start and equals the maximum take off weight of the aircraft, 351534 kg for the Boeing 777. W_{final} is the landing weight of the aircraft, when all the fuel is burned. This weight is assumed to be equal to the operative empty weight of the aircraft + the additional weight of the heat exchangers. For the Boeing 777 with the current turbofan engines, this weight is 206510 kg [42]. V is the cruise velocity of the aircraft and assumed to be 250 m/s. g is the gravitational acceleration on earth, 9.81 m/s². L is the lift of the aircraft and D is the drag. The ratio $\frac{L}{D}$ is assumed to be 16.

$$R = \frac{V}{g * SFC} * \frac{L}{D} * \ln\left(\frac{W_{initial}}{W_{final}}\right) \quad (3.1)$$

The Breguet range equation was chosen as the performance parameter, as it enables a very quick comparison of the performance and takes the two most important aspects of SFC in cruise flight and the weight into account.

With the given weights, and the fact that the Boeing 777 has two engines, a SFC decrease of 1.82 % is required in order to compensate an additional weight of 1000 kg per engine. This value is specific for the given aircraft on its maximum range mission. When looking at different aircraft from different range categories, this value changes a lot. Table 3.4 shows the effect for different aircraft. The values for the maximum take off weight and the fuel weight were taken from Jane's all the world's aircraft database [42]. These data show a great variation with the expected range of the aircraft. This can be explained by the different maximum take off weight of the aircraft. A regional jet has a lower maximum take off weight than a large long haul aircraft. Therefore, the engines of a long haul aircraft produce more thrust during cruise. For this reason, 1 % change

Table 3.4: Required change in SFC to compensate for 1000 kg of additional engine weight for different aircraft

Aircraft	Boeing 777	Airbus A330 NEO	Airbus A320NEO	Airbus A320	Bombardier CRJ900
Change in SFC to compensate 1000 kg extra engine weight	-1.82 %	-2.47 %	-9.8 %	-9.845 %	-25.07 %

Table 3.5: Required change power density for the supercritical cycle for different aircraft

Aircraft	Boeing 777	Airbus A330 NEO	Airbus A320NEO	Airbus A320	Bombardier CRJ900
Required power density [kW/ton]	309	289	375	371	465

in SFC due to the addition of the supercritical power requires much more power output of the supercritical cycle for the long haul aircraft. Thus it makes sense to look at the absolute required power density. Table 3.5 shows the required power densities for the aircraft in order to make the addition of a supercritical cycle beneficial. To get these values, a thrust at cruise of 0.205 kN per ton of MTOW and a cruise velocity of 236 m/s was assumed. These values represent a typical cruise Mach number of 0.8 and the mean value of the investigated aircraft.

The results indicate that the power density requirement for the supercritical cycle is lower for long haul aircraft and thus the combined cycle engine is best suited for long haul aircraft. This was expected, as for long haul missions, the fuel makes up a bigger portion of the total weight. For the same reason, already today long haul aircraft engines are optimized more for fuel efficiency and weight penalties are accepted for lower specific fuel consumption. In this thesis, only the maximum range mission will be investigated. This assumes that the aircraft starts at its maximum take off weight and lands at its operational empty weight. This represents the mission, where the combined cycle engine will be most beneficial.

3.2.1. COMPARISON TO A TURBOFAN ENGINE

In order to estimate the improvements of the base design, the performance is compared to a turbofan model. This turbofan has the same OPR, TIT and component efficiencies and produces the same thrust of 72 kN at the same operating conditions. Table 3.6 shows and compares the performance of the two engines. The specific fuel consumption of the combined cycle engine is 1.55 % lower than for the turbofan engine. At the same time, the required airflow decreased by 0.46 % compared to the turbofan. Therefore, the specific thrust of the CCE is higher in this case. However, the weight penalty of 2768 kg outweighs the advantage of a lower SFC. This is the reason that the range according to equation 3.1 decreases by 3.65 %.

3.2.2. DESIGN SENSITIVITIES

The main design parameters of the supercritical cycle have a big influence on the performance of the combined cycle engine. Therefore, it is important to understand their influence and identify the most important parameters. For this purpose, the effects of the design parameters on the system performance metrics SFC, weight and range are analysed. The term weight only takes into account the additional weight of the heat exchangers.

Table 3.6: Comparison between baseline 2035 CCE and the corresponding turbofan engine

	Turbofan	CCE	Difference in %
Thrust [kN]	72	72	0
SFC [kg/kN*h]	48.36	47.62	-1.53
Massflow [kg/s]	655.647	652.62	-0.46
Weight [kg]	0	2768.68	∞
Range [km]	20183	19447	-3.65

The minimum cycle pressure determines the possible pressure ratio, as the maximum pressure is limited to 400 bar. It should be matched to the minimum cycle temperature, as the peak in C_p values shift with temperature and pressure as can be seen in figure 3.4. The peaks in this graph are called pseudo critical points. As can be seen, the peaks in fluid properties become less severe and less sensitive to changes in pressure and temperature, when the conditions are further away from the critical conditions. It is beneficial, to start the compression at the peak, as a higher C_p value decreases the required work for the compression process. In that sense, the critical point is the best starting point for the compression process.

The pressure ratio has an important effect on the cycle efficiency. A higher pressure ratio increases the cycle efficiency but decreases the effect of the regenerator. At the same time, the weight of the regenerator and heater will increase, as the stresses in the heat exchanger walls increase and thus require a higher thickness. The effect of thicker walls in the regenerator is more than the effect of a lower heat duty. In total the regenerator weight increases for a higher pressure ratio of the cycle.

The pinch temperature of the heater determines the maximum temperature in the cycle. A lower pinch temperature in the heater increases the maximum cycle temperature and thus the cycle efficiency. At the same time, the weight of the heater increases and so do the pressure losses in the heat exchanger.

The pinch temperature in the cooler determines the minimum temperature in the cycle. A lower pinch temperature in the cooler causes a lower minimum cycle temperature and increases the size of the cooler. For the highest cycle efficiency, the pinch temperature should be matched, to achieve a minimum cycle temperature close to the critical temperature of the working fluid.

The pinch temperature of the regenerator determines the heat duty and thus size of the regenerator. A lower pinch temperature increases the heat duty of the regenerator and increases the efficiency of the cycle. At the same time, the size of the heater and cooler decrease.

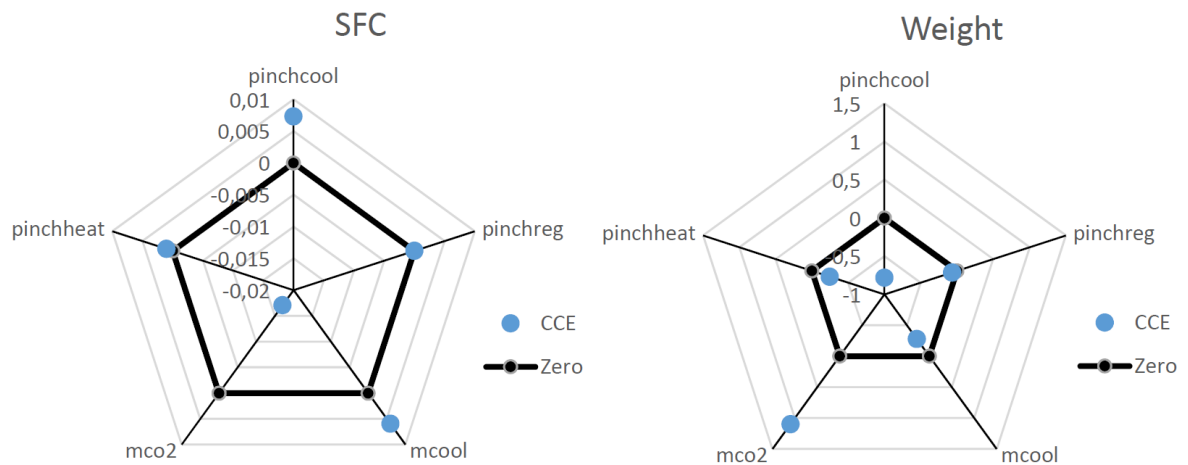
The amount of cooling air has an effect on the pressure losses and the size of the cooler. Also the maximum heat duty of the cooler is affected. A higher cooling air mass flow decreases the cooler size and allows for a lower CO₂ outlet temperature. This is because for a higher cooling air mass flow, the cooling air temperature increases less for a given energy input. As a consequence the temperature difference in the cooler increases. At the same time, the velocity of the cooling air increases. This further increases the heat transfer but also the pressure losses.

The amount of supercritical working fluid has an influence on the power output as well as the weight of the heat exchangers. A higher mass flow increases the weight of all heat exchangers, as more energy has to be transferred. At the same time, the internal pressure losses increase, as the flow velocity increases. An increased working fluid mass flow also increases the power output of the cycle.

The described effects are quantified in figure 3.3. The effect of the pressure ratio and minimum cycle pressure are excluded from these figures, as the initial design point is far away from the critical pressure and thus the calculated results are not representable for most designs. The calculated sensitivities are defined in equation 3.2. In this equation P is a generic performance index, for example the range and DV is a generic design variable, for example the mass flow rate of the working fluid.

$$S = \frac{\frac{\Delta P}{P}}{\frac{\Delta DV}{DV}} \quad (3.2)$$

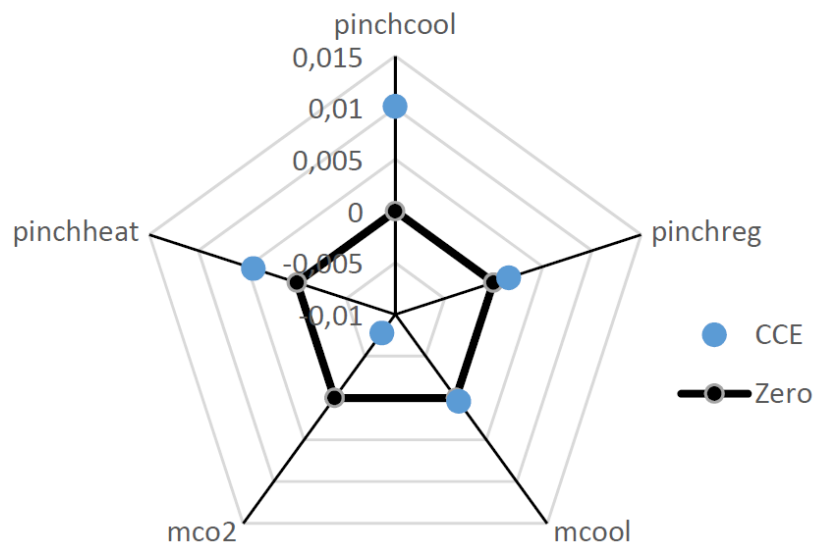
As can be seen, the effects on the weight are much bigger than on the SFC or the range of the aircraft. This follows from the fact that the additional supercritical cycle produces only a small amount of the total power and makes up only a small part of the total weight of the aircraft. Therefore, its effect on the SFC or range are very small. The weight metric however is only related to the weight of the heat exchangers of the supercritical cycle itself. Therefore, the design parameters have a much bigger influence on it. All design parameters have an opposite sign for the sensitivity on weight and SFC this means that a lower weight corresponds to a higher SFC and vice versa. Therefore, the optimal design has to be a trade off between these two properties and between the different design parameters. The mass flow rate as well as the pinch temperature of the cooler are



(a) Effect of the parameters on the SFC

(b) Effect of the parameters on the weight

Range



(c) Effect of the parameters on the range

Figure 3.3: Sensitivities of the cycle parameters

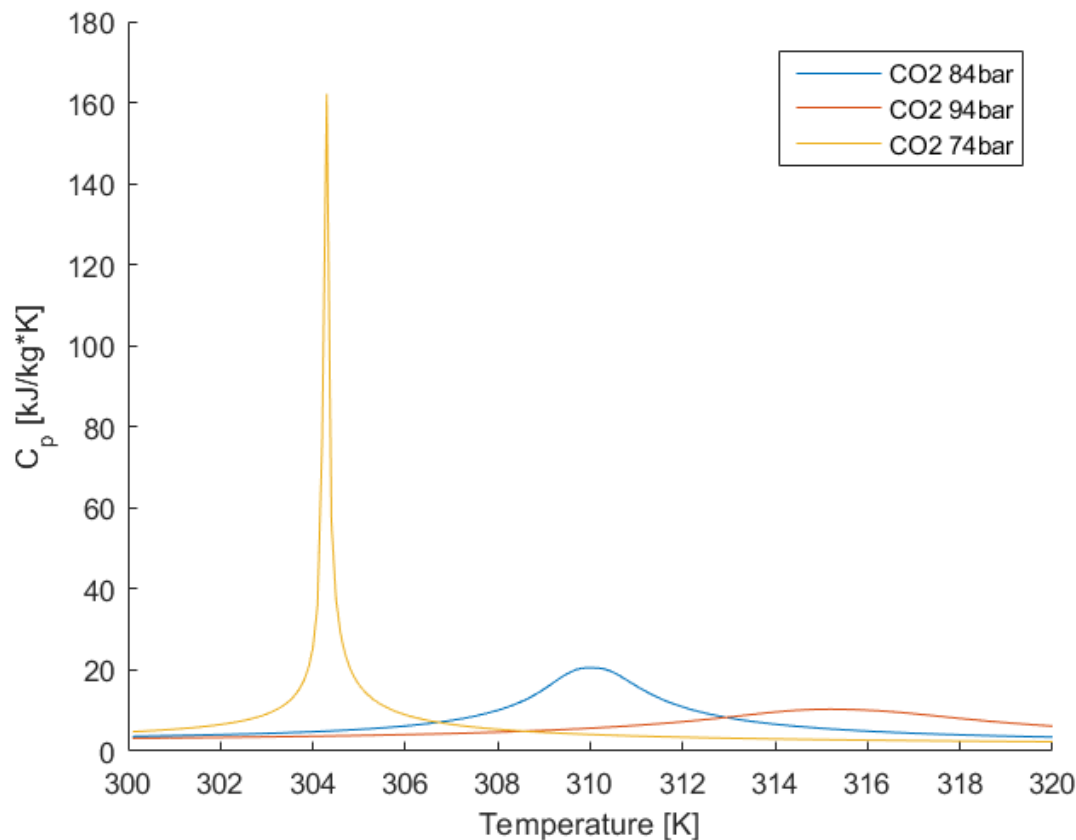


Figure 3.4: C_p value of CO_2 for different temperatures and pressures

the most sensitive design parameters. The amount of cooling air is also important for the weight and the SFC. These two effects, however, cancel out each other. For this reason, the amount of cooling air has almost no effect on the range of the aircraft. At the initial point the effect of the pinch temperature in the regenerator is almost negligible. The pinch temperature in the heater has a moderate effect on the range. All values except for the CO_2 mass flow rate should increase, in order to increase the range performance of the system.

All these sensitivities strongly depend on the design point that they are calculated at. For this reason, no direct quantitative conclusions about the optimal design can be drawn. An extensive optimization routine is necessary, to find the best design option.

3.2.3. HEAT EXCHANGER BEHAVIOUR

The heat exchangers are the most important components of the supercritical cycle. For this reason, it is important to understand the processes inside them. Figure 3.5 shows the temperature profiles inside the heater and the cooler. The hot medium is coloured red and the cold medium blue. For clarity reasons, only the mean value of the CO_2 temperature is plotted. When the full profile is plotted, the CO_2 temperatures represent a fan similar to the one visible for the air/flue gas temperature. These fans are caused by the cross flow configuration of the heat exchangers. I.e. in figure 3.5 (a), the red line with the strongest decrease represents the flue gas that flows along the tubes, where the cold CO_2 just entered the tubes. Accordingly, a lot of energy is transferred in this area and the flue gas temperature drops. The red line with the smallest decrease in temperature represents the flue gas that flow around the tubes, where the heated CO_2 leaves the tubes. The CO_2 at this location has already a high temperature and thus the heat transfer is low.

As can be seen, at the beginning of the heat exchangers, a large temperature difference exists. As expected for a cross flow configuration, the temperature difference decreases towards the end and the lowest temperature difference, the pinch point is at the exit of the heat exchanger. The temperature change of the air and flue gas

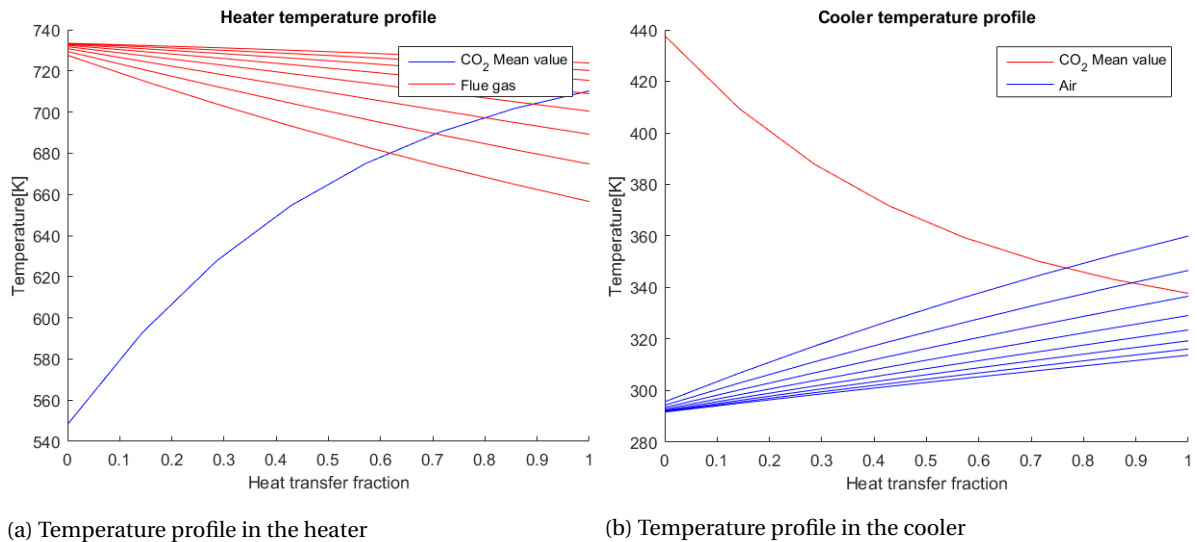


Figure 3.5: Temperature profile in the heat exchangers

are very linear, while the change of the CO₂ temperature is not. This shows that the C_p value of CO₂ changes inside the heat exchanger and for the gases it stays almost constant. The stronger curvature of the plot of the CO₂ temperature in the cooler shows that the fluid properties vary more, when the CO₂ is close to its critical temperature.

To get a better understanding of the processes and the behaviour of the heat exchangers, the temperature distribution in the high pressure side of a regenerator is shown in figure 3.6. To show the differences more clearly, this regenerator is discretised in 14*14 elements. The cold, high pressure working fluid flow from the bottom to the top, the hot, low pressure working fluid flows from left to right. The big temperature difference at the outlet of the regenerator is clearly visible. This makes mixing of the outflowing fluid necessary and shows the need for a 2-D heat exchanger model.

3.3. CONCLUSIONS

In this chapter the initial design of the combined cycle engine has been analysed using the simulation framework. The results were compared to the corresponding turbofan engine. The specific fuel consumption could be reduced by 1.53 %. However due to the additional weight of 2768 kg, the range decreased by 3.65 %. The system performance is a trade off between the system weight and the improvements in thrust specific fuel consumption. The Breguet range equation was found to be a good metric to measure the system performance. Based on this metric it was found that the application to a big long haul aircraft is the most logical application aircraft for the combined cycle engine, as it demands the lowest power density in terms of kW/kg. For the chosen aircraft, the Boeing 777 a decrease in SFC of 1.82 % per 1000 kg of additional weight per engine is required to make the system beneficial. This translate to a required power density of 309 kW/ton. The most important parameters for the performance of the supercritical cycle have been identified and analysed at the initial design point. The most important parameters at this point are the pinch temperatures in the cooler and heater and the mass flow rate of the supercritical working fluid. However, these design drivers can change at different design points and therefore, a sophisticated optimization routine is necessary to find the best design. The influence of the real gas effects can be clearly recognised in the heat exchanger performance.

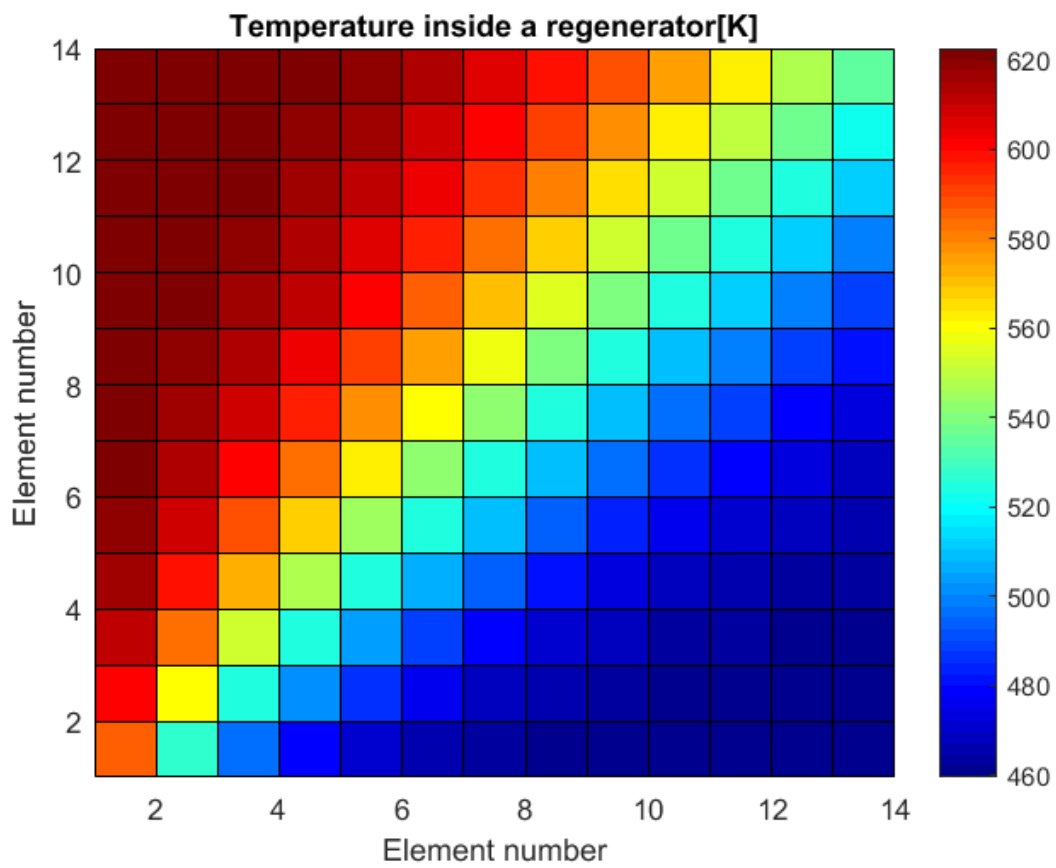


Figure 3.6: Temperature distribution in the high pressure side of a regenerator

4

ANALYSIS OF THE COMBINED CYCLE ENGINE

Based on the findings from the investigation of the initial design, strategies to improve the performance of the combined cycle engine will be developed in this chapter. For this reason, the effect of different parameters will be analysed and presented. The findings will be used to propose new configurations to find the optimal combined cycle engine in later chapters.

4.1. OPTIMIZATION

The sensitivity analysis of the initial combined cycle engine design showed the influence of the supercritical cycle parameters on the system performance. It is possible to find parameters, that yield a better system performance. The influence of the parameters strongly depends on the given situation. To find the optimal set of parameters, an optimization routine is required. The chosen optimization process and the results are shown in this section.

4.1.1. OPTIMIZATION SET-UP

The optimization was set-up in MATLAB, using the well known `fmincon` function with the `sqp` algorithm. This approach was chosen, as the author is familiar with this approach and it is a common approach for such problems. The gradient based optimization method delivers reliable results with relative few function evaluations. The `sqp` algorithm can handle calculation errors in the objective function. This allows a wide design space to be evaluated as areas with potential calculation problems do not have to be excluded. As the objective function, the range based on the Breguet range equation has been selected to account for the effect of SFC reduction and weight penalty simultaneously. The objective function J is defined in equation 4.1. In this equation $R_{Turbofan}$ is the range of the turbofan engine and R_{Design} the range of the considered design.

$$J = \frac{R_{Turbofan}}{R_{Design}} \quad (4.1)$$

As the design variables, the pinch temperatures of the three heat exchanger, the amount of cooling air, the mass flow of CO_2 as well as the minimum pressure and pressure ratio of the CO_2 cycle have been selected. These values have been selected as they have a direct influence on the performance of the supercritical cycle and are not limited by technological burdens. All design variables were bound by upper and lower limits to exclude non-feasible designs and thus speed up the process. In particular, a phase change of the working fluid and unreasonable large or small heat exchangers were prevented by the bounds on the minimum temperature and the minimum pressure. These properties were limited by the critical point of the working fluid.

Two design constraint have been added to the optimization problem.

- The maximum pressure in the supercritical cycle can not exceed 400 bar. This represents the limit to which CO_2 has been handled so far at the expected temperatures [43].

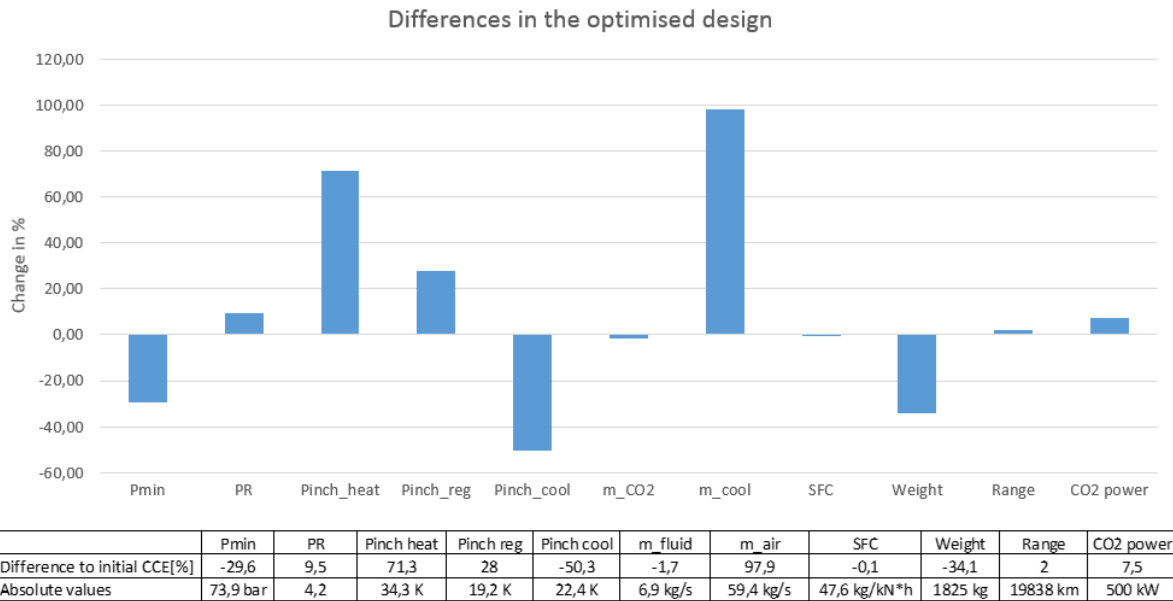


Figure 4.1: Changes between initial and optimized CCE design

Table 4.1: Overview of different engine performances

	SFC [kg/kN*h]	Weight [kg]	Range [km]
GE90-77B	54.55	0	17893
Baseline turbofan 2035	48.36	0	20183
Baseline CCE 2035	47.62	2768.68	19447
Optimized CCE 2035	47.58	1824.9	19838

- The supercritical cycle has to deliver a net power of 500 kW.

The second constraint is necessary, as the baseline CCE is not beneficial when compared to a turbofan. As a result, an optimizer would try to get rid of the additional cycle instead of optimizing it. Furthermore, lower power outputs are not feasible for the supercritical cycle, as the turbomachinery is becoming too small. 500 kW has been used as the value as it represents 1.8 kN of thrust, a similar value as has been used in earlier studies.

4.1.2. RESULTS

The optimization could improve the range of an aircraft by 2.01 % compared to the initial CCE design. The optimization could decrease the SFC of the engine as well as the weight penalty of the heat exchangers. However, the improvements are not enough to yield an absolute positive effect on the system. This means that the turbofan without supercritical cycle still outperforms the combined cycle engine. The advantage of the conventional turbofan decreases to 0.98 %.

The design was changed to lower pressures and in general towards a lower temperature difference in the cooler. This is to get the minimum temperature in the cycle towards the critical temperature of the carbon dioxide. This greatly increases the efficiency of the waste heat recovery unit but also increases the weight of the cooler at the same time. The design changes are summarized in figure 4.1. The amount of cooling air increased by 77 % as the additional effect of the pressure losses was compensated for by the lower cooler weight that resulted from this. The pinch temperatures of heater and regenerator increased considerably, to decrease the weight without sacrificing too much the efficiency of the cycle. The performance that has been achieved with this design is compared to other engine designs in table 4.1. As can be seen, the range of an aircraft equipped with the optimized CCE 2035 is still lower than the range of the corresponding turbofan engine. This means the addition of the supercritical waste heat recovery unit is not beneficial but increases the fuel burn instead.

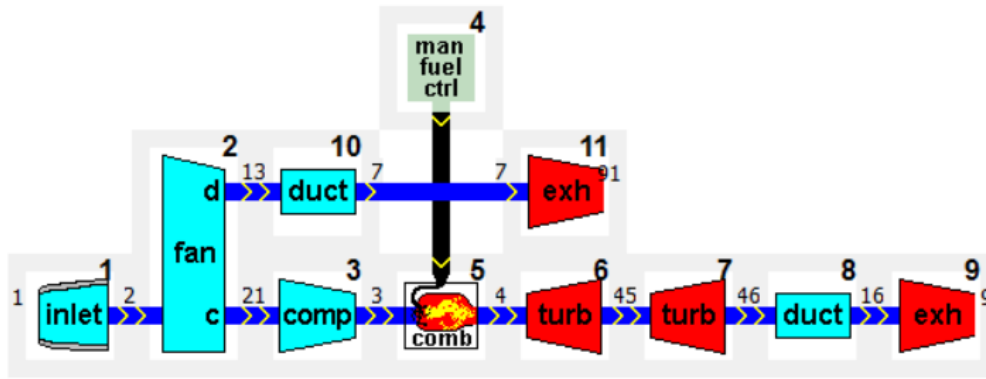


Figure 4.2: GSP model to represent the combined cycle engine

Table 4.2: Top level sensitivities

	Change in SFC [%]	Change in Range [%]
1000 kg of weight	0	-1.812
1 MW heat addition in the cooler	-0.78	0.787
1 % pressure loss in the cooler	1.746	-1.716
1 % pressure loss in the cooler 10% bypass fraction	0.185	-0.185
1 % pressure loss in the heater	0.164	-0.164
1 MW heat removal in the heater	0.511	-0.511
1 MW additional power	-4.9	5.15

4.2. TOP LEVEL ANALYSIS

From the results of the previous optimization of the supercritical cycle, it can be concluded that the optimization gives considerable improvements in the performance of the system. These improvements alone are not sufficient to deliver a system that is superior to an equivalent turbofan. For this reason, the effects of the different components will be analysed in a more isolated way. This highlights improvement possibilities of the system.

For the purposes of the top level analysis, a GSP turbofan model representative of the optimized year 2035 CCE was used. The model was equipped with two ducts that represent the effects of the heat exchangers. These ducts are placed between fan and bypass nozzle and between LPT and the core nozzle. In these ducts, variable pressure losses and heat duties can be applied. The mission component was again investigated using the Breguet range equation for a maximum range mission of the Boeing 777-300ER. Figure 4.2 shows the configuration in GSP. The effect of pressure losses, heat duties, additional thrust and weight on the specific fuel consumption and range of the aircraft were investigated. The results are summarized in table 4.2. The results show that the aircraft range is most sensitive to the weight and the additional power of the cycle. The effect of the pressure loss acts through an increase in SFC of the engine. The positive effect of 1 MW of energy added to the bypass stream outweighs the negative effect of 1 MW being removed from the exhaust gas. This means that a pure heat transfer between exhaust and bypass stream would have a beneficial effect, if the weight is neglected.

In a second stage, these top level sensitivities were grouped to represent the actually occurring phenomena in the different heat exchangers. In this way, the positive and negative effects of the heat exchangers could be isolated and quantified. The results are shown in table 4.3.

As can be seen, the weight is an important factor for the range of the aircraft. The additional weight of the supercritical cycle is the most important reason for the poor performance of the supercritical cycle. Another important effect that decreases the performance is the heat removal from the exhaust gas before the

Table 4.3: Applied top level sensitivities

	Change in SFC [%]	Change in weight [kg]	Change in Range [%]
Pressure loss cooler (1.84 %)	0.31	0	-0.31
Heat addition cooler (1.46 MW)	-1.31	0	1.33
Weight cooler	0	701.53	-1.27
Cooler total	-0.82	701.53	-0.45
Pressure loss heater (1.91 %)	0.31	0	-0.31
Heat removal heater (1.98 MW)	1.03	0	-1.02
Weight heater	0	991.54	-1.8
Heater total	1.34	991.54	-3.09
CO ₂ power	-2.53	0	2.59
CO ₂ cycle total	-2.08	1824.9	-1.24
CO ₂ cycle no weight	-2.08	0	2.12
CO ₂ cycle no extra power	0.47	1824.9	-3.75

Table 4.4: Breakdown of the three heat exchangers

	Weight [kg]	Surface area [m ²]	Volume [m ³]
Cooler	701.53	148.54	10.22
Heater	991.54	518.1	3.19
Regenerator	131.83	73.07	0.0849

expansion in a nozzle. The pressure losses in the heat exchangers have a negative effect as well, but they are of less importance. Positive effects are additional power of the supercritical cycle but also the heat addition in the bypass stream. This heat addition accounts for a third of the total SFC reduction. It is interesting to see that the positive effect of the heat addition in the cooler outweighs the negative effect of the heat removal in the heater even though less heat is transferred in the cooler. To increase the performance of the system, the weight of the heat exchangers has to be decreased. At the same time, it would be beneficial to decrease the negative effect of the heat removal. Please note, as there exists a slight difference between GSP and Dymola, the values for the effect on range and SFC of the total cycle do not exactly match the results from table 4.1. The differences are below 1 %.

4.2.1. WEIGHT BREAKDOWN

Table 4.4 shows the weight and volume of the three heat exchangers for the optimized CCE that was presented before. As can be seen, the heater is the heaviest component even though the cooler is much bigger. This is caused by the higher thickness of the heater that is necessary due to the higher operating pressure and temperature. Without this thickness constraint, the weight of the heater would decrease by 789 kg to 202 kg, when a wall thickness of 0.3 mm is assumed. The regenerator is the smallest component and very compact. The weight of the cooler and the regenerator are limited by the technological limit imposed on the minimum wall thickness of 0.2 mm for the cooler and 0.4 mm for the regenerator. If this constraint can be lowered, the weight of the cooler and regenerator would further decrease. The differences in the minimum wall thickness are caused by the different heat exchanger types and the difference in the operating temperature.

4.2.2. THERMODYNAMIC ANALYSIS

In this section, the heat extraction will be analysed in more detail. As has been identified previously, the heat removal in the heater is the biggest loss term associated with the application of the supercritical CO₂ cycle. Therefore, it is necessary to minimize the negative effect of the heat extraction on the main cycle while maintaining a high power output of the supercritical cycle. In order to assess the impact of the heat extraction on the whole system, three aspects have to be taken into account. These are:

- The implication for the thermodynamics of the main engine
- The implications for the thermodynamics of the supercritical cycle

- The effect on the weight of the heat exchangers and the entire system.

IMPLICATIONS FOR THE MAIN ENGINE

The heat removal after the low pressure turbine has negative consequences for the main engine, as it causes a decrease in the core thrust. To investigate the behaviour of this expansion process, an isentropic, choked convergent nozzle with ideal gas is investigated. For a choked convergent nozzle, the flow is sonic at the exit. This enables the calculation of the static conditions at the outlet based on the total conditions at the inlet by the use of the isentropic flow relations. Equation 4.2 shows the relation for the static outlet temperature, equation 4.3 for the static outlet pressure. Station 7 is at the inlet of the nozzle and station 8 at the outlet. Station 0 refers to the ambient conditions and subscript t refers to total properties. In the following derivation, F is the thrust of the nozzle, T the temperature, P the pressure, η the isentropic efficiency, κ the specific heat ratio, ρ the density, R the individual gas constant, A the cross sectional area of the nozzle, m the massflow rate and V the velocity.

$$T_8 = T_{t7} \frac{2}{\kappa_{gas}} \quad (4.2)$$

$$P_8 = \frac{P_{t7}}{\frac{1}{1 - \frac{1}{\eta_{nozzle}} * \frac{\kappa_{gas}-1}{\kappa_{gas}+1}} * \frac{\kappa_{gas}}{\kappa_{gas}-1}} \quad (4.3)$$

The outlet velocity of the gas is equal to the local speed of sound and can be calculated using equation 4.4.

$$V_8 = \sqrt{\kappa_{gas} * R * T_8} \quad (4.4)$$

Similar the static density 4.5 and the required cross sectional area of the nozzle 4.6 can be calculated.

$$\rho_8 = \frac{P_8}{R * T_8} \quad (4.5)$$

$$A_8 = \frac{m_8}{\rho_8 * V_8} \quad (4.6)$$

The thrust force that the nozzle generates is composed of the pressure difference and the velocity difference of the exhaust gas. This is shown in equation 4.7.

$$F = m_8 * (V_8 - V_0) + A_8 * (P_8 - P_0) \quad (4.7)$$

Substitution 4.2 into 4.4, the exit velocity becomes a function of the total temperature at the inlet.

$$V_8 = \sqrt{\kappa_{gas} * R * T_{t7} \frac{2}{\kappa_{gas}}} \quad (4.8)$$

Similarly substituting 4.2 and 4.3 into 4.5 gives an expression for the static density.

$$\rho_8 = \frac{\frac{P_{t7}}{\frac{1}{1 - \frac{1}{\eta_{nozzle}} * \frac{\kappa_{gas}-1}{\kappa_{gas}+1}} * \frac{\kappa_{gas}}{\kappa_{gas}-1}}}{R * T_{t7} \frac{2}{\kappa_{gas}}} \quad (4.9)$$

$$A_8 = \frac{m_8}{\frac{P_{t7}}{\frac{1}{1 - \frac{1}{\eta_{nozzle}} * \frac{\kappa_{gas}-1}{\kappa_{gas}+1}} * \frac{\kappa_{gas}}{\kappa_{gas}-1}} * \sqrt{\kappa_{gas} * R * T_{t7} \frac{2}{\kappa_{gas}}}} \quad (4.10)$$

Finally substituting the previous results 4.10, 4.8 and 4.3 into the equation for the thrust 4.7 gives the desired equation for the thrust produced by the nozzle.

$$F = m_8 * \left(\sqrt{\kappa_{gas} * R * T_{t7} \frac{2}{\kappa_{gas}}} - V_0 \right) + \frac{m_8}{\frac{P_{t7}}{\frac{1}{1 - \frac{1}{\eta_{nozzle} * \kappa_{gas} + 1}} * \frac{\kappa_{gas} - 1}{\kappa_{gas} + 1}} * \sqrt{\kappa_{gas} * R * T_{t7} \frac{2}{\kappa_{gas}}}} * \left(\frac{P_{t7}}{\frac{1}{1 - \frac{1}{\eta_{nozzle} * \kappa_{gas} + 1}} * \frac{\kappa_{gas} - 1}{\kappa_{gas} + 1}} - P_0 \right) \quad (4.11)$$

Rearranging, expanding the brackets and combining term gives

$$F = \left(m_8 * \sqrt{\kappa_{gas} * R * \frac{2}{\kappa_{gas}}} + \frac{m_8 * R * \frac{2}{\kappa_{gas}}}{\frac{1}{1 - \frac{1}{\eta_{nozzle} * \kappa_{gas} + 1}} * \frac{\kappa_{gas} - 1}{\kappa_{gas} + 1}} * \frac{1}{\sqrt{\kappa_{gas} * R * \frac{2}{\kappa_{gas}}}} * \frac{1}{1 - \frac{1}{\eta_{nozzle} * \kappa_{gas} + 1}} * \frac{\kappa_{gas} - 1}{\kappa_{gas} + 1}} \right) * \sqrt{T_{t7}} \quad (4.12)$$

$$- m_8 * V_0 - \frac{m_8 * R * \frac{2}{\kappa_{gas}}}{\frac{1}{1 - \frac{1}{\eta_{nozzle} * \kappa_{gas} + 1}} * \frac{\kappa_{gas} - 1}{\kappa_{gas} + 1}} * P_0 * \frac{\sqrt{T_{t7}}}{P_{t7}}.$$

In the present analysis, m_8 , R , κ_{gas} , η_{nozzle} , V_0 and P_0 stay constant. Rearranging and substituting the constant factors 4.13, 4.14 and 4.15, the thrust force of the nozzle becomes a straight forward function of the total pressure and total temperature at the nozzle inlet 4.16.

$$k_1 = m_8 * \sqrt{\kappa_{gas} * R * \frac{2}{\kappa_{gas}}} + \frac{m_8 * R * \frac{2}{\kappa_{gas}}}{\frac{1}{1 - \frac{1}{\eta_{nozzle} * \kappa_{gas} + 1}} * \frac{\kappa_{gas} - 1}{\kappa_{gas} + 1}} * \frac{1}{\sqrt{\kappa_{gas} * R * \frac{2}{\kappa_{gas}}}} * \frac{1}{1 - \frac{1}{\eta_{nozzle} * \kappa_{gas} + 1}} * \frac{\kappa_{gas} - 1}{\kappa_{gas} + 1}} \quad (4.13)$$

$$k_2 = \frac{m_8 * R * \frac{2}{\kappa_{gas}}}{\frac{1}{1 - \frac{1}{\eta_{nozzle} * \kappa_{gas} + 1}} * \frac{\kappa_{gas} - 1}{\kappa_{gas} + 1}} * \sqrt{\kappa_{gas} * R * \frac{2}{\kappa_{gas}}} * P_0 \quad (4.14)$$

$$k_3 = m_8 * V_0 \quad (4.15)$$

$$F = k_1 * \sqrt{T_{t7}} - k_2 * \frac{\sqrt{T_{t7}}}{P_{t7}} - k_3 \quad (4.16)$$

It is beneficial to have the minimum loss in thrust per unit of heat removed before the nozzle. As we are considering the flue gases to be an ideal gas, the temperature change of the gas is proportional to the heat removal. The derivative of the thrust with respect to the inlet temperature gives us the desired relation. This is shown in equation 4.17.

$$\frac{dF}{dT_{t7}} = 0.5 * k_1 * \frac{1}{\sqrt{T_{t7}}} - 0.5 * k_2 * \frac{1}{P_{t7} * \sqrt{T_{t7}}} \quad (4.17)$$

When considering that the two constant coefficients are always positive, equation 4.17 states that the thrust loss due to the heat extraction decreases for the higher pressures. The influence of the temperature is less obvious as the first term suggests a high temperature to be better for the heat extraction whereas the second term suggests a low temperature to be beneficial. However, when considering the typical values of k_1 and k_2 , it becomes clear that k_1 is dominating and accordingly, the thrust loss of the nozzle due to a given heat removal at a given inlet and outlet pressure is smaller, the higher the total inlet temperature is.

IMPLICATIONS FOR THE ADDITIONAL CYCLE

The maximum temperature of the working fluid in the additional cycle is dependent on the flue gas temperature at the location where the heat is extracted from the main cycle and has a big influence on the efficiency of the additional cycle. The dependency of the cycle efficiency on the maximum cycle temperature for a recuperated sCO₂ cycle is shown in figure 4.3. As can be seen, the efficiency of the additional cycle increases, when the maximum temperature increases. Therefore, heat extraction from the main engine at high temperature is beneficial.

IMPLICATIONS FOR THE WEIGHT PENALTY

The heat transfer in the heat exchangers happens via a combination of conduction and convection. Both physical phenomena are proportional to the temperature difference between the media as can be seen in equation 4.18 and equation 4.19. In these equations h is the convective heat transfer coefficient and k the conductive heat transfer coefficient. A is the area, t the thickness of the material and ΔT the temperature difference. Therefore, the system weight for a given heat transfer decreases with higher temperatures. The power density of the additional cycle thus increases for higher temperature and a heat extraction at high temperatures is thus beneficial from this point of view.

$$Q_{convection} = h * A * \Delta T \quad (4.18)$$

$$Q_{conduction} = k * A * \frac{\Delta T}{t} \quad (4.19)$$

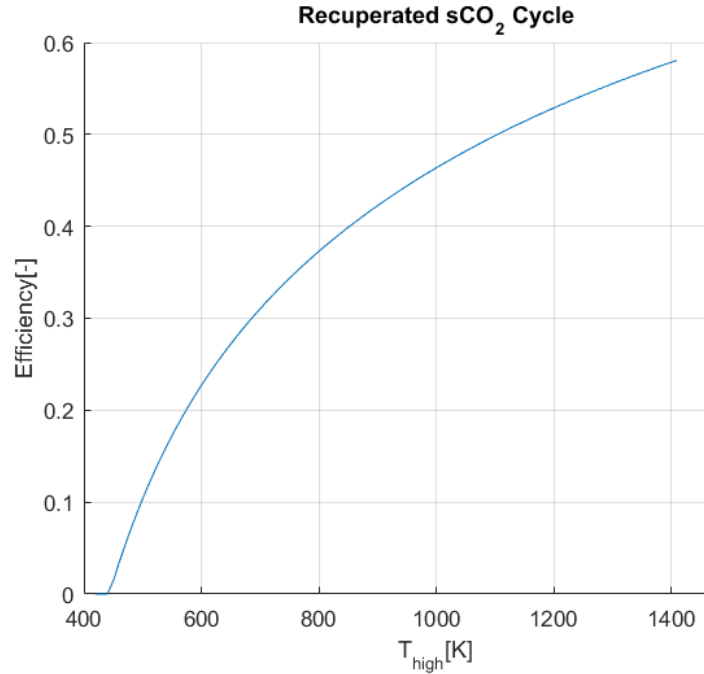


Figure 4.3: Efficiency variation of a recuperated sCO₂ cycle with maximum temperature

4.2.3. PRESSURE LOSSES

The pressure losses in the heat exchangers have an influence on the performance of the main cycle. As for the heat removal, the pressure losses only have an influence on the expansion in the nozzle. Building the derivative with respect to the total inlet pressure yields the desired relation 4.20.

$$\frac{dF}{dP_{t7}} = \left(\frac{m_8 * R * \frac{2}{\kappa_{gas}}}{\frac{1}{\frac{\kappa_{gas}}{\kappa_{gas}-1}} * \sqrt{\kappa_{gas} * R * \frac{2}{\kappa_{gas}}}}} \right) * \frac{\sqrt{T_{t7}} * P_0}{P_{t7}^2} \quad (4.20)$$

It becomes clear that for lower pressures, the pressure losses become more important as the total inlet pressure is in the denominator of the equation. At the same time, their importance increases for higher temperatures. The behaviour of the nozzle can be seen in figure 4.4. In order to have the lowest possible effect of the pressure losses associated with the use of heat exchangers, the heat exchanger should be placed at a high pressure ratio and low temperature. These findings are confirmed by a check in GSP. For this check, the effect of additional pressure losses and heat removal before the nozzle was investigated for turbofan engines with different turbine outlet temperatures and pressures.

4.2.4. SYSTEM LEVEL

When combining the three previously investigated factors for the heat removal, it becomes clear that the optimal application of a supercritical waste heat recovery cycle is with the heat extraction taking place at the lowest possible pressure to ensure little influence on the main cycle and the highest possible temperature

to enable a high power density and efficiency of the supercritical cycle. For the lowest effect of the pressure losses, a high pressure and a low temperature are beneficial. However, the effect of the heat removal is bigger and more sensitive to the operating conditions than the effect of the pressure losses.

Figure 4.5 shows the h-s diagram of the ideal cycle for the application of a supercritical waste heat recovery cycle. The cycle contains an isothermal expansion of the flue gases to the ambient pressure. In this way both criteria are fulfilled. The heat extraction happens at the lowest pressure and the highest temperature of the cycle. However, this cycle is very difficult to achieve due to the required heat addition during the expansion. A more realistic alternative is the use of an inter turbine burner. An exemplary h-s diagram of a Brayton cycle with inter turbine burning, also called reheating, is shown in figure 4.6. When used in an turboshaft configuration, the heat extraction can take place at almost atmospheric conditions and at still high temperatures. Furthermore, the inter turbine burner increases the specific thrust of the core engine, compensating for the additional weight of the waste heat recovery unit. Inter turbine burners have not been introduced in civil aircraft engines yet, as they tend to increase the specific fuel consumption of the engine. However a recent investigation by Yin *et al.* [41] showed a potential decrease in SFC, as the application of an inter turbine burner eases the design constraints of a hot day take off. At the same time, the lower temperature at the outlet of the combustion chamber reduces the NO_x emissions and increases the lifetime of the engine. This makes a turboshaft engine using an inter turbine burner the best candidate for the successful application of an supercritical waste heat cycle.

This has already been proven by the gas turbine manufacturer ABB. They developed a gas turbine for power applications with a reheat stage and applied a regenerator to it. This increases the power density without sacrificing the specific fuel consumption. At the same time, the lifetime increased [44].

4.2.5. DERIVATION NON CHOKED NOZZLE

Previously, the effects of pressure losses and heat removal on a choked nozzle have been investigated. When the pressure ratio over the nozzle decreases, the nozzle can become unchoked. This can happen for the bypass nozzle, when a fan with a low pressure ratio is used. The behaviour of the nozzle changes, as the flow becomes subsonic in the throat. Therefore, it is important to know the effect of pressure losses and heat removal in the case of an unchoked nozzle. This knowledge will be gained in the following analysis. In an unchoked nozzle, the fluid is expanded to atmospheric pressure.

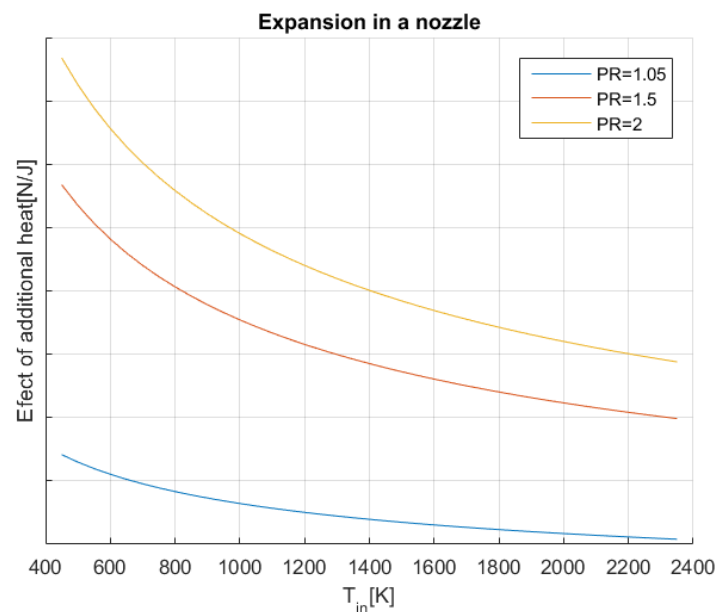


Figure 4.4: Effect of added heat in front of a converging nozzle

$$P_8 = P_0 \quad (4.21)$$

With this knowledge, the outlet temperature can be calculated using the isentropic flow relations 4.22.

$$T_8 = T_{t7} \frac{P_8}{P_{t7}}^{\frac{\kappa_{gas}-1}{\kappa_{gas}}} \quad (4.22)$$

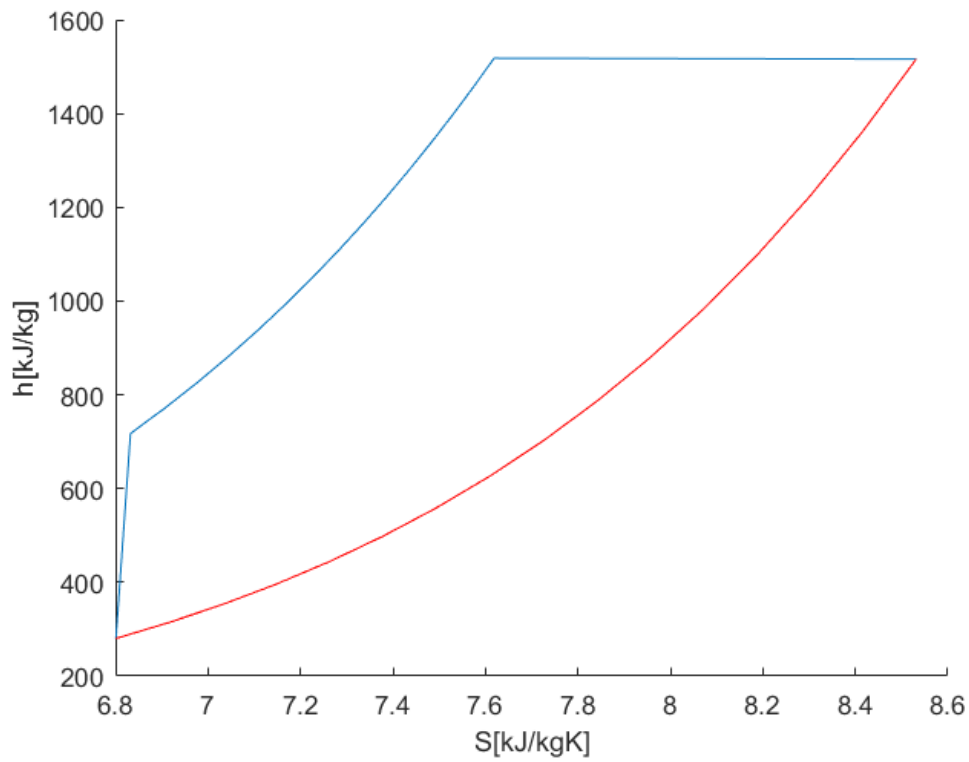


Figure 4.5: h-s diagram of the optimum cycle for the application of waste heat recovery

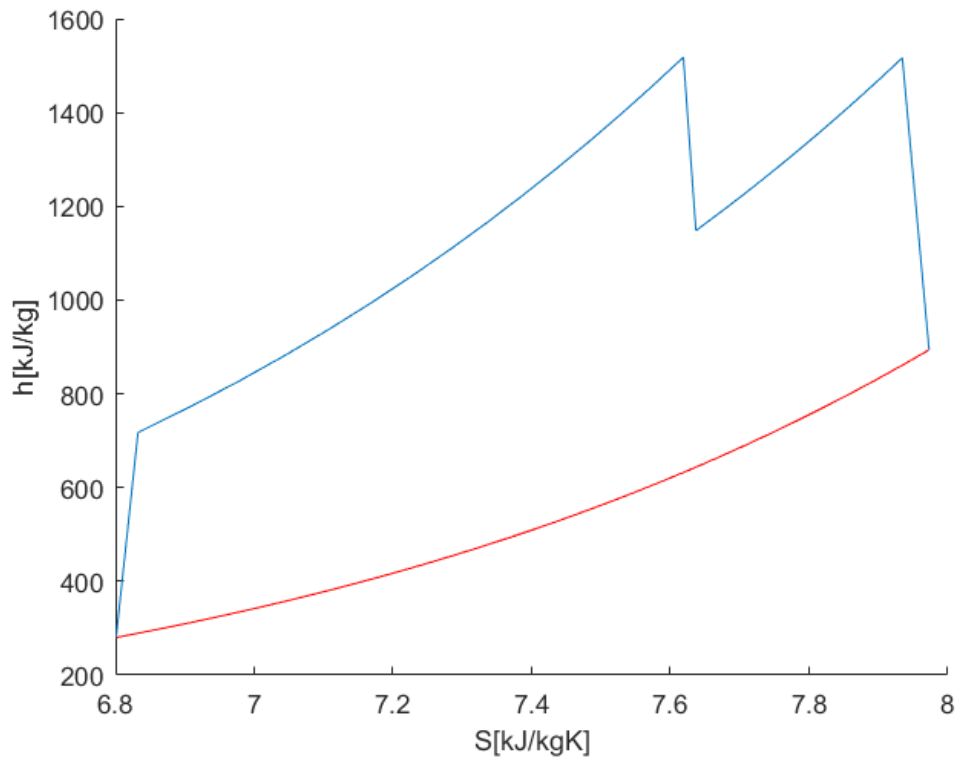


Figure 4.6: h-s diagram of an inter turbine burner cycle

The equation for the outlet velocity is shown in equation 4.23

$$V_8 = \sqrt{2 * c_p * (T_{t7} - T_8)} \quad (4.23)$$

As the fluid is expanded to ambient pressure, the thrust of the nozzle is caused by the change in velocity only 4.24.

$$F = m_8 * (V_8 - V_0) \quad (4.24)$$

Substituting equations 4.22 into equation 4.23 and the result into equation 4.24 results in an expression for the thrust of the nozzle that is only dependent on the inlet temperature and the pressure ratio 4.25.

$$F = m_8 * \left(\sqrt{2 * c_p * T_{t7} * \left(1 - \frac{P_8}{P_{t7}} \frac{\kappa_{gas} - 1}{\kappa_{gas}} \right)} - V_0 \right) \quad (4.25)$$

Again we are interested in the effect of the heat removal. For this reason, the derivative with respect to the total inlet temperature is calculated.

$$dF/dT_{t7} = m_8 * 0.5 * \left(2 * c_p * T_{t7} * \left(1 - \frac{P_8}{P_{t7}} \frac{\kappa_{gas} - 1}{\kappa_{gas}} \right) \right)^{-0.5} * 2 * c_p * \left(1 - \frac{P_8}{P_{t7}} \frac{\kappa_{gas} - 1}{\kappa_{gas}} \right) \quad (4.26)$$

As the total inlet pressure P_7 is constant in this case, the expression can be rewritten as equation 4.27.

$$dF/dT_{t7} = k_1 * \sqrt{\frac{\left(1 - \frac{P_8}{P_{t7}} \frac{\kappa_{gas} - 1}{\kappa_{gas}} \right)}{T_{t7}}} \quad (4.27)$$

where

$$k_1 = m_8 * \sqrt{\frac{c_p}{2}}. \quad (4.28)$$

For the pressure losses, the derivative with respect to the total inlet pressure is calculated to be

$$dF/dP_{t7} = 0.5 * m_8 * \left(2 * c_p * T_{t7} * \left(1 - \frac{P_8}{P_{t7}} \frac{\kappa_{gas} - 1}{\kappa_{gas}} \right) \right)^{-0.5} * 2 * c_p * T_{t7} * \frac{(\kappa_{gas} - 1) * P_8 * \frac{P_8}{P_{t7}} \frac{-1}{\kappa_{gas}}}{\kappa_{gas} * P_{t7}^2}. \quad (4.29)$$

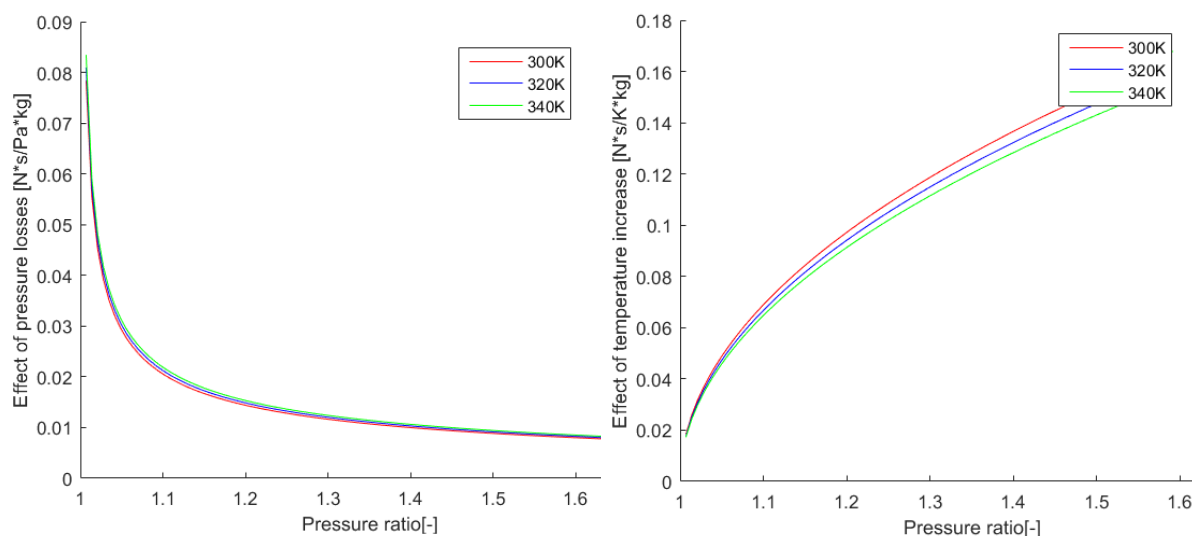
This equation can be rewritten as well. This shows the correlation more clearly 4.30.

$$dF/dP_{t7} = k_2 * \frac{\sqrt{T_{t7}} * P_8 * \frac{P_8}{P_{t7}} \frac{-1}{\kappa_{gas}}}{P_{t7}^2 \sqrt{\left(1 - \frac{P_8}{P_{t7}} \frac{\kappa_{gas} - 1}{\kappa_{gas}} \right)}} \quad (4.30)$$

in this equation

$$k_2 = \frac{m_8 * (\kappa_{gas} - 1) * \sqrt{c_p}}{\sqrt{2} * \kappa_{gas}}. \quad (4.31)$$

The equations are slightly more complex than for the choked case. However, it becomes clear that the pressure losses become more severe at higher temperatures. Furthermore, the effect of the pressure losses decreases for higher pressure ratios. The effect of the heat addition is bigger at high inlet pressures and lower temperatures. To gain the biggest thrust increase through the heat addition, the cooler should be placed at high pressure and low temperature. For a small negative effect of the associated pressure losses, the cooler should be placed at a high pressure and low temperature. Note that the same recommendation could have been derived from the choked case. The effects of pressure loss and heat extraction are shown in figure 4.7. As can be seen, the effect of the pressure ratio is much bigger than the effect of the temperature.



(a) Effect of the pressure losses for nozzles of different pressure ratios (b) Effect of the temperature increase for nozzles of different pressure ratios

Figure 4.7: Effect of pressure losses and temperature increase on an exemplary unchoked nozzle

4.2.6. PLACEMENT OF THE COOLER

In the initial design, the cooler was placed in the bypass duct and connected to a second nozzle. The heat transfer and pressure loss of the cooler have an influence on the performance of the main engine. This influence depends on the pressure and temperature of the cooling air. Therefore, a second investigation is made to find out the optimal location of the cooler. However, this time heat is added to the flow before the expansion in a nozzle. This means that a big effect of the heat addition is beneficial. Furthermore, a lower air temperature results in smaller heat exchanger as it increases the temperature difference between the two media. In addition to this, the minimum temperature of the supercritical cycle is fixed by the critical temperature of the working fluid. Therefore, the air temperature has no influence on the supercritical cycle efficiency. However, the cooling air temperature does have an effect on the pinch temperature and thus the weight of the cooler. The effect of the internal pressure losses is neglected in this analysis, as the changes are very small.

For the most beneficial effect on the main cycle, the cooler should be placed at high pressure and low temperature. These conditions enable the biggest effect of the associated heat addition to the air stream as can be seen in figure 4.4. To enable compact heat exchangers, the cooler should extract heat at a location with low temperature. As an adiabatic rise in pressure, as it happens in a fan, is always associated with an increase in temperature, the placement of the cooler becomes a trade-off between the weight of the heat exchanger and the thermodynamic performance.

There are several possibilities: The cooler could be placed in the bypass stream as has been done in the initial design. This results in higher pressure but also higher temperature of the air. To decrease the temperature, the bypass air could be cooled before being led to the cooler. This would decrease the efficiency of the heat addition. However, energy would be lost beforehand through the cooling process and an additional heat exchanger between the bypass air and free stream air would be required, bringing an additional weight penalty. Another possibility would be the placement of the cooler in air streams that are tapped off the first compressor stages. This would result in high pressure but also high temperature air. At the same time, the propulsive efficiency would decrease, as the high pressure results in very high exhaust velocities. The last possibility is to place the cooler in the free air stream. This would result in low temperature, low pressure air.

The previous description shows that the best placement of the heat exchanger is either behind the fan or in free air. The optimal solution depends on the given circumstances. For the cooler of the CCE2035 engine, the results of the analysis is presented in table 4.5. It is observed that there is a trade off between the thermodynamic performance and the weight. For the given situation, a compromise between thermodynamic

Table 4.5: Weight estimation of the cooler

	No fan	Fan with pressure ratio 1.2	Fan with pressure ratio 1.44
Cooling air temperature [K]	251.71	266.23	281.59
Weight [kg]	303.31	367.39	474.19
Extra equivalent in power [MW]	0.121	0.141	0.157
Outlet CO ₂ temperature [K]	313.16	312.96	313.29
Pressure loss [%]	0.819	0.723	0.689
Change in SFC [%]	-0.8	-0.936	-1.042
Change in Range [%]	0.251	0.271	0.182

performance and weight is the best solution. Thus for the given situation, the placement of the cooler behind a fan with very low pressure ratio is the best option as it has the most positive effect on the range of the aircraft. All three positions for the cooler have a positive effect on the range. The higher pressure loss in the free stream placement can be explained by the higher velocity in the heat exchanger due to the low density. However, the best placement depends on many aspects:

- The fan efficiency
- The cruise speed
- The ambient temperature
- The ambient pressure
- The cooler inlet temperature of the working fluid
- The pinch temperature of the cooler

4.3. APPLICATION TO AN INTER TURBINE BURNER TURBOSHAFT

A turboshaft engine has been identified as a thermodynamically more favourable application case for a waste heat recovery unit. The application of an inter turbine burner promises further improvement potential, as it increases the temperature at the location of the heater. In this section a preliminary analysis for the possible benefits of the application to these engine types will be conducted.

4.3.1. REFERENCE ENGINES

The reference turbofan engine had to produce 72 kN of thrust at the cruise velocity of 237 m/s. Assuming a propulsive efficiency of the turboshaft engine propulsor of 90 %, the required shaft power output of the equivalent turboshaft engine becomes

$$72000N * 237 \frac{m}{s} \cdot 0.9 = 18.96MW \quad (4.32)$$

The OPR for all engines is 70 and the TIT is 1900 K. When an ITB is present, the temperature after the ITB is 1400 K. All components have the same efficiencies for all engines.

Once again, the top level sensitivities were investigated. For this purpose GSP models of a conventional turboshaft and a turboshaft with inter turbine burner with a shaft power of 19 MW were created and the effect of pressure losses and heat extraction were investigated. The properties at the location of the heat removal are given in table 4.6. The results are summarized in table 4.7. For simplicity, the supercritical cycle of the previously optimized design has been used. Only the effects of the heater are investigated as the designs do not have a fan any more and thus the cooler has to be placed at a location outside the engine, where it does not have any influence on the engine performance itself. Therefore, the influence of the cooler will be identical for both engines.

Table 4.6: Flue gas properties

	ITB turboshaft	Turboshaft
Temperature [K]	887.9	704
Pressure [bar]	0.2263	0.2263
Mass flow [kg/s]	17.75	21.48
Oxygen fraction [%]	8.3	11.5
Water fraction [%]	5	3.9
CO ₂ fraction [%]	12.9	10
Nitrogen fraction [%]	72.4	72.9

Table 4.7: Top level sensitivities of the heater for different architectures, values give the change in SFC in %

	ITB turboshaft	turboshaft	ITB turbofan	turbofan
1.91 % pressure loss	0.437	0.416	0.36	0.31
1.98 MW heat removal	0	0	1.07	1.03
Both effects	0.437	0.416	1.43	1.34
Both effects and additional power	-2.093	-2.114	-1.1	-1.19

As can be seen, the effect of the heat extraction is zero for both configurations, as the flue gases are expanded to atmospheric pressure in the turbine and no more expansion takes place in the nozzle. The effect of the pressure loss is bigger for the engine with ITB. This can be explained with the higher working potential of the LPT when an inter turbine burner is applied. The effect of the pressure drop on both engines is considerably higher than for the turbofan application. This is as expected from the previous analysis.

The comparison to the turbofan engines with and without ITB shows that the importance of the pressure losses increases, while the effect of the heat removal diminishes for turboshaft engines. The application of ITB for the turbofan has similar effects for turbofan engines. The pressure losses as well as the heat removal have a bigger negative effect on the specific fuel consumption. This can be explained by the higher pressure ratio in the nozzle and the higher temperatures and is inline with the expectations from the previous analysis.

From this analysis, it can be expected that the ITB turboshaft is a worse candidate than the conventional turboshaft. The same holds for a turbofan engine. In this case the difference is even bigger than for the turboshaft. However, the ITB offers higher temperatures, which enable smaller heat exchanger and thus offers an weight advantage for the same maximum temperature in the additional cycle. At the same time, the mass flow of the ITB engine is less, as it has a higher specific thrust. This would induce bigger heat exchangers. Therefore, it has to be analysed if there exists a difference in the heater size between the two configurations and what that difference is. Also it has to be taken into account that the pressure losses will decrease, if the heater size decreases. Lastly, it has to be analysed whether the addition of the supercritical cycle to the turboshaft engines is beneficial for the aircraft mission.

For this purpose, it is important to be able to calculate the weight of the heat exchangers for the two configurations. For this purpose, a new stand alone heat exchanger model was created. The inlet conditions are specified in table 4.6. As can be seen, the turboshaft with inter turbine burner has the flue gas at a higher temperature. However, the flue gas mass flow is lower. The effect of the different flue gas composition of the two engines is neglected in this simple analysis. For the comparison, the mass flow rate and the inlet temperature of CO₂ as well as the heat duty are fixed. Table 4.8 summarises the results. As can be seen, the weight of the heat exchanger at the engine with inter turbine burner is 4434 kg lower than for the engine without inter turbine burner due to the higher temperature of the flue gases. The power and fluid outlet temperature are comparable. However, the weight for the engine without inter turbine burner is extremely high, as the temperature difference is very small. Therefore, the heat exchanger becomes impracticably large.

Table 4.8: Weight estimation of the heater

	ITB turboshaft	Turboshaft	2035 Turbofan
Power [MW]	1.9835	1.98	1.9854
Outlet flue gas temperature [K]	786.92	619.12	692.26
Outlet CO ₂ temperature [K]	698.39	696.95	689.59
Pressure loss [%]	0.187	1.872	1.917
Weight [kg]	552.86	4986.8	991.54

To make a second comparison between the two concepts, the supercritical cycle is altered to circulate 10 kg/s of CO₂. This will decrease the CO₂ outlet temperature and will thus increase the temperature difference. This analysis will only look at the weight of the heater, to get a feel for the effect of the inter turbine burner. At the same time, the cooler will have to be designed much larger and the supercritical cycle will be less efficient and produce less power as the maximum cycle temperature and thus the cycle efficiency decreases. In this second comparison the weights of the heater become 475.46 kg and 1448.5 kg for the turboshaft engine without ITB and with ITB respectively.

The performance of the engines can be compared through tables 4.8 and 4.7 and equation 3.1. The addition of the supercritical cycle increases the range of the turboshaft with ITB by 1.209 %. This is a notable number compared to the range decrease of 1.709 % for the application at the baseline 2035 turbofan. The range of the aircraft with the conventional turboshaft engine decreases by 6.839 % through the addition of the supercritical cycle. This shows that the chosen supercritical cycle is very suboptimal because of the too high heat extraction in the heater. It can be concluded that likely a turboshaft with ITB is a better application case than a conventional turboshaft as the heater can be designed much lighter, while the effect of the pressure loss and heat extraction differ only slightly. The difference in those values accounts for a change of range of 0.03 % only. This is underlined by the second investigated supercritical cycle. In this case the CO₂ mass flow rate is increased to 10 kg/s. This causes the weight of the heater to decrease, as the temperature difference increases. The difference in range between the engine with ITB and without decreases from 8.05 % to 1.78 %. This is still a big difference, as it causes the system to be beneficial in the first case and not beneficial in the later case.

The analysis shows that the exhaust temperature is a very important parameter for the weight of the system. For this reason, a turbofan engine can also be more beneficial than the turboshaft engine. Also the option of coupling the power of the supercritical cycle to the low pressure spool of the turbofan engine as has been done in the paper of Jacob *et al.* [4] can be an attractive solution. The best solution however strongly depends on the specific case under consideration.

4.4. INFLUENCE OF THE SUPERCRITICAL WORKING FLUID

Most research on supercritical cycles uses CO₂ as the working fluid because it has favourable properties for the use in terrestrial power production, the main application that has been investigated. Other reasons, are the experiences with CO₂ at high pressures and temperatures, the availability and the extensive research on CO₂ itself. However, one can think of different working fluids or mixtures of fluids for the application in the supercritical cycle. In this section, the aspects of the working fluid selection will be elaborated on and a selection of possible working fluids will be presented and evaluated.

4.4.1. FLUID REQUIREMENTS

In order to have a suitable working fluid, the following characteristics have to be considered. The working fluid has to be as inert as possible within the temperature and pressure range that is reached in the cycle. This is to ensure the durability of the piping and heat exchanger and prevent corrosion. Furthermore, the working fluid has to be chemically stable. The working fluid operates in a closed cycle, chemical reactions at elevated temperatures and pressure would prevent the continuous operation.

In addition to these properties, it is desirable for the working fluid to be non toxic, not flammable and readily available. These are practical requirements, that are not necessary for the proof of concept. However at later stages, when the feasibility of the concept for a product will be evaluated, they will become important.

Table 4.9: Properties of the candidate working fluids

	CO_2	Xe	C_4F_{10}
T_{crit} [K]	304.13	289.73	386.33
P_{crit} [bar]	73.77	58.42	23.23
ρ [kg/m ³]	1.7842	5.3241	9.9707
C_p [kJ/kg*K]	850.76	160.07	816.54

4.4.2. CRITICAL TEMPERATURE

In order to benefit the most from low compression work of the fluid, the minimum cycle temperature should be close to the critical temperature of the working fluid. A lower critical temperature can increase the efficiency of the cycle, as it enables higher temperature ratios for the same maximum temperature. At the same time, a lower critical temperature decrease the temperature difference in the cooler. This increase the weight of the cooler for the same heat duty. The critical temperature has to be above the ambient temperature in order to enable the cooling of the working fluid up to its critical point.

4.4.3. CRITICAL PRESSURE

The critical pressure of the working fluid has a big impact on the system design as well. Furthermore, the critical pressure is the optimum low pressure, as the benefits of low compression work are the highest at this pressure. Also the pressure ratio and thus the efficiency of the cycle are dependent on the critical pressure of the working fluid. For this reason, a lower critical pressure is beneficial, as it enables higher pressure ratios. Next to this thermodynamic effect, the pressure in the cycle has also an influence on the weight of the heat exchangers. A higher pressure requires thicker tubes and thus increases the weight. For those two reasons, the critical pressure of the working fluid should be as low as possible.

4.4.4. CANDIDATE FLUIDS

Based on their properties, candidate fluid for the application as working fluid in the supercritical waste heat recovery cycle were identified. Only fluids that can be calculated with Refprop have been considered. The candidate fluids are:

- Carbondioxide
- Xenon
- C_4F_{10} (Perfluorobutane)

Table 4.9 summarizes their most important properties. The values for the density and C_p values are given for atmospheric conditions of 25° C and 1 bar. All three fluids are gases at atmospheric conditions. Furthermore they are non toxic, non flammable and not very reactive. Xenon has the lowest critical temperature of 290 K. C_4F_{10} has the highest critical temperature of 386 K. This shows a remarkable big difference in the critical temperature. Also the densities vary greatly from 1.8 kg/m³ for CO_2 to 10 kg/m³ for C_4F_{10} . This difference will be smaller in the cycle, as C_4F_{10} has a much lower critical pressure, but still a noticeable difference at the operating conditions of the supercritical cycle exists.

4.4.5. PERFORMANCE COMPARISON

To get a first impression of the performance of the different working fluids, supercritical cycles are compared. The cycles are applied to similar operating conditions. The minimum pressure equals the critical pressure of the working fluids and the minimum temperature of the cycle is 10 K above the critical temperature of the fluid. To be able to make a useful comparison of the results, the pressure ratio, maximum cycle temperature and component characteristics are identical for the different cycles. In addition to this, the effect of the working fluid on the heater and cooler was tested. For the test of the heater, the heat transfer for a heater with fixed dimensions and operating conditions for the three working fluids was calculated. For the cooler, the dimensions of the cooler were fixed but the operating conditions were different to ensure meaningful results. To be more specific, the working fluid entry temperature was fixed to 60 K above the critical temperature. In this way the occurring conditions of a cycle with the working fluid are approximated. Two cases were considered for the conditions of the cooling air. In the first case $Cooler_{sameT}$, the cooling air has a temperature of 280 K for all working fluids. In the second case $Cooler_{variableT}$, the cooling air has a temperature of 20 K below

Table 4.10: Operating conditions of the heat exchangers

	Heater	$Cooler_{sameT}$	$Cooler_{variableT}$
m_{gas} [kg/s]	42	60	60
$m_{supercriticalfluid}$ [kg/s]	7	7	7
$T_{gas_{in}}$ [K]	750	280	270/285/366
$T_{supercriticalfluid_{in}}$ [K]	480	350/365/446	350/365/446
Number of rows [-]	60	25	50
$P_{supercriticalfluid}$ [bar]	350	63/78/28	63/78/28

Table 4.11: Performance of the working fluids for different heat exchangers

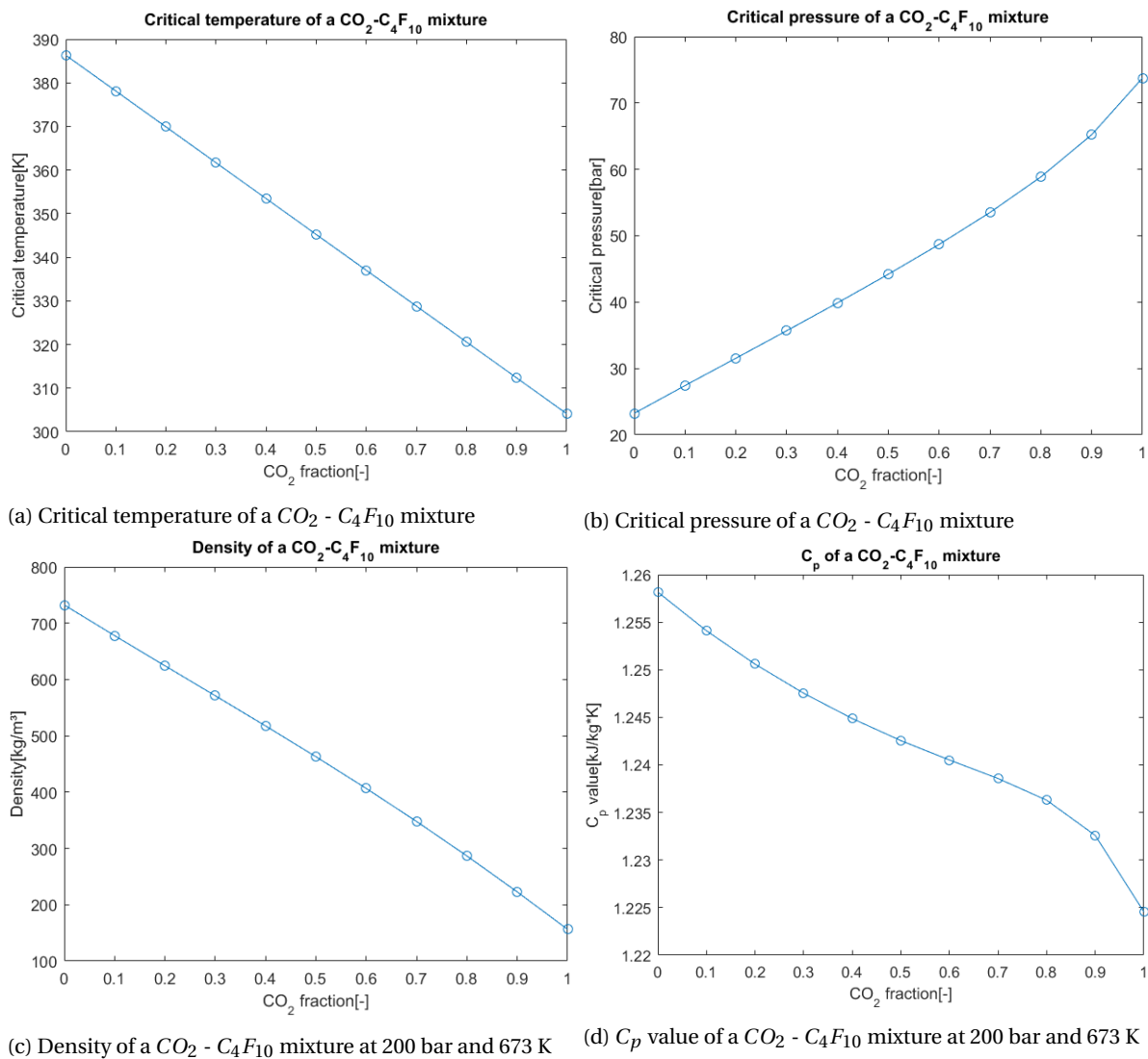
	CO_2	Xe	C_4F_{10}
Q_{heater} [kW]	1992	448	1830
$Q_{cooler_{sameT}}$ [kW]	349	155	668
$Q_{cooler_{variableT}}$ [kW]	510	270	494
W_{heater} [kg]	668	678	684
$W_{cooler_{sameT}}$ [kg]	73	84	83
$W_{cooler_{variableT}}$ [kg]	148	179	159
$T_{out_{heater}}$ [K]	687.5	738	691
$T_{out_{cooler_{sameT}}}$ [K]	333.5	300.6	389.67
$T_{out_{cooler_{variableT}}}$ [K]	322.7	293.9	397.8
$T_{Pinch_{heater}}$ [K]	15.35	3.35	15.58
$T_{Pinch_{cooler_{sameT}}}$ [K]	48.46	18.74	99.34
$T_{Pinch_{cooler_{variableT}}}$ [K]	29.81	20.06	24.73

the critical temperature of the working fluid. These conditions ensure that a big amount of effects is covered by the investigations. Specifically, the effect of the critical temperature and thus the expected temperature difference in the cooler are represented. Furthermore, the effect of the fluid properties with identical temperature differences are investigated. In this way it becomes possible to isolate the effects of different property values.

Table 4.11 shows the results for the investigations of the heat exchangers. The operating conditions of the heat exchangers are shown in table 4.10. Looking at the weight of the heat exchangers, only small differences are present. This is no surprise, as the heat exchanger have equal size, the only difference in weight is due to the different amount of working fluid inside the heat exchanger. This amount is proportional to the density of the working fluids at the specified conditions. In the heater, the heat duty of Xenon is much smaller than for the other two working fluids. This is caused by the low C_p value of Xenon. Accordingly the temperature change of Xenon is very high. The performance of CO_2 and C_4F_{10} is very similar, when the temperature difference is similar. The much higher critical temperature of C_4F_{10} causes very high heat transfer in the cooler with the cooling air temperature of 280 K.

To summarize, Xenon enables high maximum temperatures and has a very high density. The low C_p value causes a low heat duty. This makes Xenon well suited for the application in very efficient cycles. The cycle however requires very large mass flow rates to achieve a sufficient power output. The low critical temperature requires cold cooling air. CO_2 offers very high heat duties and low temperature changes. C_4F_{10} shows a similar behaviour but offers the advantage of a very high critical temperature, low critical pressure and a high density. This allows very compact coolers and turbomachinery but results in low cycle efficiencies. The optimal working fluid thus depends on the given operating conditions and the importance rating of efficiency and weight.

To compare the effects of the working fluids on the supercritical cycle, the cycles have to be optimised for a given main engines. This will be done in chapter 5.

Figure 4.8: Thermodynamic properties of a $CO_2 - C_4F_{10}$ mixture dependent on the mixture fraction

4.4.6. MIXTURES OF WORKING FLUIDS

Next to pure working fluids, the use of mixtures of working fluids is also a possibility. Especially a mixture of CO_2 and C_4F_{10} seems promising, as the mixture can combine the positive aspects of both fluids. The fluid properties depending on the mixture fraction are shown in figure 4.8. As can be seen, the fluid properties vary almost linearly with the mixture fraction. A mixture of around 50 % CO_2 and 50 % C_4F_{10} shows very favourable properties. A high density, relatively low critical pressure, a high C_p and a critical temperature that allows a compact cooler design and yet enables a high energy extraction from the exhaust gases.

4.5. TECHNOLOGICAL BARRIERS

Next to the aspects already discussed, the possible performance of the system depends on technological limitations as well. Many of these are related to the design of the heat exchangers and are presented in this section.

- Minimum wall thickness:

The wall thickness of the cooler and the regenerator are not constraint by the pressure difference but rather by the ability to produce such thin walled tubes. The possibility to produce thin tubes would decrease the weight of the heat exchangers considerable. At the same time, the heat transfer and pressure losses would decrease slightly, as the inside dimension would reduce for the same outside dimensions.

- **Minimum tube diameter:**
The possibility to produce tubes with a smaller diameter has the potential to decrease the weight of the heat exchangers, as it produces a bigger surface area to cross sectional area ratio. At the same time, a smaller diameter decreases the stresses due to the pressure difference. This allows the application of thinner tubes. The introduction of smaller tubes causes the internal pressure losses to increase. However, the internal pressure losses are currently still at a negligible level.
- **Specific yield strength of material at high temperatures:**
Through the high pressure of the working fluid, the wall thickness of the heater is likely to be limited by the stresses. A higher specific yield strength of the material at the high operating temperatures of the heater will decrease the weight of the heater and thus increase the performance of the system. This change can be realised through a different material choice.
- **Maximum cycle pressure:**
The maximum pressure in the system is limited to 400 bar, as only little experience exists for the handling of Carbon dioxide above this pressure. If this limit was not present, higher pressures could be achieved. This would in turn allow for higher pressure ratios in the cycle and thus higher thermal efficiencies. However, also the weight of the regenerator would increase, as the stresses due to the pressure losses would increase. At the same time, the regenerator would become less beneficial and higher maximum cycle temperature would be required. For these reasons, the constraint of the maximum pressure is not limiting. Especially when working fluids with a lower critical pressure are considered.
- **Maximum cycle temperature:**
The maximum cycle temperature can be limited by the capability of the heat exchangers to withstand the elevated temperatures. However, for the considered engines, the exhaust gas temperature is below this limit. For this reason, the maximum temperature of the cycle is not actually limited by technological barriers.
- **Component efficiencies:**
More efficient turbomachinery in the supercritical cycle has many positive effects. It increases the efficiency of the cycle. This in turn leads to a smaller cooler and heater for the same power output. The efficiency of the turbine is the more important parameter. This is caused by the compressor being operated close to the critical point of the working fluid. Therefore, the compression work is low any ways and changes in the compressor efficiency have only a small influence. A more efficient compressor increase the heat recovery potential of the regenerator slightly as the temperature difference increases. A more efficient turbine has the opposite effect, as more energy is extracted from the fluid in the turbine.

4.6. INFLUENCE OF THE HEAT EXCHANGER DESIGN

As has been demonstrated in the previous section, many technological barriers are related to the design of the heat exchangers. Therefore it is important to understand the effect of these barriers in more detail and be able to quantify them. In addition to this, there are design parameters of the heat exchangers, that are not limited by the technology. These design options will also be elaborated on.

4.6.1. EFFECT OF THE WALL THICKNESS

The wall thickness of the tubes is either limited by the requirement to withstand the pressure difference or by the minimum wall thickness associated to the chosen manufacturing technique. Accordingly, the wall thickness can be decreased by the usage of more advanced production methods, a decrease in the tube diameter, a decrease in the aspect ratio of the tubes or by the usage of a material with a higher yield strength at the operating conditions. When the thickness decreases, the outside dimensions of the tubes stay the same and the cross sectional area as seen by the fluid on the inside increases. On the gas flow on the outside, a change in thickness has no immediate effect. On the inside, the flow velocity decreases, as more area is available to the same mass flow. This decrease in velocity reduces the heat transfer coefficient and thus the heat duty of a given heat exchanger slightly. This decrease is in the order of magnitude of 1 % per 0.1 mm reduction of wall thickness. In addition to this, also the pressure losses inside the tubes decrease slightly. However, this effect is negligible for most applications. Next to this effect, the decrease of thickness causes an almost proportional decrease in heat exchanger weight as less material is used. Another effect of a decreased thickness

is a lower heat resistance of the wall and thus a higher heat transfer in the heat exchanger. However, this effect is negligible compared to the other effects.

4.6.2. EFFECT OF THE HEAT EXCHANGER TUBE DIAMETER

The ability to produce tubes with a smaller diameter has many advantages. The weight decreases, as the tubes become smaller and contain less fluid. The smaller diameter decreases the required thickness as well. This is the case, when the pressure requirement is limiting the tube thickness and would increase the weight savings even more. The flow areas increase on the outside, as the blockage of the tubes decreases and it decreases on the inside of the tubes, as the diameter decreases. This in turn causes a higher flow velocity and thus pressure losses and heat transfer coefficient on the inside and the opposite on the outside. At the same time, the smaller diameter of the tubes increases the heat transfer on the outside, cancelling the effect of the lower velocity. The total heat transfer coefficient of the tubes increases. In addition to this, the surface area of the tube and thus the area over which the heat transfer takes place, decreases. The total effect of the tube diameter on the heat transfer, and thus the required amount of tubes, depends on the given configuration. At very small tube diameters, the internal pressure losses begin to rise very strong and the increase in total heat transfer coefficient begin to stagnate, leading to a decrease in the total heat transfer.

4.6.3. EFFECT OF THE THERMAL CONDUCTIVITY OF THE MATERIAL

The thermal conductivity of a material determines how well heat travels through this material. A higher thermal conductivity of the wall material is beneficial, as it increases the heat transfer. A big variation in thermal conductivity exists between different materials. While titanium has a thermal conductivity of around 20 W/m*K, copper has a thermal conductivity of around 400 W/m*K. However, as the heat exchanger walls are very thin, the effect of the thermal conductivity of the material is very small. For an heat exchanger of a given size and wall thickness, an increase in thermal conductivity of the wall material from 20 to 400 W/m*K, increases the heat transfer by only 0.017 %.

4.6.4. EFFECT OF THE SPACING BETWEEN HEAT EXCHANGER TUBES

The spacing of the tubes is specified in the radial direction and along the rotational axis of the main engine. The model that is being used, does not take the effect of the lateral spacing into account. For this, higher fidelity models of the effect on the heat transfer coefficient are required. This is beyond the scope of the thesis, as the main focus is on the system optimization. However, the radial spacing is taken into account as it influences the flow through the heat exchanger. A smaller radial spacing of the heat exchanger tubes places more tubes in a single row. This decreases the available area for the gas flowing outside the tubes. As a consequence, the flow velocity increases as well as the heat transfer coefficient and the pressure losses. The static temperature of the gas decreases due to the higher velocity. This is beneficial for the cooler but not for the heater.

The effect of a higher radial spacing between the tubes is small. For a cooler, the increase in the radial spacing from 15 mm to 25 mm, the heat transfer decreased by 1.8 % and the pressure losses increased from 1.83 % to 2.28 %. When the radial spacing was decreased to 12 mm, the heat transfer increased by 1.4 %. At the same time, the pressure losses stayed almost constant. For a heater, the results are different. The radial spacing had almost no influence on the heat transfer. The effect on the pressure loss was similar as for the cooler. For this experiment, the amount of rows of tubes was changed, to keep the weight of the heat exchanger constant. This means that in case the radial spacing was increased, more row of tubes were used and thus the length of the heat exchanger increased. The results show that the effect of the radial spacing is low and very dependent on the design of the heat exchanger and the conditions it operates at.

4.6.5. EFFECT OF THE TUBE ASPECT RATIO IN THE HEAT EXCHANGER

The aspect ratio of the heat exchanger tubes is another important parameter of the heat exchanger design. A higher aspect ratio decreases the pressure losses on the outside of the heat exchangers. At the same time, the stress in the tube walls increase. Also the surface area that is available for the heat transfer increases, when the maximum diameter stays constant and the aspect ratio increases.

A sizing exercise for the heat exchangers was used to quantify the effect of the aspect ratio on the heat exchanger performance. In these simulations, the performance of heat exchangers of equal size and maximum

tube diameter were calculated for different aspect ratios. For a heater, an increase in the aspect ratio by 10 % from 2 to 2.2, increased the weight by 14 %. The heat transfer increased by 3.5 % and the pressure losses on the gas side reduced by 27 % from 4.54 % to 3.37 %. When the aspect ratio was decreased by 10 % to 1.8, the weight decreased by 17 %, the heat transfer decreased by 5.4 % and the pressure losses increased by 40 % to 6.37 %. For the cooler, a comparable effect was observed. When the aspect ratio of the cooler tubes was decreased by 10 %, the weight decreased by 20 %, the heat transfer decreased by 1 % and the pressure losses on the air side increased by 40 %.

These results show that the behaviour is less dependent on the heat exchanger design and operating conditions and that the aspect ratio of the tubes has a big influence on the pressure ratio and weight of the heat exchanger but not so much on the heat transfer.

4.7. INFLUENCE OF THE SUPERCRITICAL CYCLE CONFIGURATION

So far, only the simple recuperated cycle configuration has been considered for the supercritical cycle. However, several different cycle configurations exist and have been investigated already. These cycles have been designed for the use in terrestrial power plants and focus on a high thermal efficiency of the cycle. The recompression cycle is the most investigated cycle configuration and has been identified as a good compromise between high efficiency and simple cycle layout. The main idea of the recompression cycle is to reduce the effect of the pinch point problem and thus enable more heat to be recovered in the recuperators. The layout of the recompression cycle is shown in figure 4.9. The fluid starts in the cooler and is compressed in the compressor from state 1 to state 2. Heat is then added in the two recuperators and the heater before the fluid is expanded in the turbine. Heat is then removed from the fluid in the two recuperators. A part of the stream flows through the cooler and starts the cycle again. Another part of the fluid does not go through the cooler and is directly compressed instead. This recompressed fluid is then inserted in between the two recuperators.

The advantage of the recompression cycle is the reduced heat duty in the cooler, as less fluid runs through the cooler. This brings a higher thermal efficiency of the cycle. However, the operational complexity of the cycle is increased and a second compressor as well as a second regenerator is necessary for the recompression cycle.

There are many more cycle configurations. However, the problem of the increased complexity and thus weight remains. Previous research found a possible efficiency gain of around 5 % for more complex cycle layouts at the maximum temperature under consideration [3]. This translates to 25 kW of additional power output and a roughly 5 % lighter cooler. Taking only these effects, and none of the associated negative effects into account, the range of the aircraft would increase by 0.17 %. The real effect however will be lower, as the weight of the additional compressor and regenerator is not taken into account. Moreover, less heat will be added to the bypass stream, thus sacrificing some of the efficiency gain. This does not justify the added complexity of the cycles. Therefore, different cycles will not be investigated in this thesis. For an extensive discussion on different cycle layouts one can refer to the paper of Moisseytsev and Sienicki [33].

4.7.1. EFFECT OF THE SUPERCRITICAL CYCLE COMPONENTS

The efficiency of the turbomachinery components plays an important role for the system performance. Due to the small size of the turbomachinery, rather low isentropic efficiencies are assumed. The assumptions are 85 % for the compressor and 90 % for the turbine. The mechanical efficiency is assumed to be 99 %. The values seem realistic, when the experience from supercritical CO_2 test loops is taken into account [19]. However, achieving these efficiency values remains a challenge due to the small dimensions and the rapidly changing fluid properties.

The turbine efficiency is the most important parameter. Its effect is almost twice the effect of the compressor efficiency. An increase in the efficiency of the turbine of 1 % increases the range of the aircraft by 0.055 %. For the compressor this value is 0.028 %. The effect of the mechanical efficiency is much lower. This can be explained, as this efficiency only counts for the connection between compressor and turbine. It corresponds to a 1 % higher compressor work but without the negative effect of the higher compressor outlet temperature. As the weight estimation and thus also the range estimation is affected by the numerical inaccuracies of the heat exchanger sizing process, it is interesting to investigate the change in power output of the supercritical

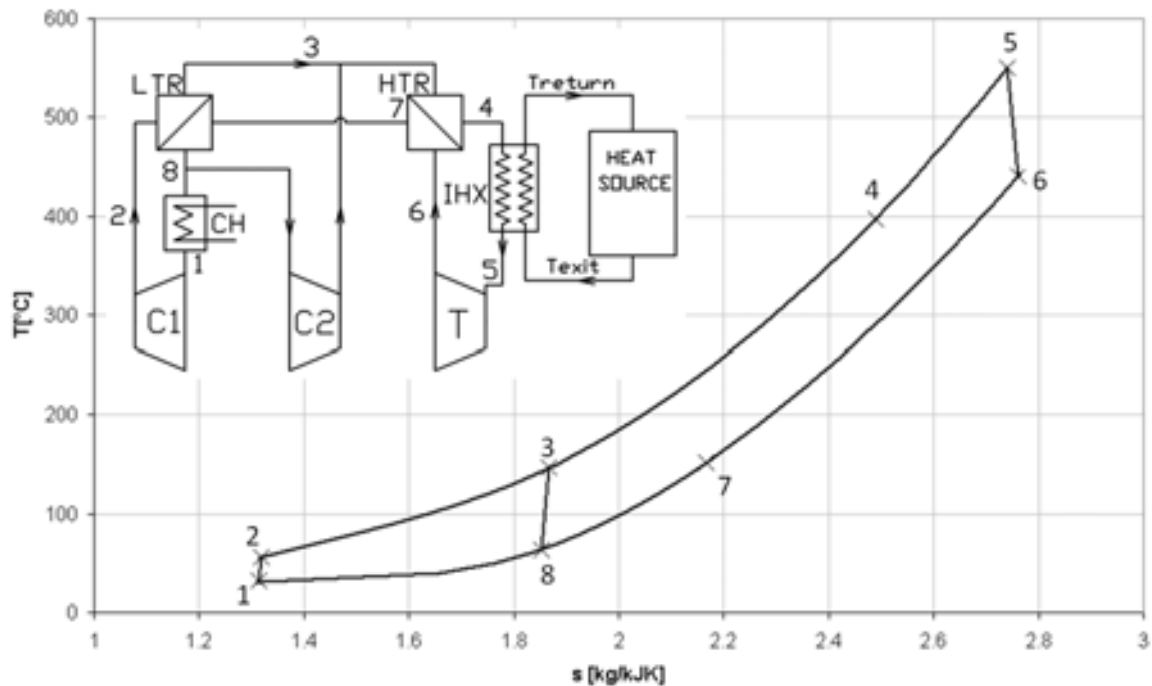


Figure 4.9: Layout of a recompression cycle from [3]

cycle. Looking at this metric, an increase of 1 % in isentropic turbine efficiency increases the power output by 2.15 %, for the compressor, this value becomes 1.19 % and the mechanical efficiency has the lowest value of 0.99 %. This shows that the focus of further research should lie on the development of more efficient turbines.

4.8. CONCLUSIONS

In this chapter, the behaviour of the combined cycle engine has been analysed and the effects of several parameters has been identified. The optimization of the supercritical cycle operating parameters for the given conditions of the main engine proved to be an important process in the optimization of the system. In this way it is possible to increase the power output of the supercritical cycle while decreasing its weight at the same time. As the optimal parameters depend strongly on the given application, no general trends can be recognised and an extensive optimization process has to be conducted for every new application.

The top level system analysis showed that the heat removal in the heater has a strong negative effect on the system performance. This negative effect can be reduced by extracting the heat at a lower pressure. Therefore, the application of a waste heat recovery unit to a turboshaft engine can be more beneficial. The application of an inter turbine burner can reduce the weight penalty associated with the lower exhaust temperature of a turboshaft engine. The exhaust gas temperature proves to be a very important parameter for the system. The optimal placement of the cooler results from a trade off between high pressure and low temperature of the cooling air. This translates to a trade off between the weight of the heat exchanger and the additional thrust of heat being added to the cooling air. The placement in a separate duct proves to be close to the optimal point for many applications.

The choice of the working fluid has a big influence on the performance of the engine. Especially the critical temperature and the critical pressure are of importance for the system performance. Based on typical conditions of an aircraft engine, Carbon dioxide, Xenon and Perfluorobutane haven been identified as promising candidate working fluids. The resulting supercritical cycles are very different. A mixture of CO_2 and C_4F_{10} shows to be a good candidate, combining the good properties of both fluids. However, the performance on a system level has yet to be investigated.

The effect of technological barriers was also investigated. It was found that the most severe limitations are

associated with the production of the heat exchanger. Improvements in the ability to produce smaller tubes with thinner walls can increase the performance of the system by decreasing the weight. To increase the efficiency of the supercritical cycle, more efficient components, especially the turbine, are the most promising solution, however the possible gains are limited. The effect of the internal pressure losses on the cycle efficiency are very small.

The heat exchanger design plays an important role in the performance of the system as the heat exchangers determine the additional weight of the supercritical cycle and the pressure losses on the gas side have an important influence on the performance of the main engine. The wall thickness and the tube size proved to be very important parameters, having a big influence on the weight of the heat exchanger. The aspect ratio in turn has a big influence on the weight as well as the pressure loss on the gas side. The spacing between tubes has less influence on the performance but is not negligible either. The effect of the thermal conductivity of the tube material however, is negligible.

The potential of different supercritical cycle layouts was estimated to be below 0.17 %. This is a theoretical upper bound and the real improvements will be less, if there are any. This does not justify more in depth investigations into this option at this point of the research. Different cycle layout will therefore, not be accounted for.

Based on this knowledge a lot of improvement potential has been identified. As for the main cycle parameters, the effect of different aspects is highly dependent on the current design point. Therefore, it is not possible, to conclude an optimal design based on these findings. It has yet to be proven that the application of these improvements is actually beneficial and enables the combined cycle engine to outperform a corresponding conventional aircraft engine. For this purpose, predicted turbofan and turboshaft engines with and without inter turbine burner for the year 2035 will be modified to combined cycle engines. Different working fluids will be tested and the supercritical cycles will be sized according to the application. The resulting performances of the engines will be compared to identify the best combination and gain additional knowledge about further improvement potential.

5

SYSTEM OPTIMIZATION

The previous analysis showed many possibilities to improve the performance of the combined cycle engine. The most promising options were the optimization of the supercritical cycle parameters, the application to a turboshaft engine, possibly with ITB, and the use of different supercritical working fluids. The optimization of the heat exchanger design showed to have a big impact on the performance as well. However, this will only be applied, once the best candidate for a high system performance has been identified.

To identify the best combination, equivalent turbofan and turboshaft engines with and without ITB will be equipped with optimized supercritical Brayton cycles with Carbon dioxide, Xenon or Perfluorobutane. The performance of the resulting combined cycle engines will be compared and the most promising candidate for more in depth optimization will be identified. The results will also show whether the concept of the combined cycle engine is capable of improving the fuel efficiencies of an aircraft along a mission.

5.1. MODIFIED METHODOLOGY

During the optimization of the system layout, a more flexible approach is required in order to exploit the full design space in an efficient manner. For this reason the combination of a MATLAB code to calculate the properties of the supercritical cycle and the heat exchangers and GSP, to calculate the behaviour of the main engine is used. GSP is used, as it is a validated tool for the simulation of gas turbines. MATLAB enables the efficient calculation of the heat exchangers and fluid properties. The working of this method is explained in this section.

Figure 5.1 shows the interaction between the two models. At first, GSP simulates the main engine. The operating conditions for the heat exchangers are then parsed to MATLAB. The script calculates the performance of the cycle and sizes the heat exchangers. The resulting pressure losses and the heat power exchanged with the flue gasses and the bypass air are put back into GSP. The performance of the main engine is then calculated. As a last step, the output of the single cycles is combined, to calculate the system performance.

The interaction with GSP is realised through an API. Refprop is used for the calculation of the fluid properties on both sides to take into account the non linear behaviour of the fluid properties. Due to the high density of the working fluid, the method calculates the wet weight of the heat exchangers.

5.1.1. NUMERICAL IMPLEMENTATION

The structure of the code is shown in figure 5.2. The lowest level is the calculation of a heat exchanger of a given size. The procedure uses the approach as in the Dymola model with the difference that the fluid properties of gases and supercritical fluid are calculated with Refprop. A finite differences method calculates the properties in the cells. In case of an error in the fluid property calculation or non convergence, a temporary back up of the last successful iteration is done. Initially a constant pressure is imposed for all cells in the discretisation. The initial temperature distribution is a linear temperature change along the flow direction between the inlet and expected outlet temperature. Convergence is reached when the total heat transfer of three consecutive iterations is within $\pm 0.25\%$. An exemplary initial and final temperature distribution is

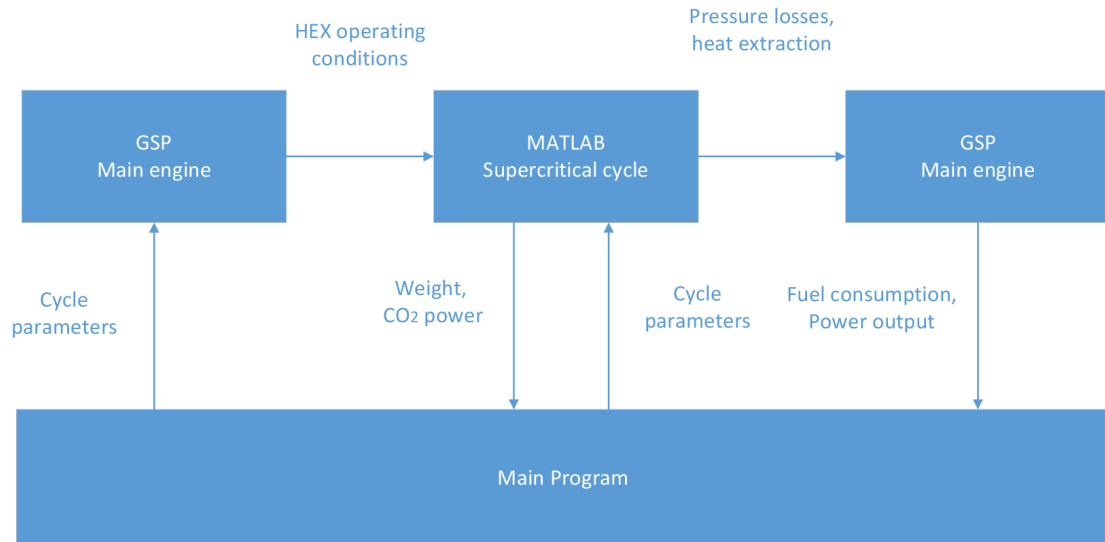


Figure 5.1: Information flow in the new simulation framework

shown in figure 5.3. The working fluid is CO_2 with a mass flow rate of 7 kg/s and an inlet temperature of 446 K. At the same time 53 kg/s of cooling air with an inlet temperature of 290 K stream through the cooler. The fluid flows from the left to the right. The temperature variation perpendicular to the flow direction is not accounted for in the initial temperature distribution. The initial temperature is often higher than the final temperature. This causes an overestimation of the initial heat transfer, as the temperature difference in the heat exchanger is overestimated. However, the approach is very general and enables a quick convergence.

The convergence history for a cooler with CO_2 as working fluid is shown in figure 5.4. The heat power is negative, as heat is extracted from the cycle. The value overshoots slightly and converges to the final solution after one oscillation. The convergence criterion is fulfilled after 13 iterations. This is represented by the green dot in the plot.

The next higher level is the sizing of the heat exchangers. The scheme determines the size of the heat exchanger based on the required heat transfer. This loop uses the Newton scheme to determine the required size. In case the calculation of the heat exchanger fails in the function, the amount of elements for the discretisation is increased and the calculation is re initiated. Convergence is reached, when the difference between actual heat transfer and required heat transfer is below 0.5 %.

The top level function calculates the performance of the system of the combined cycle engine. For this function, the mass flow rates, pinch point values and component efficiencies are fixed through the input parameters. The procedure it follows is shown in figure 5.5. As a first step, the properties of the main engine are loaded from the GSP results. With these information and the input parameters, the supercritical cycle is uniquely defined. The maximum as well as the minimum temperature and pressure are known and the calculation starts at the working fluid outlet of the cooler with the specified pressure and temperature. The estimations are straightforward until the regenerator is reached. The heat duty of the regenerator is not known yet. The calculation continues after the heater, with the specified heater outlet temperature. An inter-

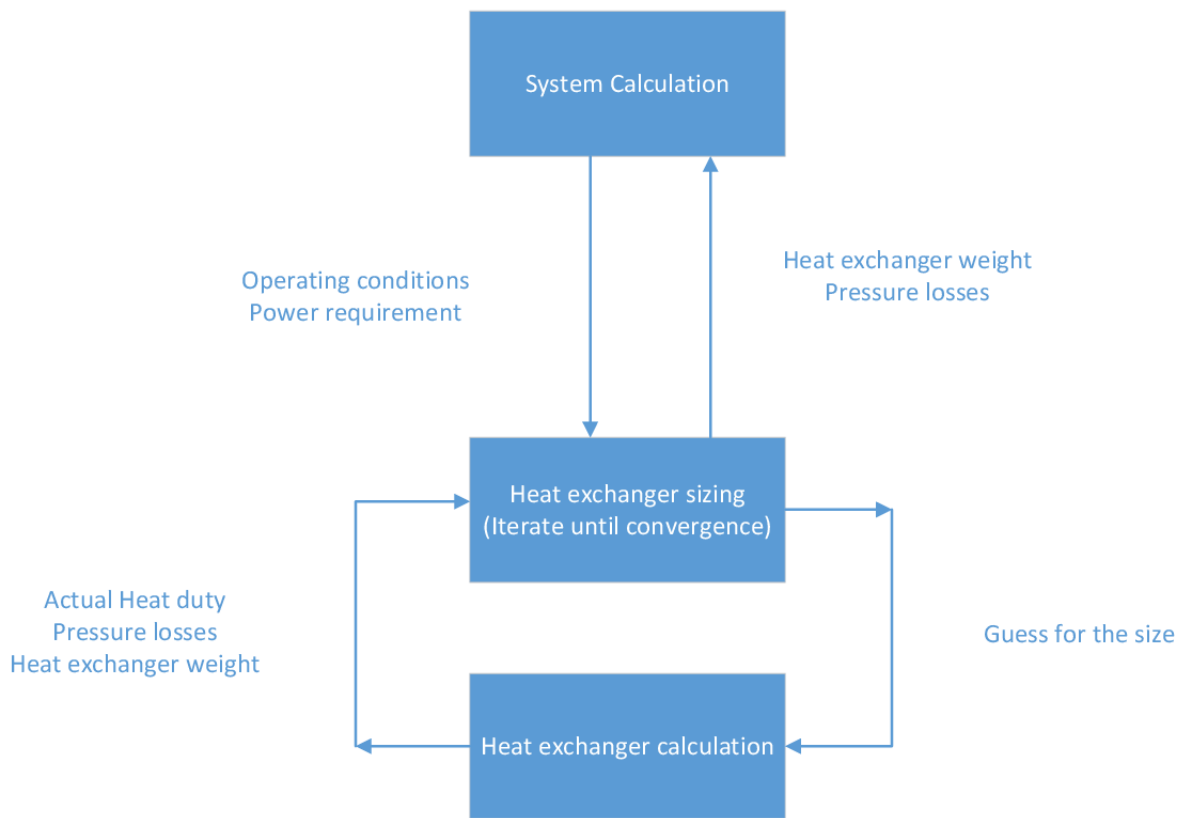
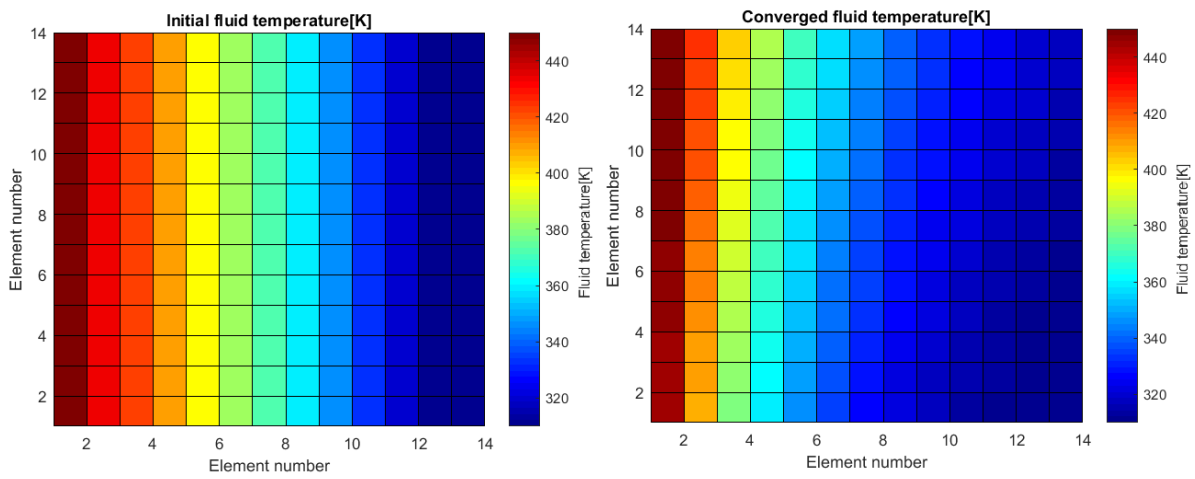


Figure 5.2: Main calculation steps in the system simulation



(a) Initial fluid temperature in a cooler

(b) Final fluid temperature in a cooler

Figure 5.3: Initial and final temperature distribution of a cooler with CO₂

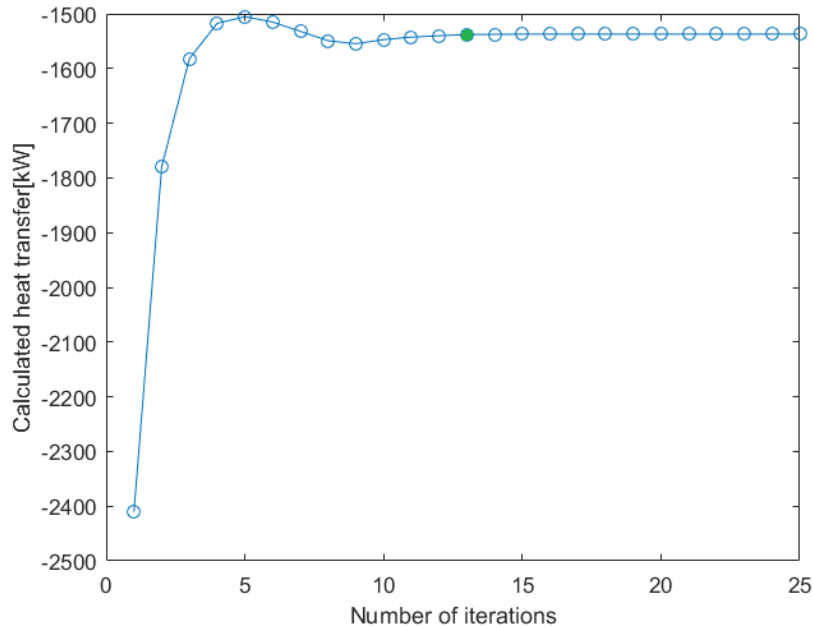


Figure 5.4: Convergence history of a typical cooler with CO₂

nal pressure loss of 1 % is assumed for the heater and the cooler and 0.5 % for both sides of the regenerator. With this assumptions, the inlet conditions of the regenerator are known and the outlet conditions as well as the heat duty of the regenerator can be computed. As a last step also the heater inlet conditions can be determined. Now all inlet conditions and heat duty requirements for the heat exchangers are known. The sizing of the heat exchangers starts in parallel. Once the three heat exchangers have been sized, the cycle is solved again but this time, the calculated internal pressure losses are used. The power output of the supercritical cycle is evaluated and then the heat duty and external pressure losses are put into GSP to calculate the final performance of the main engine. As a last step, the performance of the supercritical cycle and the main engine are combined to determine the system performance.

Only one iteration is present in the top level calculation. The accuracy of the method could be increased, when the method would execute several iterations of the internal pressure losses and thus the heat duties of the heat exchangers. However, it was found that the internal pressure losses show small variations and have only little influence on the cycle performance. At the same time, the implementation of this iteration would greatly increase the required computation time and thus decrease the ability to investigate a big design space in the given time. Another way of increasing the accuracy of the method would be to adjust the air mass flow rate of the main engine to keep the produced thrust or power constant and then iterate the supercritical cycle design based on the new operating conditions. This would again greatly increase the computation time and the typical error by not conduction this additional iteration, is below 1 %. This is acceptable and therefore, the iteration is not implemented.

5.1.2. VERIFICATION

In order to validate the script, the results for a supercritical cycle of Dymola and the Matlab code are compared, see table 5.1. As can be seen, the changes in the thermodynamic properties are within a few percent. This can be explained by different flue gas compositions and a different fluid model for the air. On the CO₂ side, the pressure losses in the heater and cooler show high deviations which are caused by an improved calculation of the pressure losses. In addition to this, the effect of these pressure losses on the system performance is negligible, as has been proven before. The modified method calculates a lower weight for the cooler and heater and a higher weight for the regenerator. The change in the heater and cooler can be explained by the different gas models and more exact calculation of the heat exchanger geometry. This change causes a roughly 5 % higher heat duty for heat exchangers of the same dimensions. Figure 5.6 shows the heat exchanger weight for a given heat duty and operating conditions. As can be seen, a small change in the heat

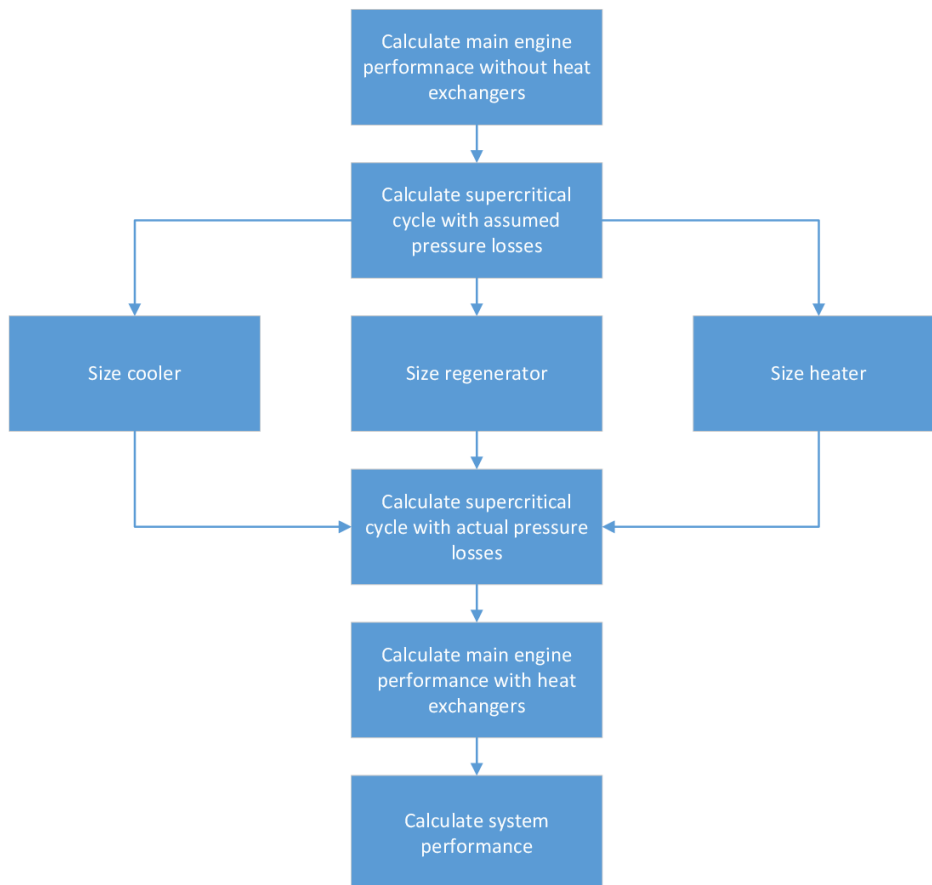


Figure 5.5: Main calculation steps in the system simulation

Table 5.1: Comparison of results from Dymola and the modified methodology

	Dymola	Modified methodology	Difference in %
Q_{Heater} [MW]	1.985	1.994	0.45
Q_{Cooler} [MW]	1.469	1.469	0
$Q_{Regenerator}$ [MW]	0.525	0.517	-1.55
W_{Heater} [kg]	991.54	883.1	-12.28
W_{Cooler} [kg]	701.53	581.81	-20.58
$W_{Regenerator}$ [kg]	131.83	147.01	10.32
$dp_{Heater_{fluegas}}$ [%]	1.92	1.95	0.15
$dp_{Heater_{CO_2}}$ [%]	0.017	0.007	-41.1
$dp_{Cooler_{air}}$ [%]	1.81	1.36	-33
$dp_{Cooler_{CO_2}}$ [%]	0.003	0.002	-50
$dp_{Regenerator_{Hp}}$ [%]	0.004	0.004	0
$dp_{Regenerator_{Lp}}$ [%]	0.092	0.09	-2.22
Cycle Power [MW]	0.5	0.525	4.76

duty can cause a big difference in the weight of the heat exchanger. The weight increases almost exponentially with the required heat duty, as a higher heat duty decreases the temperature difference at the end of the heat exchanger. Therefore, the required surface area for any additional heat duty increases. The higher weight of the regenerator is due to the addition of the working fluid weight. The method gives good results and uses more sophisticated assumptions than the Dymola model. Therefore, the method will be used for further analysis.

5.2. MAIN ENGINES

The reference engines are taken from the paper of Yin and Rao [41]. In order to obtain the same total thrust as for the previous analysis, the total mass flow of the engines is scaled up. The ITB energy fraction ITB_{frac} , defined as

$$ITB_{frac} = \frac{E_{in_{ITB}}}{E_{in_{ITB}} + E_{in_{CC}}}, \quad (5.1)$$

gives the percentage of the total energy input, that is added in the second combustion chamber, the inter turbine burner, and is defined in equation 5.1. In this equation $E_{in_{ITB}}$ is the energy input in the inter turbine burner and $E_{in_{CC}}$ the energy input in the combustion chamber. The comparison is carried out for engines without ITB and for engines with ITB_{frac} of 15 % and 30 %. These values are investigated, because for an energy fraction of 15 % the lowest SFC has been found in previous research and 30 % is the highest ITB_{frac} that data is available about. This enables to investigate whether the beneficial effect of more energy added in the ITB can justify the higher SFC of the main engine. The engine models are similar to the one used as a starting point for the investigation. However, the model is more elaborate with especially the effects of the turbine cooling being modelled in more detail. This model takes the location of the cooling air extraction as well as the pressure losses and efficiency deterioration of the cooling itself into account. Furthermore, the cooling air requirement is calculated for every stage of the turbines based on the occurring temperatures. In that way, the engine models can reproduce the results from Yin [41]. This enables a better comparison between the different engines.

To build a turboshaft model from the existing turbofan models, the fan was replaced by a compressor and a free power turbine is placed behind the LPT. This is to ensure that the operating conditions of the other turbines remain the same for the turboshaft and turbofan engines and to ensure the correct modelling of the required turbine cooling and the effects on the turbine efficiency. The cooler is placed in a separate duct without fan. To deliver a similar power as the turbofan engines, 19 MW of shaft power are required, see equation 4.32. The engines are scaled to this shaft power by adjusting the air mass flow entering the inlet. Figure 5.7 shows the turbofan and turboshaft models that are used. For the turbofan model, the bypass stream is split in two parts. The upper part passes through the heat exchanger before being expanded in the nozzle. The lower path passes just through the bypass duct before being expanded in the nozzle. To account for the lower pressure of the flue gases in the heater, the diameter of the duct was increased for the turboshaft engines. The

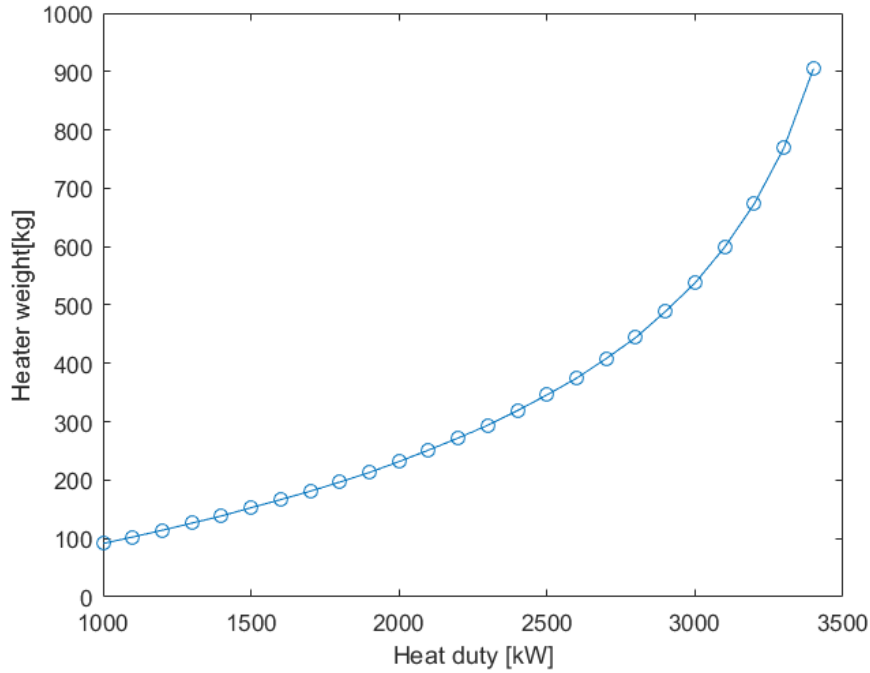


Figure 5.6: Heat exchanger weight for a given heat duty

Table 5.2: Performance of the engines without waste heat recovery unit

	Turbofan 1	Turbofan 2	Turbofan 3	Turboshaft 1	Turboshaft 2	Turboshaft 3
ITB energy fraction [%]	0	15	30	0	15	30
TSFC [kg/kN*h]	49.55	47.37	48.39	42.32	41.46	42.31
Core mass flow [kg/s]	54.46	48.29	48.07	45.95	41.9	41.64
Exhaust temperature [K]	616.5	644.1	662.7	556.6	576.5	594.1
Exhaust pressure [bar]	0.338	0.352	0.350	0.226	0.226	0.226
Cooling air temperature [K]	273.7	273.7	273.7	244.38	244.38	244.38
Cooling air pressure [bar]	0.499	0.499	0.499	0.345	0.345	0.345

diameter of the engine has to increase to be able to house the additional free power turbine. The operating conditions of the engines are summarized in table 5.2.

As can be seen, the addition of an inter turbine burner with an ITB_{frac} of 15 % reduces the specific fuel consumption for the turbofan and turboshaft engine. The reduction is around 4.4 % for the turbofan and 2 % for the turboshaft architecture. The SFC reduction of the inter turbine burner decreases for an ITB_{frac} of 30 %. For the turbofan engine, the application of an ITB with ITB_{frac} of 30% decreases by 2.3 % for the turboshaft engine, the SFC is almost the same as without ITB. This change in effect of the ITB is due to the more severe effect of the pressure losses in a turboshaft configuration. The application of an inter turbine burner causes additional pressure losses in the second combustion chamber. Thus the benefit of the ITB is smaller for a turboshaft.

The addition of an interturbine burner decreases the core mass flow and increases the exhaust temperature. This effect becomes bigger for higher energy fractions. Overall, this decreases the size of the heat exchangers. The change from turbofan to turboshaft engine reduces both, the exhaust temperature and the core mass flow rate. This has a very negative effect on the heat exchangers as their size has to increase.

In general, the specific fuel consumption of the turboshaft engines is much lower than for the turbofan engines. This difference can be explained by the assumed propulsive efficiency of 90 % for the turboshaft en-

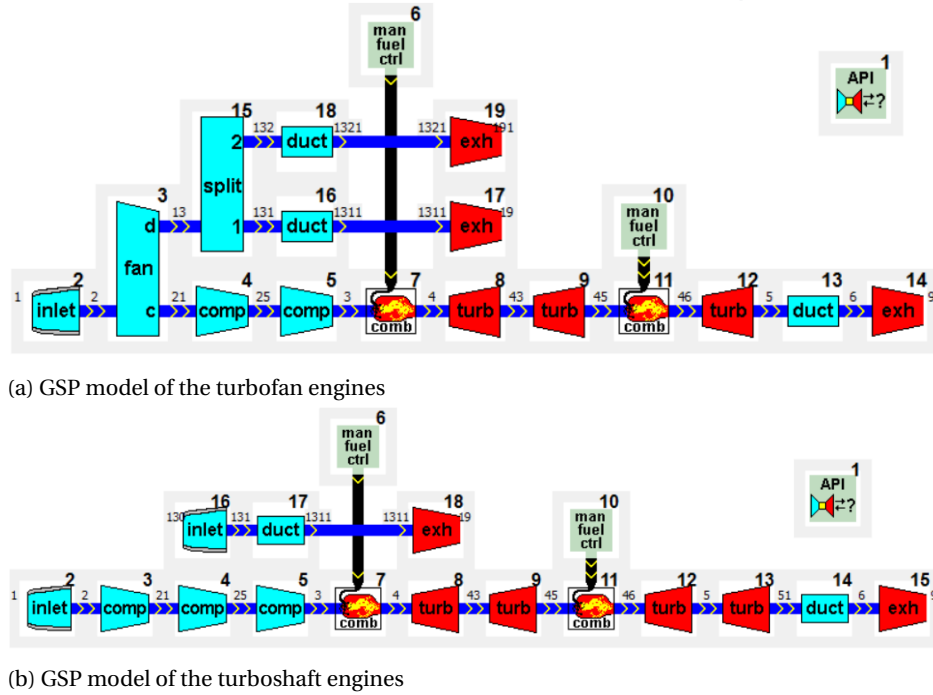


Figure 5.7: GSP models of the main engines

gines. This number is an assumption of the expected efficiencies and higher than the propulsive efficiency of the turbofan engines. This assumption is based on the ability to use more advanced concepts like the distributed propulsion [45]. This higher propulsive efficiency of the turboshaft engines explains the differences of around 25 % in SFC. As this effect on the propulsive efficiency and the realisation of this benefit is beyond the scope of the thesis, no comparison between turbofan and turboshaft engines in an absolute sense will be made. For this thesis, the main focus will lie on the effect of the additional supercritical cycle on the system. I.e. does an additional supercritical cycle have a more positive effect on a turbofan rather than a turboshaft engine?

5.3. RESULTS

The results for the turbofan engines are shown in table 5.3, the ones for turboshaft engine in table 5.4. For all engines with C_4F_{10} as working fluid no suitable design could be found, as the requirement of 500 kW of additional power could not be fulfilled with acceptable heater size and pressure losses. The critical temperature of C_4F_{10} is very high. Therefore, the possible temperature gain in the heater is low, as the fluid enters at an already high temperature. At the same time, low pressure ratios are required to keep the compressor outlet temperature at acceptable ranges. This results in low cycle efficiencies and thus a high energy input to achieve the required shaft power output of 500 kW. The combination of a high required heater power and a low temperature difference results in a very big heater. This causes high pressure losses of the heater which limit the work potential of the main engine turbine. The main engine could not be sized due to the too high pressure losses in the heater.

The data show that the application of the candidates is not beneficial and the range decreases due to the additional supercritical cycles. They also show that the application of an ITB is beneficial for the supercritical cycle in that it reduces the weight of the heater. However, the effect of ITB on the main engine is stronger than the effect on the additional cycle. Therefore, the optimal ITB_{frac} remains at 15 %. Looking at the working fluids, pure C_4F_{10} can be said to be not suitable as a working fluid for the CCE. Xenon and CO_2 show similar performance but result in very different designs. While the mass flow rate for the Xenon cycle is around 90 kg/s, it is only 13 kg/s for the CO_2 cycle. This can also be recognized in the internal pressure losses in the heat exchangers. They are higher for the Xenon cycle. While this is not a problem in the current designs, it limits the potential for more efficient heat exchanger designs, as the size of the tubes can not be reduced as

Table 5.3: Performance of the investigated turbofan engines

	Turbofan 1	Turbofan 2	Turbofan 3
ITB energy fraction [%]	0	15	30
TSFC without WHR cycle [kg/kN*h]	49.55	47.37	48.39
TSFC with CO ₂ cycle [kg/kN*h]	48.30	46.45	47.45
TSFC with Xe cycle [kg/kN*h]	48.98	46.50	47.46
TSFC with C ₄ F ₁₀ cycle [kg/kN*h]	—	—	—
Weight with CO ₂ cycle [kg]	3970	2407	2122
Weight with Xe cycle [kg]	3205	2079	1890
Weight with C ₄ F ₁₀ cycle [kg]	—	—	—
Range with CO ₂ cycle [km]	15018	16082	15827
Range with Xe cycle [km]	15026	16164	15892
Range with C ₄ F ₁₀ cycle [km]	—	—	—
Range without WHR unit [km]	15787	16513	16166
Maximum range with WHR unit [km]	15026	16164	15892
Maximum change in range [%]	-4.82	-2.11	-1.69

Table 5.4: Performance of the investigated turboshaft engines

	Turboshaft 1	Turboshaft 2	Turboshaft 3
ITB energy fraction [%]	0	15	30
TSFC without WHR cycle [kg/kN*h]	42.32	41.46	42.31
TSFC with CO ₂ cycle [kg/kN*h]	42.47	41.49	42.32
TSFC with Xe cycle [kg/kN*h]	42.28	41.33	42.19
TSFC with C ₄ F ₁₀ cycle [kg/kN*h]	—	—	—
Weight with CO ₂ cycle [kg]	3571	3351	3061
Weight with Xe cycle [kg]	2426	1981	1934
Weight with C ₄ F ₁₀ cycle [kg]	—	—	—
Range with CO ₂ cycle [km]	17209	17691	17438
Range with Xe cycle [km]	17659	18217	17860
Range with C ₄ F ₁₀ cycle [km]	—	—	—
Range without WHR unit [km]	18484	18868	18489
Maximum range with WHR unit [km]	17659	18217	17860
Maximum change in range [%]	-4.46	-3.45	-3.40

much.

In general, as was expected, the weight of the supercritical cycle and the pressure losses increase. These effects overcompensate for the additional power of the supercritical cycle. It can be seen that the optimal pressure ratio for turboshaft engines is lower than for the turbofan engines, as the maximum cycle temperature decreases due to the lower exhaust gas temperature. As a consequence the heat load of the regenerator increases. This causes a weight increase in the regenerator. The lower pressure ratio decreases the efficiency of the cycle and thus more energy has to be extracted from the exhaust at a lower temperature. For this reason, the heater becomes heavier as well.

The weight distribution of different candidate systems is shown in figure 5.8. For all systems the heater is the heaviest heat exchanger, due to the high thickness required for the range of design pressures. The data also show that the weight fraction of the heater decreases with higher ITB_{frac} and thus higher exhaust gas temperature. The cooler of systems with a turbofan as main engine makes up a much bigger fraction of the total weight. For the turbofan system with an ITB_{frac} of 15 %, the regenerator weight of the system with Xenon is much lower than for CO_2 . This can be explained by the much lower heat capacity of Xenon and the higher internal flow velocity due to the higher mass flow.

5.3.1. CARBON DIOXIDE CYCLES

Carbon dioxide has been the standard working fluid in this study, as it is the most investigated supercritical working fluid in literature.

The highest range is achieved with the combination of a turbofan engine with an ITB_{frac} of 15 %. However, the additional weight of the supercritical cycle outweighs the effect of the additional power. Therefore, the range of the aircraft decreases, when compared to just the main engine. For the turbofan engine with an ITB_{frac} of 30 %, the benefit of the additional cycle is bigger. However, the main engine has a higher SFC. This outweighs the effect of the supercritical cycle. The range of the aircraft is lower than for an ITB_{frac} of 15 %.

The design of the carbon dioxide cycles is characterised by relatively low mass flow rates. At the same time, high pressure ratios are achieved. Together with the high critical pressure, this results in a heavy heater. The high pressure ratio also causes a small regenerator. The cooler has a rather high temperature difference and still enables a minimum cycle temperature close to the critical temperature.

5.3.2. XENON CYCLES

The low C_p value of Xenon causes very high temperature changes of the working fluid in the heat exchangers. To enable a high enough energy input into the system, very high mass flow rates are required. These are in the order of 90 kg/s. This also requires higher cooling air mass flows. The minimum cycle temperature of the optimized supercritical cycles is even higher than for CO_2 even though the critical temperature is lower. This shows the difficulties in the cooler design due to the high mass flow rates. As the high mass flow rate and the low critical temperature cause a very high cooler weight, when the minimum temperature equals the critical temperature, a lower efficiency is unavoidable and thus a lighter cooler outweighs the efficiency loss

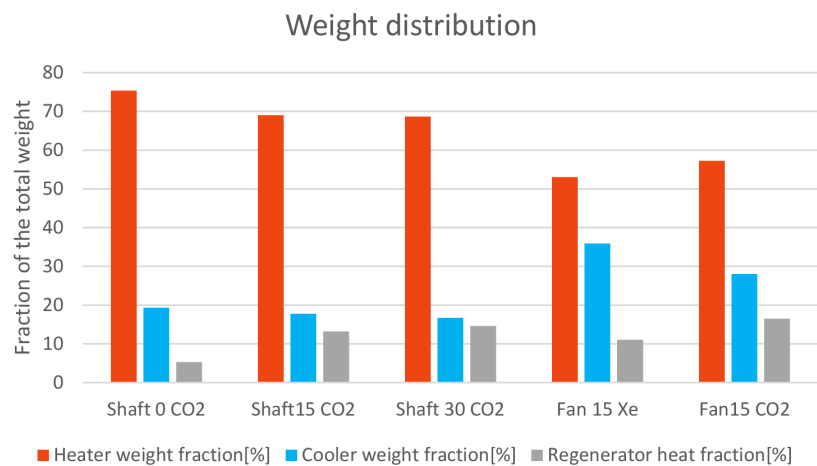


Figure 5.8: Weight distribution of different CCE configurations

in the supercritical cycle. The low critical pressure does not influence the cooler design, as the wall thickness is limited by the production process and equal to the one for CO_2 . At the heater and regenerator however, thinner tubes can be used due to the lower critical pressure and pressure ratio.

The Xenon cycle in combination with a turbofan engine with an ITB_{frac} of 15 % proved to be the cycle with the best performance. This is due to the low weight of the heater and regenerator. The internal pressure losses in the heat exchangers are between 1 % and 1.5 %. This is much higher than for the CO_2 cycles and is caused by the higher mass flow rates and thus internal flow velocities. While these losses have not a big influence on the current designs, they limit the ability to use smaller tubes in the heater and cooler, as the internal pressure losses increase quickly for smaller tubes and can outweigh the benefits of lower external pressure losses and lower weight, if the tubes are too small.

5.3.3. PERFLUOROBUTANE CYCLES

It was not possible, to create suitable CCE designs with C_4F_{10} as working fluid. Perfluorobutane has a very low critical pressure and a high critical temperature. This enables a high temperature difference in the cooler. To keep the working fluid in its supercritical state, the cooler exit temperature has to be rather high. For this reason, only a small temperature increase can be realised in the heater. This also limits the achievable pressure ratios, as a higher pressure decreases the temperature difference in the heater even more. This results in a low cycle efficiency and a low power input. For these reasons, it is not possible to create a cycle that fulfils the 500 kW shaft power requirement. The required heater for such a cycle is too big and the associated pressure loss prevents the operation of the main engine. Therefore, pure Perfluorobutane is not a suitable working fluid for the supercritical cycle.

5.4. CONCLUSIONS

In this chapter, the best candidate for a more in depth analysis was found. For this purpose a new simulation methodology based on GSP and MATLAB was introduced and the performance of several system configurations was investigated and compared.

It was found that the turbofan engine with a moderate ITB_{frac} of 15 % is the best main engine for the application of a supercritical waste heat recovery unit. This is because of its superior SFC and the good operating conditions it provides for the heater. A higher ITB_{frac} makes the supercritical cycle more beneficial, however, this effect can not outweigh the diminishing SFC of the main engine due to the higher ITB_{frac} .

Xenon was found to give the best system performance of the investigated working fluids. However, the designs require very high mass flow rates to fulfil the minimum power constraint. CO_2 was chosen as the best candidate for further investigations, as it performs almost as good as Xenon but requires much lower mass flow rates. This enables the use of smaller tubes, when the heat exchanger design is optimized. Therefore, CO_2 has a bigger potential for weight reduction.

Turboshaft engines are less suited for the application of a supercritical waste heat recovery unit. The reason for this is the lower exhaust gas temperature. This increases the weight and associated pressure losses of the heat exchangers and outweighs the thermodynamic benefits this architecture has on the main engine. C_4F_{10} was found to be not suitable for the use as working fluid in the combined cycle engine due to its too high critical temperature. This results in a too low temperature difference in the heater and thus prohibitively large heaters.

In the next chapter, the heat exchanger geometry will be optimized, to improve the system performance even more and check whether the additional cycle can be beneficial in terms of aircraft maximum range mission range. For this, the combination of a turbofan engine with an ITB_{frac} of 15 % and a carbon dioxide cycle is used as a basis. In addition to the optimal heat exchanger design, also the effect of a mixture of CO_2 and Xenon or C_4F_{10} will be investigated.

6

RESULTS

Based on the findings from chapter 5, the combination of a supercritical cycle, with a mixture of CO_2 and C_4F_{10} as working fluid, with a turbofan engine with 15 % ITB_{frac} in the inter turbine burner was selected as the most promising candidate system for further optimization. In this chapter, two versions of the combined cycle engine are tested. In one case, the power of the supercritical cycle is used to produce thrust outside the engine. In the second case, the power is transferred into the low pressure spool of the main engine. While the second option does not present as many thermodynamic benefits, it ensures a higher exhaust gas temperature. As has been seen in the previous analysis, this is very beneficial as it allows a lower weight of the heater.

6.1. OPTIMIZATION OF THE SYSTEM

To show the full potential of the system, the design space for this optimization has been expanded to also include the mixture fraction of the working fluid and the heat exchanger design. The methodology is the same as has been introduced in chapter 4 and has been used in chapter 5. For this investigation, the minimum pressure in the supercritical cycle is fixed to be 1 bar above the critical pressure of the working fluid. The design variables are:

- Pressure ratio in the supercritical cycle
- Pinch temperature of the heater
- Pinch temperature of the regenerator
- Pinch temperature of the cooler
- Mass flow rate of the supercritical working fluid
- Mass flow rate of the cooling air
- Mixture fraction of CO_2
- Aspect ratio of the heat exchanger tubes
- Maximum diameter of the heat exchanger tubes
- Radial spacing of the heat exchanger tubes

The minimum wall thickness of the heat exchangers was reduced to 0.2 mm and the minimum major axis diameter of the cooler and heater tubes was set to be 3.6 mm. This fits well with the experience from heat exchangers made by MTU [46].

Table 6.1: Properties of the investigated cases

	Engine 1	Engine 2	Engine 3	Engine 4
Working fluid	$CO_2 - C_4F_{10}$	CO_2	CO_2	Xe
Cooler location	Behind the fan	Behind the fan	In free stream	Behind the fan
Use of additional power	Additional thrust	In LP spool	Additional thrust	Additional thrust

Table 6.2: Results of the second optimization step

	Engine 1	Engine 2	Engine 3	Engine 4
SFC [kg/kN*h]	46.23	46.57	46.41	46.11
Weight [kg]	987.5	1093.6	818.2	1990
Change in range [%]	+0.4644	-0.4784	+0.3755	-1.13

6.1.1. INVESTIGATED CASES

Four different engines have been optimised in the extended design space. This is to find the best configuration and have a realistic estimation of the performance. The cases are summarized in table 6.1.

- Engine 1: This engine uses a variable mixture of CO_2 and C_4F_{10} as working fluid for the supercritical cycle. The power of the WHR is transformed to thrust with an efficiency of 90 %. The cooler is placed behind the fan of the main engine.
- Engine 2: Based on the findings of engine one, pure CO_2 is used as the working fluid for this engine. In this case, the additional power is directly transferred into the low pressure spool of the main engine. The cooler is placed behind the fan of the main engine.
- Engine 3: This engines uses pure CO_2 as well. The power of the WHR is transformed to thrust with an efficiency of 90 %. The cooler is placed in a duct in free stream. No Fan is upstream of the cooler.
- Engine 4: Engine 4 is the same as engine number 1 with the difference that Xenon is used as the working fluid. This engine is a test case to check whether the assumption about the potential of Xenon as a working fluid is indeed correct.

6.2. RESULTS

The results are summarized in table 6.2. Engine 1 is the best engine configuration. It uses the additional power to produce thrust and has the cooler placed behind the fan. The optimization of the system could increase the range of the maximum range mission of the aircraft by 0.46 % compared to the turbofan without additional cycle. Even though a mixture was specified as the working fluid, the optimized mixture fraction was 1 and thus pure CO_2 . Both a mixture with C_4F_{10} as well as Xenon proved to be less beneficial.

Engine 3 has a very similar performance and has a better performance than the turbofan engine. The range of the aircraft can be increased by 0.38 %. This engine has the cooler placed in free stream conditions. As expected, the SFC is higher but the weight of the system is lower. This is due to the higher air pressure and temperature at the cooler. However, the difference between the two designs does not match the one in table 4.5. The placement behind the fan is more beneficial. This shows that the heat exchanger design has a big influence on the system behaviour. At the current design point, the cooler weight is lower and less sensitive to the air temperature. At the same time, the influence of the pressure is almost unchanged, as the heat addition is of similar magnitude.

Engine 2 transfers the power of the supercritical cycle into the LP spool. This is less beneficial than using the power directly for the generation of thrust. This was expected, as the propulsive efficiency of the main engine is much lower than the assumed efficiency when the power of the supercritical cycle is directly used to produce thrust. The weight of the system increases due to a heavier regenerator. The higher exhaust gas temperature and pressure make the pressure losses of the heater more important. This means that a small heater is more beneficial and also easier to achieve due to the higher temperature. A bigger regenerator compensates for the lower heat power of the smaller heater. In this way, the external pressure losses are kept low

but the total weight increases.

Engine 4 achieves the lowest SFC of the investigated engines but is also the heaviest engine. Therefore, it has the worst performance. However, this result is influenced by an error in the optimization process. The process was stopped, before the termination criteria was reached, thus no final conclusions can be drawn from the result. Yet some trends can be identified. The high mass flow rate causes high internal pressure losses. To limit these pressure losses, the heat exchanger tubes are bigger than for the engine with CO_2 as working fluid.

6.2.1. THE OPTIMAL DESIGN

The optimal design of the combined cycle engine uses pure CO_2 as working fluid and its characteristics are summarised in table 6.3. The heat exchanger uses very small tubes and a slightly higher aspect ratio of the tubes. The radial spacing between the tubes also decreases by around 15 %. The pressure ratio is around 2.8. This results in a maximum pressure of 211 bar, much lower than the maximum allowed pressure of 400 bar. The minimum cycle temperature is 313 K. This is close to the critical temperature of 305 K. Still the pressure loss of the cooling air in the cooler is low with only 0.76 % and only the cooling airflow of 34 kg/s is effected by this pressure loss. The pressure loss of the flue gas in the heater is 2.33 %. These low pressure losses are made possible by the small heat exchanger tubes. The internal pressure losses are bigger than at the previous cycle but still below 1 % and show the potential to decrease the tube size even more.

Table 6.3: Characteristics of the optimized engine 1 design

Cooling air temperature [K]	274
Flue gas temperature [K]	644
Minimum WHR cycle temperature [K]	314
Maximum WHR cycle temperature [K]	621
Minimum WHR cycle pressure [bar]	74.77
WHR cycle pressure ratio [-]	2.825
Pinch temperature cooler [K]	40
Pinch temperature heater [K]	23.23
Pinch temperature regenerator [K]	24.45
Cooling air mass flow [kg/s]	34.26
CO_2 mass flow [kg/s]	10.69
Heat exchanger tube aspect ratio [-]	2.3
Heat exchanger tubes major axis length [mm]	3.6
Cooler wall thickness [mm]	0.2
Regenerator wall thickness [mm]	0.2
Heater wall thickness [mm]	0.53
Cooler weight [kg]	324
Heater weight [kg]	448
Regenerator weight [kg]	215
Cooler power [kW]	1713
Heater power [kW]	2219
Regenerator power [kW]	1140
Internal pressure loss cooler [%]	0.05
External pressure loss cooler [%]	0.76
Internal pressure loss heater [%]	0.24
External pressure loss heater [%]	2.33
Internal pressure loss regenerator Hp [%]	0.01
Internal pressure loss regenerator Lp [%]	0.01
WHR cycle efficiency [%]	22.8

The wall thickness of the heater tubes is 0.53 mm. The wall thickness of the cooler and regenerator is limited by the minimum wall thickness of 0.2 mm. The supercritical cycle produces 507 kW of power. This shows that the cycle is beneficial, as the minimum power constraint is not active any more. The maximum cycle temperature is 621 K. This is 23 K below the flue gas temperature. In general, the heat exchanger pinch temperatures are similar to the results from the candidate cycles from chapter 5. The biggest difference is 15 % in the heater. In this case, the smaller heat exchanger tubes make a lower pinch temperature more beneficial, as the weight and pressure penalty is lower. The pressure ratio and CO_2 mass flow rate did only change a few percent, when the design space was enlarged. The amount of cooling air reduced by 20.6 % due to the modified heat exchanger design. Due to the smaller cooler tubes and thus lower weight, the saving in cooler weight did not justify the higher thrust losses due to the pressure losses. These changes in the optimized design show that there is a clear relation between the heat exchanger design and the optimal design parameters of the supercritical cycle. Yet the resulting supercritical cycles are similar and always result from a trade off between thermodynamic performance and weight.

6.3. EFFECT OF TECHNOLOGICAL BARRIERS

The given design is based on estimations of the potential technology that will be available at

the possible entry into service period in 2035. However, more sophisticated technologies and component performances can improve the performance of the system. The heat exchangers are the components with the highest impact on the system performance. When the heat transfer coefficient of the heat exchangers can be increased by 10 %, the range of the aircraft can be increased by 0.23 %. A 10 % reduction in the internal and external pressure losses increases the range by 0.08 %. This shows that the heat transfer of the heat exchangers is more important than the associated pressure losses. Further investigations are required to understand how such improvements can be realised.

Two parameters that affect the heat exchanger performance are the wall thickness and the tube size. The wall thickness of the cooler and the regenerator are still limited by the capabilities of the production process. A reduction of the minimum wall thickness from 0.2 mm to 0.1 mm can increase the range by 0.33 %. According to Parsons [47], a wall thickness of 0.1 mm is achievable in series production. When this capability is combined with a smaller tube diameter of maximum 2.5 mm, the range can be increased by 0.67 % compared to the design with respect to engine 1 of table 6.2. This would mean a total range increase of 1.13 % compared to the turbofan engine.

When no production limits are present, the CCE can achieve a 2.15 % higher range than the equivalent turbofan. To achieve this result, very advanced heat exchangers are required. The axis of the elliptical heat exchanger tubes become 1.07 mm and 0.5 mm. These small dimensions decrease the pressure stresses in the tubes and the wall-thicknesses become as low as 0.034 mm for the cooler and 0.137 mm for the heater. The weight of the heat exchangers is reduced to a total of 200 kg. This demands very advanced production technologies.

Another effect that will change the potential of the combined cycle engine is the development of future airframe technology. It can be expected that the empty weight of an aircraft with a given maximum take off weight will decrease, as new materials arise and better design and production methods are used for the development of aircraft. This will increase the maximum range of the aircraft and will also benefit the combined cycle engine. As the fuel will become a bigger fraction of the total weight, savings in fuel will get a higher importance. This reduces the requirement for the power density of the supercritical cycle.

6.4. CONCLUSIONS

In this chapter the best candidate for the CCE for the year 2035 was optimized in an enlarged design space. Four versions were compared. Furthermore, the optimized design was introduced and analysed. The combined cycle engine was found to increase the range by 0.46 %, when equipped with advanced heat exchangers. The best combination is a turbofan engine with an ITB_{frac} of 15 % in combination with a supercritical carbon dioxide cycle. The cooler is placed behind the fan of the turbofan engine and the power of the supercritical cycle is used to produce thrust outside the main engine.

The possibility to produce thinner and smaller heat exchanger tubes could increase the range advantage to 1.13 %. When no production constraints are taken into account, a range increase of 2.15 % can become possible. It was also found that future development in aircraft structures will make the combined cycle engine more beneficial due to lower structural weights of the aircraft.

7

CONCLUSIONS

Aviation has to reduce its emissions. The historic way of further optimizing the turbofan engine holds only limited potential to reach this goal. Therefore, research into alternative cycles started. The concept of a combined cycle engine consisting of a main engine and an additional supercritical Brayton cycle has been proposed as part of this research. Initial investigations showed a potential for this concept. However, the application into existing engines reduced the benefits.

The present study aims at analysing this concept to find out the potential benefits. For this purpose a Dymola model of the system has been created to be able to calculate the specific fuel consumption and the weight of the system. To be more flexible in the system configuration, a model in GSP and Matlab was derived from the Dymola model. As a performance metric, the maximum mission range of an aircraft according to equation 3.1 has been used. It was found that the application to long range aircraft is the most beneficial one. However, for the CCE to be beneficial, a SFC reduction of at least 1.82 % per ton of additional engine weight is required. In absolute terms, this requires a power density of the supercritical cycle of 309 kW per ton of additional engine weight.

The effect of several parameters on the system performance was investigated. It was found that the supercritical cycle operating parameters as well as the heat exchanger design have a big impact on the performance. The influence of a single parameter on the system performance strongly depends on the design point. This makes the use of optimization routines to find the best set of parameters necessary. The main engine configuration and the working fluid of the supercritical cycle have a big influence as well. The best combination found is a turbofan engine with inter turbine burner and CO_2 as working fluid for the additional cycle. The configuration of the supercritical cycle appears to have only a small influence on the system performance. The simple recuperated configuration was chosen as a compromise between complexity and performance.

The optimization process pointed out that the combined cycle engine can increase the range of an aircraft by 0.46 %. It was also found that the heat exchanger design has an effect on the optimal cycle parameters and that the capabilities in the heat exchanger production have a big influence on the performance of the combined cycle engine. In addition to that, it was found that more advanced aircraft structures have a beneficial effect on the combined cycle engine. When the production constraints on the minimum wall thickness and tube diameter are removed, the CCE can increase the range of an aircraft by 2.15 %.

The combined cycle engine can have a small contribution towards more efficient aviation. Also the best configuration of the combined cycle engine has been found and ways to further improve the system have been shown. However, the contribution is only limited and not enough to make the CCE a competitive solution yet. The achievable gains are very small and negative installation effect, like increased wetted area and the weight of ducting and the additional turbomachinery will further reduce the achievable fuel burn reduction. These improvements do not justify the efforts of a real product development, until very advanced heat exchanger technology becomes available.

7.1. RECOMMENDATIONS

Many possibilities of improving the system performance have been investigated. Further aspects, that have not been investigated are listed and motivated below.

The presented analysis was conducted in design conditions during cruise flight. To be able to estimate the effects of the engine on the aircraft mission performance, the performance along the entire mission has to be investigated. The performance increase by the addition of an inter turbine burner in the paper of Yin *et al.* [41] was based on the loosening of the hot day take off constraint. It is interesting what effect the addition of a supercritical waste heat recovery unit has on these kinds of design constraints.

The heat exchangers are a critical part of the concept of the combined cycle engine. The heat exchangers have been analysed extensively in this study. Yet not all possible design factors have been incorporated into the model. It is advisable to extend the model to include additional design parameters such as the amount of rows and the spacing of the tubes. In addition to this, the results depend on two correlations. More detailed correlations have to be adopted to increase the accuracy of the weight estimation. A first investigation in this direction is the work of Vidyarthi [48].

This study approximated the total weight of the system with the wet weight of the heat exchangers, neglecting other components. To have a more complete evaluation of the system performance, other components like the turbomachinery or ducting of the working fluid should be taken into account as well. However, this also requires a more detailed design of the main engine and the aircraft.

The effect of different supercritical cycle configurations have been estimated to be not more than 0.17 % of the aircraft range at best. While more in depth research on these configurations was not conducted in this thesis work, it might be worthwhile in further research.

In this thesis, the performance of the combined cycle engine was estimated, for the maximum range mission of the aircraft only. This is the most beneficial case for the application of the combined cycle engine. However, in the commercial use of an aircraft, this mission is of minor importance. Therefore, it is advisable to investigate the performance of the combined cycle engines for different, more common missions of an aircraft. This includes different payload, range missions and gives a better understanding of the performance of the combined cycle engine in everyday airline operation.

The presented research focused on the influence of the new engine concept on the aircraft by means of changes in SFC and weight. In further studies, the feasibility of the combined cycle engine should be proven by additionally taking into account the required volume of the additional cycle and the effect it has on the aircraft design. A different cooler location can potentially allow for a greater benefit than has been found in this study. For example, the cooler could be placed at the wing tips and thus reduce the wing bending moment and act as a winglet as has been presented in [45]. Also more futuristic concepts like the usage of turbomachinery and engine surfaces as heat exchangers as proposed by Ito *et al.* [49]. In this way, a small amount of energy could be transferred between the air in the main compressor and the supercritical cycle, increasing the efficiency of both cycles.

It has already been noted that parts of the supercritical working fluid might change phase inside the cooler. Based on [19], it was assumed that this does not pose a problem for the stability of the operation. However, in further studies this should be investigated more closely. The finding can also be used to show the feasibility of a supercritical condensation cycle. The possibility of a phase change from the supercritical state into the liquid phases has not been considered in this study and can potentially increase the efficiency of the additional cycle.

Many assumption have been made during the research for this thesis. A big effort has been made to verify the results and make sure that the results are correct. The lack of experimental data however, does not allow for the validation of the results. The validation of the results with experimental data is desirable.

BIBLIOGRAPHY

- [1] Y. Cengel and M. Boles, *Thermodynamics: An Engineering Approach*, 6th ed. (2007).
- [2] C. De Servi, L. Azzini, M. Pini, A. Gangoli Rao, and P. Colona, *Exploratory assessment of a combined cycle engine concept for aircraft propulsion*, in *Global propulsion and power society forum 2017*.
- [3] M. Kulhanek and V. Dostal, *Thermodynamic analysis and comparison of supercritical carbon dioxide cycles*, in *Supercritical CO2 power cycle symposium 2011*.
- [4] F. Jacob, A. Rolt, J. Sebatianpillai, V. Sethi, M. Belmonte, and P. Cobas, *Performance of a supercritical co2 bottoming cycle for aero applications*, *Applied sciences* (2017).
- [5] D. Lee, D. Fahey, P. Forster, P. Newton, R. Wit, L. Lim, B. Oweb, and R. Sausen, *Aviation and global climate change in the 21st century*, *Atmospheric Environment* **43** (2009).
- [6] N. Cumpsty, *Preparing for the future: Reducing gas turbine environmental impact-igti scholar lecture*, *Journal of Turbomachinery* **132** (2010).
- [7] X. Zhao, *First and second law analysis of intercooled turbofan engine*, *Journal of Engineering for Gas Turbines and Power* **138** (2016).
- [8] L. Xu, K. Kyprianidis, and T. Groenstedt, *Optimization study of an intercooled recuperated aero-engine*, *Journal of Propulsion and Power* **29** (2013).
- [9] S. Kaiser, A. Seitz, S. Donnerhack, and A. Lundblad, *Composite cycle engine concept with hectopressure ratio*, *Journal of Propulsion and Power* **32** (2016).
- [10] C. Perullo, D. Mavris, and E. Fonseca, *An integrated assessment of an organic rankine cycle concept for use in onboard aircraft power generation*, in *ASME Turbo Expo 2013*.
- [11] E. Feher, *The supercritical thermodynamic power cycle*, *Energy Conversion* **8** (1968).
- [12] G. Angelino, *Carbon dioxide condensation cycles for power production*, *Journal of Engineering for power* (1968).
- [13] V. Dostal, M. Driscoll, and P. Hejzlar, *A Supercritical Carbon Dioxide Cycle for Next Generation Nuclear Reactors*, Report MIT-ANP-TR100 (MIT, 2004).
- [14] Petr V., Kolovratnik M, Hanzal V, "On the Use Of CO2 Gas Turbine in Power Engineering (in Czech)", *Czech Technical University in Prague, Department of Fluid Dynamics and Power Engineering, Division of Power Engineering, Departmental report Z-530/99, January, (1999)*, Report.
- [15] P. Jiang, F. Zhen, and R. Xu, *Thermodynamic analysis of a solar-enhanced geothermal hybrid power plant using co2 as working fluid*, *Journal of applied thermal engineering* **116** (2017).
- [16] T. Paris de Bollardiere, T. Verchere, M. Wilson, P. O'Sullivan, S. Heap, A. Thompson, S. Jewer, and P. Beeley, *Design of a supercritical carbon dioxide cooled reactor for marine applications*, in *International Congress on advances in nuclear power plants*.
- [17] Y. Ahn, S. Bae, M. Kim, S. Cho, S. Baik, J. Lee, and J. Cha, *Review of supercritical co2 power cycle technology and current status of research and development*, *Nuclear Engineering and Technology* **47** (2015).
- [18] M. Utamura, T. Fukuda, and M. Aritomi, *Aerodynamic characteristics of a centrifugal compressor working in supercritical carbon dioxide*, *Energy Procedia* **14** (2011).
- [19] J. Noall and J. Pasch, *Achievable efficiency and stability of supercritical co2 compression systems*, in *Supercritical Co2 Power Cycle Symposium*.

- [20] S. Wright, R. Radel, T. Conboy, and G. Rochau, *Modeling and Experimental Results for Condensing Supercritical CO₂ Power Cycles*, Report SAND2010-8840 (2011).
- [21] E. Clementoni and T. Cox, *Steady-state power operation of a supercritical carbon dioxide brayton cycle*, in *The 4th international Symposium-Supercritical CO₂ Power Cycles*.
- [22] K. Kimball, K. Rahner, J. Nehrbauer, and E. Clementoni, *Supercritical carbon dioxide brayton cycle development overview*, in *ASME Turbo Expo 2013*.
- [23] J. Cha, S. Bae, J. Lee, S. Cho, and J. Lee, J. and Park, *Operation results of a closed supercritical co₂ simple brayton cycle*, in *The 5th International Symposium-Supercritical CO₂ Power Cycles*.
- [24] G. Rochau, *Commercializing the sco₂ recompression closed brayton cycle*, <http://www.swri.org/4org/d18/sco2/papers2014/systemConcepts/63PPT-Rochau.pdf>, [Online; accessed 4 December 2016].
- [25] <http://energy.gov/under-secretary-science-and-energy/articles/doe-announces-80-million-investment-build-supercritical>, [Online; accessed 4 December 2016].
- [26] [http://www.gastechnology.org/news/Pages/GTI-Selected-to-Lead-a-Supercritical-CO₂-Project.aspx](http://www.gastechnology.org/news/Pages/GTI-Selected-to-Lead-a-Supercritical-CO2-Project.aspx), [Online; accessed 4 December 2016].
- [27] J. Sarkar, *Thermodynamic analysis and optimization of a recompression n₂o brayton power cycle*, *Energy* **35** (2010).
- [28] J. Perez, *Evaluation of ethane as a power conversion system working fluid for fast reactors*, Thesis (2008).
- [29] W. Jeong and Y. Jeong, *Performance of supercritical brayton cycle using co₂-based binary mixture at varying critical points of sfr applications*, *Nuclear engineering and design* **262** (2013).
- [30] W. Jeong, J. Lee, and Y. Jeong, *Potential improvements of supercritical recompression co₂ brayton cycle by mixing other gases for power conversion system of a sfr*, *Nuclear Engineering and Design* **241** (2011).
- [31] L. Vesely and V. Dostal, *Research on the effect of the pinch point shift in cycles with supercritical carbon dioxide*, in *The 4th international symposium-Supercritical CO₂ power cycles*.
- [32] T. Neises and C. Turchi, *A comparison of supercritical carbon dioxide power cycle configurations with an emphasis on csp applications*, *Energy Procedia* **49** (2014).
- [33] A. Moisseytsev and J. Sienicki, *Investigation of alternative layouts for the supercritical carbon dioxide brayton cycle for a sodium-cooled fast reactor*. *Nuclear Engineering and Design* **239** (2009).
- [34] T. Ibrahim and A. Gooma, *Thermal performance criteria of elliptica tube bundle in crossflow*, *International Journal of Thermal Sciences* **48** (2009).
- [35] A. Sogni and P. Chiesa, *Calculation code for helically coiled heat recovery boilers*, in *68th Conference of the Italian Thermal Engineering association*.
- [36] A. Cioncolini and L. Santini, *On the laminar to turbulent transition in diabaic helically coiled pipe flow*, *Experimental thermal and fluid science* **30** (2006).
- [37] D. Fryer and J. Harvey, *High pressure vessels*, 1st ed. (Springer, 1998).
- [38] R. Manglik and A. Bergles, *Heat transfer and pressure drop correlations for the rectangular offset strip fin compact heat exchanger*, *Experimental Thermal and fluid Science* **10**, 171 (1995).
- [39] F. Ghezze, *Thermodynamic analysis and preliminary design of a combined-cycle engine for next generation civil aircraft*, Thesis (2016).
- [40] W. Visser, *Generic analysis methods for gas turbine engine performance*, Thesis (2015).
- [41] F. Yin and A. Rao, *Off-design performance of an interstage turbine burner turbofan engine*, *Journal of Engineering for Gas Turbines and Power* **139** (2017).

- [42] *Janes's all the world's aircraft: In service*, (2017).
- [43] S. Dewson and C. Graby, *Hetric workshop at mit*, (2003).
- [44] K. Vogeler, *The potential of sequential combustion for high bypass jet engines*, in *International Gas turbine and Aeroengine congress and exhibition*.
- [45] J. Felder, H. Kim, and G. Brown, *Turboelectric distributed propulsion engine cycle analysis for hybrid wing body aircraft*, in *47th AIAA Aerospace sciences Meeting*.
- [46] H. Gonser, *Untersuchung zum Einsatz von Wärmetauschern in zivilen Turboflugtriebwerken*, Thesis (2008).
- [47] E. Parsons, *Development fabrication and application of a primary surface gas turbine recuperator*, SAR Papers (1985).
- [48] K. Vidyarthi, *Design of heat exchangers for combined Brayton cycle engines*, Thesis (2017).
- [49] Y. Ito and T. Nagasaki, *Suggestion of intercooled and recuperated jet engine using already equipped components as heat exchangers*, in *47th AIAA/ASME/SAE/ASEE Joint Propulsion Conference and Exhibit*.